POLITECNICO DI MILANO
DEPARTMENT OF CIVIL AND ENVIRONMENTAL ENGINEERING
DOCTORAL PROGRAMME IN ENVIRONMENTAL AND
INFRASTRUCTURE ENGINEERING

NUMERICAL MODELLING OF FLOW-INDUCED NOISE EMITTED BY CONTROL DEVICES

Doctoral Dissertation of:
Luca Fenini

Supervisor:
Prof. Stefano Malavasi

Tutor:
Prof. Stefano Malavasi

The Chair of the Doctoral Program:
Prof. Riccardo Barzaghi

2019 – XXXI Cycle

A Holly

Acknowledgements

Il più sentito ringraziamento per questo lavoro va a Stefano che è colui che mi ha dato l'opportunità di effettuare questo percorso e che mi ha stimolato ponendomi davanti a problemi che non avrei mai pensato di volere e potere affrontare. Allo stesso modo voglio ringraziare Pibiviesse che ha finanziato questa ricerca e che ha attivamente collaborato al suo sviluppo. Un ringraziamento particolare va a tutte le persone con cui ho avuto l'occasione di confrontarmi e da cui ho potuto imparare ad analizzare i problemi con una prospettiva applicativa. Quindi ringrazio Danilo, Bruno, Valerio, Marco e soprattutto Filippo che è stato il primo a farmi sentire la parola 'aeroacustica'.
Il ringraziamento va poi a Maria Vittoria, Marco, Giacomo, Marco, Gianandrea e Simone, colleghi a cui ho sempre potuto chiedere un consiglio ma soprattutto amici che hanno contribuito a creare un ambiente lavorativo in cui è stato ed è ancora adesso piacevole stare.

Ci sono poi le persone fuori dall'ufficio che fanno parte della mia vita: i miei genitori che mi hanno sempre sostenuto in qualsiasi occasione, i miei amici (in particolare Davide, Andrea e Guido che conosco da una vita) e Ambra che mi ha aiutato a concentrarmi su questa tesi quando è stato il momento.

E siccome questo lavoro lo posso considerare come la conclusione del mio percorso di studio, un pensiero va anche al mio compagno di studi che c'è stato dal primo giorno in cui ho imparato a leggere fino a quando ha capito che ormai ero pronto a finire di studiare.

Abstract

This study explores different numerical approaches for the investigation of the noise emitted by a gas flowing inside a pipeline and perturbed by the presence of a flow-control device. Laws about maximum human noise exposure force industries to cut down the acoustical emissions coming from any possible source, control devices included. The characterization of control valves' noise emission is thus a crucial task for the manufacturers of these devices.

This is the motivation that raised up this research on the aero-dynamic noise. The analysis presented in this thesis is made with a numerical approach which is a suitable tool for obtaining information in shorter times and with lower costs than the experimental approach. Numerics is used for the investigation of different aspects of the aero-dynamic noise that are about the physical description of the noise dynamics (generation mechanisms, interaction with the flow and propagation) and about its intensity prediction.
The study has been conducted with the industrial purpose to achieve the information of interest in the lowest time. Because of the complexity of the phenomenon, the numerical models and approaches are chosen as the most efficient for collecting only the information of interest. In fact, suitable numerical methods for a complete description of all the aero-acoustic features would have complexity and burden that go far over the industrial resources and return a large amount of uninteresting data.

The physical investigation of the noise generation and propagation

downstream of an orifice is thus performed thanks to the resolution of a system of Acoustic Perturbation Equations (APE) developed in literature. The noise dynamic within the pipe reveals the nature of the acoustic sources and returns noise prediction along the duct. In particular, the noise prediction 1 meter downstream of the control device plays a relevant role because it is identified by the international standards as the reference measure for the acoustical characterization of a device.
The APE system proposed in literature returns a noise description wider than what is sought by valves' manufacturers. An innovative APE system is thus presented as a faster way to collect the information of interest without wasting resources in the simulation of undesired details. This system is tested and its reliability on the noise prediction far from the device is verified.

An even faster approach for obtaining estimation about devices' noise emission is based on the application of the prediction procedure described by the international standards that rule the aero-dynamic noise. In this procedure four parameters are identified as the fundamental for the acoustical characterization of a device; valves' manufacturers must provide their values to the customers. Different numerical methods can be used for the evaluation of each of them. In this work the focus is on the application of numerics for the estimation of the valve correction factor for acoustical efficiency A_η which is the parameter the external noise is most sensitive to. Aero-acoustic models are applied to fluid-dynamic simulation in order to estimate A_η taking into account its dependency on the flow condition unlike the international standards that provide only constant values for it.

A plant for experimental tests on small devices is finally designed in order to collect further data for future analysis on the aero-dynamic noise.

Contents

Abstract **I**

Contents **III**

List of Figures **X**

List of Tables **XI**

List of Acronyms **XIII**

List of Symbols **XV**

1 Introduction **1**

2 Literature Background **7**

2.1 Fundamentals of Acoustics 8
2.2 Elementary Acoustic Sources 10
2.2.1 Monopole 10
2.2.2 Dipole 11
2.2.3 Quadrupole 12
2.3 Aero-Acoustics Background 13
2.4 Acoustic Analogies 16
2.4.1 Lighthill Analogy 17
2.4.2 Ffowcs Williams - Hawkings Analogy 19
2.4.3 Lilley Analogy 20

2.5 Acoustic Perturbation Equations 21
2.5.1 APE Modelling 23

3 Numerical Resolution of APE 27
3.1 Implementation and Resolution of the APE 28
3.1.1 New Solver for the APE System 29
3.2 APE Validation 35
3.2.1 Monopole 35
3.2.2 Dipole 37
3.2.3 Quadrupole 39
3.2.4 Propagation in Sheared Flow 40
3.3 APE for Aero-Acoustics 43
3.3.1 Stochastic Noise Generation and Radiation (SNGR) Model 44
3.3.1.1 Energy spectrum 46
3.3.1.2 Random Variables in SNGR models 48

4 Numerical Investigation of the Noise Generated by an Orifice 51
4.1 Fluid-Dynamic Characterization of the Orifice 52
4.2 Noise Prediction with APE 54
4.2.1 Comparison with LES 58
4.2.2 Influence of the Flow-Rate on the Noise Emission . 62
4.2.3 Acoustic Pressure Inside the Pipe 63
4.3 New Modified APE 66
4.3.1 Acoustic Prediction with the Modified APE 68
4.4 Main Results with APE 70

5 Numerical Evaluation of Valves' Parameters in International Standards for Industrial Aerodynamic Noise 73
5.1 Reference IEC International Standard for Control Valve Aerodynamic Noise 74
5.1.1 Estimation of the Fluid-Dynamic Parameters $\mathbf{F_L}$ and $\mathbf{F_d}$ 76
5.1.2 Estimation of the Acoustic Parameters $\mathbf{A}_\eta$ and $\mathbf{St_p}$. 78
5.2 Estimation of $\mathbf{A}_\eta$ Curve from CFD 80
5.2.1 Experimental Evidences 81
5.2.2 Acoustic Model for the Numerical Estimation of W_a 82
5.2.3 Computation of A_η from the Numerical Acoustic Power 85

5.3 Numerical Prediction of the External Noise Produced by ISA Orifice 85
5.4 Main Results from the Application of Numerics on the IEC Procedure 91

6 Experimental Plant Design **93**

7 Conclusions and Future Work **99**

Appendix **103**

A Derivation of Acoustic Perturbation Equations **103**
A.1 Energy Equation 104
A.2 Continuity Equation 106
A.3 Momentum Equation 107

Bibliography **109**

List of Figures

1.1 Representation of the most common acoustical sources in ducts with both flow-induced and structure-borne sounds [43] 2

3.1 Acoustic pressure emitted by the pulsating monopole (3.6) at time $t^* = 270$. Flow from left to right with M=0.5. . . . 31
3.2 Acoustic pressure on the x-axis emitted by a pulsating monopole: analytical (red line) and numerical solution with acoustic Courant number 0.3 (blue dots) and 0.15 (black dots); $\mathrm{dx} = 1$. 32
3.3 Acoustic pressure on the x-axis emitted by a pulsating monopole: analytical (red line) and numerical solution with acoustic Courant number 0.3 (blue dots) and 0.15 (black dots); $\mathrm{dt} = 0.1$. 33
3.4 Acoustic pressure on the x-axis emitted by a pulsating monopole computed with the new solver: analytical (red line) and numerical solution with acoustic Courant number 0.3 (blue stars) and 0.15 (black dots); $\mathrm{dx} = 1$. 34
3.5 Acoustic pressure emitted by a pulsating monopole at $t^* = 150$. 36
3.6 Comparison of the analytical solution and numerical results of the acoustic pressure along the x-axis emitted by a pulsating monopole at $t^* = 150$. 37

3.7 Acoustic pressure emitted by a pulsating dipole at $t^* = 150$. 38
3.8 Comparison of the analytical solution and numerical results of the acoustic pressure along the x-axis emitted by a dipole at $t^* = 150$. 38
3.9 Acoustic pressure emitted by a pulsating lateral quadrupole at $t^* = 150$. 39
3.10 Comparison of the analytical solution and numerical results of the acoustic pressure along the x-axis emitted by a quadrupole at $t^* = 150$. 40
3.11 Mean velocity profile and acoustic pressure emitted by a pulsating monopole in a sheared flow at $t^* = 180$. 41
3.12 Acoustic pressure at the time $t^* = 180$ emitted by a pulsating monopole in a sheared mean flow computed with the APE solver (a) and obtained from literature [16] (b). . 41
3.13 Acoustic pressure at the time $t^* = 900$ emitted by a pulsating monopole in a jet computed with the APE solver (a) and obtained from literature [2] (b). Isolines from 10^{-2} to 10^{-3} (step 10^{-3}) and 10^{-4}. 43
3.14 Modified Von-Karman spectrum (a) and comparison with $k^{-5/3}$ law (dashed line) in log-log scale (b). 47
3.15 Relative error on the integral of $E(k)$ changing the number of intervals N. 48
3.16 Position of the wave vector $\mathbf{k}_n$ and the direction of the n-th Fourier mode $\boldsymbol{\sigma}_n$. 49

4.1 Technical draw of the orifice. Property of Pibiviesse S.r.l. . 52
4.2 Velocity (coloured contours) and pressure along the axis of the pipe (black line) on a slice of the pipe. Results from RANS simulation with $p_1 = 5$ barA and $p_2 = 4$ barA. . . . 54
4.3 Sound pressure level downstream of the orifice computed with different models applied on APE. 56
4.4 Instantaneous acoustic pressure p_a at time $T = 2$ms calculated with different APE models applied on the system (2.24). Contours of the mean axial velocity. Orifice's trailing edge at $x = 0$. 57
4.5 3D domain for LES simulation. 59
4.6 Time-averaged velocity along the axis of the pipe. 60

4.7 Instantaneous vorticity field: visualization of the components of $\boldsymbol{\omega}$ orthogonal to the surfaces (ω_y in the longitudinal section and ω_x in the transversal section). Flow from left to right. 60
4.8 Time-averaged turbulent kinetic energy from LES downstream of the orifice. Flow from left to right. 61
4.9 Sound pressure level downstream of the orifice computed with LES and different models applied on APE. 62
4.10 SPL on the walls of the pipe changing the pressure drop at the sides of the orifice. 63
4.11 Instantaneous acoustic pressure field downstream of the orifice on a longitudinal section of the pipe and contours of the time-averaged longitudinal velocity calculated with LES. In yellow the boundary of the acoustic source region; in grey contours of the mean axial velocity. 64
4.12 Instantaneous acoustic pressure p_a computed with different numerical methods: LES, APE system (2.24) and new modified APE (4.6). Different scales according to the own values. 68
4.13 Sound pressure level downstream of the orifice computed with different APE systems. 69

5.1 Scheme of the IEC procedure for valve aerodynamic noise prediction [28] 75
5.2 Scheme of the IEC procedure for valve aerodynamic noise prediction [28] 77
5.3 Table 4 from IEC 60534-8-3 [28] with the suggested values for the A_η and St_p parameters for particulars devices. . 79
5.4 Variability of the external noise evaluated according to the IEC procedure with the acoustic parameters A_η and St_p. 80
5.5 Noise prediction according to IEC with A_η=-4 ($\triangle$) and A_η=-4.8 ($\Diamond$) and experimental data ($\bullet$). Figure from [39] . 82
5.6 Technical draw of the orifice described in the ISA international standard [30]. 86
5.7 Acoustic power depending on the differential pressure drop ratio X: comparison of the values return from the IEC procedure with A_η=-4 and -4.8, and of the numerical prediction $\widehat{W_a}$. 87

5.8 Acoustic power depending on the velocity of the jet U_j in logarithmic scale: comparison of the values return from the IEC procedure with A_η=-4 and -4.8, and of the numerical prediction $\widehat{W_a}$. In the corner blue and green lines show the slope of the U^6 and U^8 curves. 88
5.9 Curve of the valve correction factor for acoustic efficiency A_η numerically computed with the acoustic power $\widehat{W_a}$. The horizontal lines represent the values -4 and -4.8 suggested by the IEC for a generic source and for a perforated plate. 89
5.10 Curve of the valve correction factor for acoustic efficiency A_η numerically computed with the acoustic power $\widehat{W_a}$ with the jet Mach number on the x-axis. The horizontal lines represent the values -4 and -4.8 suggested by the IEC for a generic source and for a perforated plate. 90
5.11 External noise in the position indicated by IEC 60534-8-3, depending on the differential pressure drop ratio X: comparison of the values return from the IEC procedure with A_η=-4 and -4.8, and of the numerical prediction $\widehat{W_a}$. . 90

6.1 Top-view of the plant designed for experimental campaign. 95
6.2 Possible installation for the PCB113B28 pressure sensor. . 96
6.3 Scheme of the sensors for the fluid-dynamic and acoustic measurements with the respective module and chassis for the acquisition system. 98

List of Tables

2.1 Differences about the technical and physical aspects to be cared of during numerical simulation of fluid-dynamics and acoustics. 14
2.2 Modelling for the noise propagation in different flow conditions with APE and wave equation. 24

4.1 Simulations on the orifice changing the pressure drop at its sides 62

List of Acronyms

APE	Acoustic Perturbation Equations
CAA	Computational Aero-Acoustics
CFD	Computational Fluid-Dynamic
DES	Detached Eddy Simulation
DNS	Direct Numerical Simulation
LES	Large Eddy Simulation
PPW	Points Per Wavelength
RANS	Reynolds Averaged Navier-Stokes
SNGR	Stochastic Noise Generation and Radiation
SPL	Sound Pressure Level
TKE	Turbulent Kinetic Energy

List of Symbols

α_P	Numerical constant in Proudman's equation
β	Porosity of the perforated plate
Δk	Spacing for the discretization of the energy spectrum
Δk_n	Dimension of the n-th interval of the energy spectrum
Δp	Pressure drop at the size of a device
γ	Specific heat ratio
ϵ	Energy dissipation rate
λ	Wavelength of a harmonic
ν	Kinematic viscosity
Φ	Potential for the source term $\mathbf{S_u}$
ϕ	Phase of a harmonic
Π	Natural logarithm of the pressure in Lilley equation
ρ	Density
ρ_0	Density of the fluid at the receiver
$\bar{\rho}$	Averaged density
ρ'	Density fluctuation
ρ_t	Density turbulent fluctuation
ρ_a	Density acoustic fluctuation
ρ_1	Inlet density

ρ_2	Outlet density
$\boldsymbol{\sigma}_n$	Direction of the n-th Fourier mode in SNGR
$\boldsymbol{\tau}$	Viscous stress tensor
$\tau_{i,j}$	Components of the viscous stress tensor (i,j=1,2,3)
ψ_n	Phase of the n-th Fourier mode in SNGR
$\boldsymbol{\omega}$	Vorticity field
$\overline{\boldsymbol{\omega}}$	Mean vorticity field
ω	Pulsation of a harmonic
ω_n	Pulsation of the n-th Fourier mode in SNGR
ω_x	Axial component of the vorticity $\boldsymbol{\omega}$
ω_y	Transversal component of the vorticity field $\boldsymbol{\omega}$
A	Amplitude of a harmonic
A_η	Valve correction factor for acoustical efficiency
A_H	Area of a single flow passage
c	Speed of sound
c_0	Speed of sound at the receiver (in standard conditions)
c_2	Outlet speed of sound
C	Courant number
C_a	Acoustic courant number
c_P	Specific heat at constant pressure
C_V	Flow coefficient
c_V	Specific heat at constant volume
c_{vc}	Speed of sound in the vena contracta
D	Diameter of the pipe
d	Diameter of the perforated plate
d_0	Circular equivalent diameter
d_H	Hydraulic diameter of a single flow passage
D_j	Jet diameter
dt (or Δt)	Temporal spacing
dx (or Δx)	Grid spacing
E	Kinetic energy per unity of volume
e	Internal energy per unity of mass - specific internal energy

$\mathbf{f}$	Force density in momentum equation
f	Frequency of a harmonic
F_d	Valve style modifier
f_i	Force density component (i=1,2,3)
F_L	Liquid pressure recovery factor
f_p	Peak frequency
h	Specific enthalpy
$\mathbf{I}$	Instantaneous acoustic intensity vector
I	Mean sound intensity
I_W	Wetted perimeter of a single flow passage
K (or TKE)	Turbulent kinetic energy
k	Wave number
$\mathbf{k}_n$	Wave vector of the n-th Fourier mode in SNGR
k_e	Wave number with the peak of the fluid-dynamic energy
k_K	Kolmogorov wave number
K_L	Numerical constant in the Lighthill's eighth power law
k_n	Wave number of the n-th Fourier mode in SNGR
M	Mach number
m	Mass source term
M_2	Outlet Mach number
M_t	Turbulent Mach number
M_{vc}	Mach number in the vena contracta
n_0	Number of independent and identical flow passages
$\mathbf{P}$	Opposite of the fluid stress tensor
p_0	Pressure of the fluid at the receiver
p	Pressure
$\bar{p}$	Averaged pressure
p'	Pressure fluctuation
p_t	Pressure turbulent fluctuation
p_a	Pressure acoustic fluctuation
p_1	Inlet pressure
p_2	Outlet pressure
$\mathcal{P}$	Acoustic power density

$P_{i,j}$	Components of the opposite of the fluid stress tensor (i,j=1,2,3)
p_{rsm}	Root Mean Square of the acoustic pressure
p_{vc}	Pressure in the vena contracta
Q_m	Mass flow-rate
$\bar{R}$	Specific gas constant
r	Distance of the receiver from the acoustic source
s	Specific entropy
St_p	Strouhal number for peak frequency
$\mathbf{S_u}$	Source term for the momentum equation in APE
$S_{\mathbf{u}i}$	Component of the source term for the momentum equation in APE
T	Temperature
T	Period of a harmonic
t	Thickness of the perforated plate
T_1	Inlet temperature
T_{vc}	Temperature in the vena contracta
$\mathbf{u}$	Velocity
$\bar{\mathbf{u}}$	Averaged velocity
$\mathbf{u}_t$	Velocity turbulent fluctuation
$\mathbf{u}_a$	Velocity acoustic fluctuation - acoustic particle velocity
U_j	Jet velocity
$\tilde{u}_n$	Amplitude of the n-th Fourier mode in SNGR
u_i	Velocity vector component (i=1,2,3)
$\bar{u}_i$	Component of the averaged velocity vector
u_{ti}	Component of the turbulent velocity vector
u_{ai}	Component of the acoustic particle velocity vector
W_a	Acoustic power of a source
$\widehat{W_a}$	Acoustic power numerically computed
W_D	Acoustic power of a dipole
W_M	Acoustic power of a monopole
W_Q	Acoustic power of a quadrupole
X	Ratio of pressure differential to inlet absolute pressure

$\mathbf{x}$	Position vector
x_i	Components of the position vector (i=1,2,3)
X_{cr}	Ratio of pressure differential to inlet absolute pressure in critical conditions
X_T	Ratio of pressure differential factor in chocked flow condition
Y	Expansion factor

CHAPTER 1

Introduction

The regulation of the flow is a crucial part in any industrial plant that conveys fluids such as gases, liquids, vapours or slurries. For this reason, valves are usually installed along pipelines in order to control hydraulic features as pressure and flow-rate. The functioning of a valve is based on the localized dissipation of the flow energy through the convection of the fluid in one or more passages inside the body of the valve. The dissipated energy is transmitted to the surrounding ambient in form of mechanical energy (valve's and pipe's vibrations), thermal energy (growth of the temperature of the fluid) and acoustic energy (noise). The problems associated to the noise emissions coming from pipes and ducts are indeed a distressing issue in a very wide range of engineering applications that must face problems about the quieting of industrial and civil noise and about the prevention of workers' hearing damages. The sources of the industrial acoustic pollution can be of different types: motors, fans, machineries and solid bodies' oscillations generate the so-called *structure-borne noise*. On the contrary, the term *flow-induced noise* usually refers to the sound generated by fluid-dynamic instabilities inside pipelines close to throttling devices, bends, junctions and

obstructions. This kind of noise is also known as *fluid-dynamic noise* or, when the flowing fluid is a gas as in this work, it is called *aero-dynamic noise*. The fluid-dynamic noise is a common issue for oil refineries and liquid/natural-gas plants because the mere flow of the fluid generates sound due to the turbulence inside the pipelines. In this scenario, the sources of flow-induced noise and vibrations are different and all of them cooperate in the raise of the total intensity of the emitted sound [10].
Figure 1.1 summarises the acoustical behaviour of a pipeline in which some high-speed gas is flowing highlighting all the possible noise generation mechanisms. In a straight pipe, for instance, a fully-developed flow transports turbulence that induces random pressure fluctuations inside the pipe and against the internal walls. Local singularities, as bends or

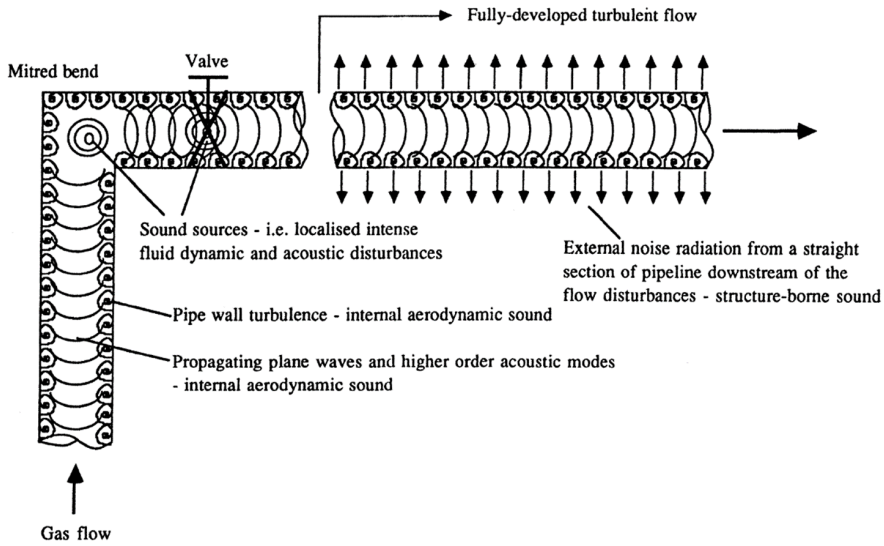

Figure 1.1: *Representation of the most common acoustical sources in ducts with both flow-induced and structure-borne sounds [43]*

valves, generate flow discontinuities that excite the fluid developing turbulent structures that impact against the walls and generate noise which travels along the pipe.

The excitation transmitted by the fluid to the bodies installed along the pipe induces mechanical vibrations that propagate along all the duct but also in the surrounding external ambient. In fact, the external noise is the result of the air excitation transmitted by the pipe's vibrating walls to the free space. The evaluation of the external *Sound Pressure Level*

SPL can be thus considered as an example of structure-borne noise.

On the contrary, inside the pipe, the noise is flow-induced; its possible sources are distributed in several regions of the pipe and are very different in strength. In general, the hierarchy of the acoustical internal sources suggests that the noise developed by the flow disturbance in proximity of discontinuities (valves, bend, etc.) is the most relevant and it dominates on the other flow-induced sources such as the wall turbulence on a straight undisturbed pipe.
Finally, the pipeline's structure and the valve's geometry play a key-role for the generation of the *tonal noise* that is generated when most of the acoustic power is concentrated in few frequencies. Such a noise seldom occurs and only in particular configurations; the noise produced in most of applications has no dominant frequencies and it is thus called *broadband noise*. This is the noise investigated in this work.

The intensity of the noise generated by all these mechanisms can reach harmful levels in critical conditions becoming even a threat for people safety; for this reason, limits on the maximum noise exposure are imposed by laws. Valves' manufacturers thus seek for methods for reducing the emissions of their devices and for knowing in advance their behaviour in different working conditions. During the design of new devices, their acoustical characterization is actually needed in order to provide estimations about the future emissions. In addition to this, valves' manufacturers have to provide to their clients all the fundamental parameters for allowing them to estimate the broadband noise intensity, in the desired operating conditions, according to the international standards.

The traditional approach followed by industries for the acoustical characterization of control devices is based on experimental campaigns because of the quality of the measured data that are representative of the tested phenomena without any modelling assumption. The experimental evaluation of the noise emitted by a control valve is regulated by international standards that are widely described in Chapter 5 and that assume the Sound Pressure Level measured in a specific point (1 meter downstream of the device and 1 meter far from the pipe's external wall) as sufficient quantity for the acoustic characterization of a device. The hardest part of the experimental approach stands in the capability to guarantee the reliability of the measures avoiding external influences such as ambient noises or instruments inefficiency due to dust, humidity and electro-magnetic fields. In addition to that, for most of the appli-

cations, the experimental approach is too expensive in terms of money and time. For instance, the characterization of a control valve requires its realization, a proper plant on which it can be installed and tested, the purchase of all the instrumentations for the measurements and the control on the hydraulic quantities. The costs of the materials and the instruments can be very high; the time for the realization of all the required pieces is too long for a quick answer to urgent requests; a wide space for the installation of a test plant for big devices is needed. The problem becomes even worse when a complete database about all the valves and their operating conditions is desired. All these issues contribute to try to find alternative approaches that return information in shorter time and with less resources available.
These are all the motivations that encouraged this work to be focused on a numerical analysis that results to be a valid alternative whereas other approaches are infeasible.

Indeed, this thesis is focused on the numerical analysis of the fluid-dynamics inside ducts, on the processes at the base of the control devices' noise generation and on its prediction. The latter, in particular, is very challenging because of the complexity of the flow close to a valve. The objective of this work is thus the exploration of different numerical approaches for the prediction of the acoustic emissions of a flow-control device. This means that the same problem is here analysed with different glasses aiming to obtain a comprehension of the noise generation mechanism close to the valve, to a description of the noise along the pipe and to a prediction of the intensity of the noise heard by the workers outside of the pipeline.

Chapter 2 deals with aero-acoustics background exploiting a brief discussion about waves, about the theoretical research developed in literature and about the possible computational approaches to the problem. At the end of this chapter the Acoustic Perturbation Equations are introduced.

In this work two numerical approaches are used for the Sound Pressure Level prediction: the first one is presented in Chapter 3 and it is based on the resolution of the Acoustic Perturbation Equations (APE) system. Its implementation is then discussed focusing on the solving algorithm, on the numerical issues and on its validation with analytical and literature cases.

Chapter 4 deals with the application of the APE to the description

of the acoustic features of an orifice installed inside a pipe. A literature APE wave-operator is tested with different models about the source terms description and about the synthetic generation of the turbulent velocity. The best ones are identified thanks to the comparison of the predicted noise with the one coming from a LES simulation. The physics of noise generation and propagation is then investigated highlighting that the perturbations close to the orifice generate a strong but fast-decaying noise. Since the reference for the acoustic characterization of a device is set by the international standards at 1 meter downstream of the device, the behaviour of the acoustic wave close to the orifice can be neglected in some circumstances. This statement is confirmed by the results obtained solving a new APE formulation which is here proposed. It neglects local effects close to the orifice, but it is anyway capable to return an accurate noise prediction far from it. Its advantage compared to the previous formulation is the 20% lower computational burden.

The second numerical approach investigated in this work is described in Chapter 5 that is about the international standards' procedure for the prediction of the control valves noise. Four valves' characterizing parameters are investigated and numerics is introduced as reliable approach for the prediction of their values. The focus is then concentrated to the valve correction factor for acoustical efficiency A_η that is involved in the description of the amount of energy converted from mechanical into acoustical. Its values suggested by the IEC international standard do not take into consideration its dependency on the flow conditions introducing relevant errors that are here highlighted thanks to previous experimental campaigns' data. An orifice described by the international standards is used as case on which the numerical models are applied for the estimation of A_η. Its dependency on the flow velocity is thus obtained and justified by theoretical discussion.

Chapter 6 is about the design of an experimental plant on which all the numerical models will be analysed thanks to a comparison with experimental data. The test campaign will be focused on the study of the influence of the pressure drop and the absolute pressure on the noise generation for different devices. It has been designed in accordance with the international standards' requests.

Conclusions and the future works are resumed in the Chapter 7.

CHAPTER 2

Literature Background

A complete description of the flow-induced noise inside pipes is an extremely challenging purpose. Several and different phenomena are in fact involved and they are about the sound generation mechanisms, the propagation of the acoustic wave and its interaction with solid bodies or with the mean flow. The merely classification of the noise in pipelines is complex. A possible distinction on the nature of the acoustic sources defines the following terms:

1. *structure-borne sound* is generated by the vibration of solid bodies that perturb the surrounding fluid. The noise heard outside of a pipe, for instance, is transported by an acoustic wave generated by the vibrations of pipe's external walls that excite the surrounding air.

2. *fluid-dynamic sound* is generated by vibrations produced by turbulence, local disturbances or unsteady flows within the fluid. Pipes' walls vibrations are induced by the impacting pressure and density fluctuations generated by the flow. When, as in this work, the fluid inside ducts is a gas we talk about *aero-dynamic noise*.

The main difference between the two kinds of noise is about the acoustic source and its location respect to the fluid in which the sound is propagated: the structure-born noise is generated by a solid (source external to the fluid), while the fluid-dynamic one is generated by disturbances inside the fluid (aero-dynamic sound sources are always contained within the fluid itself). In addition to this, inside a pipe the noise generation is strongly affected by the fluid-dynamic and different mechanisms generate sound: vibrations can be induced for instance by time-varying flow-rate (and mass), by unsteady forces from solid bodies and by turbulence [43].

In this chapter, a brief discussion on the fundamental features of acoustic and its sources is presented. The main contributes to theoretical and numerical analysis are then summarized before moving into the description of all the theories and models that can be applied for the numerical approach. They are presented with increasing complexity and with an always wider range of applicability till reaching the Acoustic Perturbation Equations that take into account all the contributes necessary for a good description of the aero-dynamic noise generated by control devices in pipelines.

2.1 Fundamentals of Acoustics

The term *noise* usually refers to an unpleasant sound that can be heard by the human ear. From a physical point of view, a sound is a pressure wave that propagates through an elastic medium inducing vibrations and particles' oscillation that transfer their motional energy. The simplest kind of noise is represented by the harmonic wave

$$x(t) = A \sin\left(2\pi f t + \phi\right). \tag{2.1}$$

An harmonic wave is defined by one and only value of its characteristic quantities:

- the speed c indicates the velocity at which the wave propagates respect to the medium;
- the amplitude A defines the intensity of the oscillation associated to the wave (intensity of the noise);
- the period T indicates how long the wave takes to repeat the same oscillation;

- the frequency f indicates how many times in a time unity a particle repeats the same oscillation. It is the reciprocal of the period T i.e. $f = 1/T$;
- the wavelength λ indicates the distance covered by a particle in one period. It satisfies the relationship $\lambda = cT = c/f$;
- the phase ϕ indicates the shift of the wave respect to the axis used for its analytical description (2.1).

A noise is usually made of several superimposed harmonics characterized by different frequencies, amplitude and phases. The contribute of each frequency to the total noise is analysed in the frequency space through its spectrum. According to its shape, it is possible to talk about white noise (constant power for all the frequencies) and pink noise (decreasing power at high frequencies) while the presence of any peak is the disclaimer between *tonal* and *broadband* noise. The former has a spectrum characterized by one or more peaks in correspondence of single frequencies. Harmonics that are propagated at those frequencies contains most of the total acoustic energy. It occurs in few and particular configurations, unlike the broadband one that is characterized by a spectrum without any dominant frequency with acoustic energy distributed in a wide range of frequencies. This is the noise whose prediction is discussed in this work.

In the evaluation of the noise intensity heard by humans, two main aspects have to be considerd. The first is that our perception of noise intensity is not linear, but it follows a logarithmic scale. For this reason, the Sound Pressure Level (quantity that measures the noise intensity) is defined as

$$\mathrm{SPL} = 20 \log_{10} \left(\frac{p_{rms}}{p_{ref}} \right), \tag{2.2}$$

where p_{rms} is the root mean squared of the acoustic pressure and p_{ref} is the reference pressure defined as the lowest pressure our ear can perceive ($p_{ref} = 2 \cdot 10^{-5}$ Pa). The SPL is measured in decibels dB.
A further particularity of human hearing system is that it cannot perceive all the frequencies, but only a limited range that goes about from 20 Hz to 20 kHz (lower frequency noises are called infrasounds, while ultrasounds propagate at frequencies higher than 20 kHz).
In addition to this, not all the frequencies in this range are heard with

the same sensitivity. Empirical band corrections are introduced to modify the noise intensity in dB taking into account the gain for each band. Therefore, we talk about dB(A) or dB(C) where the letter A and C stand for different corrections [6]. These unit of measurements are the one used by the laws for the definition of constrains: workers must not be exposed to noises more intense than 140 dB(C) and cannot work for extended periods (8 hours) with a SPL higher than 87 dB(A).

2.2 Elementary Acoustic Sources

The possible acoustic sources in the industrial applications are several and of different nature. The noise radiated by most of them, anyway, can be modelled as the one emitted by elementary sources or by a combination of them. For this reason, in this section a brief description of monopoles, dipoles and quadrupoles is discussed focusing on their features and on the intensity of the emitted noise. A visualization of the pattern of the radiated noise emitted by those three sources is given in section 3.2.
All the acoustic sources differ among them by the physical process that emits the noise, by their shape, by the noise directivity, by the modelling equations for the description of their features and by their intensity. For the latter purpose, two quantities will be introduced and they are the acoustic power W_a and the instantaneous sound intensity $\mathbf{I}$.

2.2.1 Monopole

A monopole is the simplest acoustic source and is modelled as a spherical source that, through its pulsation, produces a spherical wave radiated in the surrounding free-space. The noise is produced by the movement of the monopole's surface or through the variation of mass inside the source region.
In engineering applications, a certain type of machineries (motors and pumps) can be modelled as a monopoles, while in the aerodynamic noise such a behaviour is assumed by unsteady combustion phenomena, unsteady pulsating flows and cavitation.
The analytical description of the strength of the source make use of two fundamental quantities that are its acoustic power W_a and the instantaneous sound intensity $\mathbf{I}$. The latter is the power per unit area and its value in a point in the space is defined as the product of the acoustic pressure

and the acoustic particle velocity in that point

$$\mathbf{I} = p'\mathbf{u}'. \tag{2.3}$$

The acoustic intensity $\mathbf{I}$ is a time-dependent quantity because of the unsteady nature of the acoustic phenomenon. In the theoretical treatment it is usually preferred to exploit the discussion using a steady variable, the mean sound intensity I, defined as the time-average of the instantaneous sound intensity $\mathbf{I}$. Since the monopole creates a spherical wave, the spatial dependency of the sound intensity I is related only to the distance of the evaluation point from the source (distance r between the source and the receiver), i.e. $I = I(r)$.
The acoustic power W_a, on the contrary, is not dependent on the distance of the receiver. The evaluation of W_a is made through the integral of all the contributes of the sound intensity $\mathbf{I}$ on a generic surface that contains the acoustic source; for sake of simplicity the surface is usually chosen as a sphere (with the monopole placed in its centre) so that the intensity $I(r)$ is constant on the surface

$$W_a = \int_S I(r)\ \mathrm{dS} = 4\pi r^2 I(r). \tag{2.4}$$

The root mean square of the acoustic pressure p_{rms} can be described as function of the mean sound intensity too

$$p_{\mathrm{rms}}^2 = I(r)\rho_0 c, \tag{2.5}$$

allowing to rewrite the acoustic power (2.4) as

$$W_a = \frac{4\pi r^2 p_{\mathrm{rms}}^2}{\rho_0 c}. \tag{2.6}$$

Equations (2.4) and (2.6) suggest that the sound intensity emitted by a monopole decays with the square of the radius, while the acoustic pressure with its first power.

2.2.2 Dipole

A dipole is an acoustical source that is composed by two monopoles closed to each other that pulsate with the same strength and a phase-shift of 180°. The out-of-phase oscillation induces the formation of a nett fluctuating force that acts along the axis that separates the two monopoles. The resulting pressure radiation is a function of the radius r

and of the polar angle θ.
In industrial application a monopole placed close to a rigid reflecting body works as a dipole since, far from the source, its emission can be seen as the superimposition of two waves, i.e. the direct wave and the reflected one (phase-shifted).
The theoretical analysis of dipole intensity and power is simplified by the assumption of working in the far-field, i.e. far enough from the source to justify the assumption to consider the dipole as a point. In this case the mean sound intensity of a dipole can be described as the one of a monopole multiplied for a directivity factor $2kd\cos\theta$ that takes into account the polar angle contributes. The quantity k is the wave number of the considered frequencies $k = 2\pi/\lambda$ while $2d$ is the distance between the two monopoles. The relevancy of their contribute is clear when the acoustic power of a dipole is compared with the monopole's one: it is shown that [43]

$$\frac{W_D}{W_M} \sim \left(\frac{d}{\lambda}\right)^2 \tag{2.7}$$

where W_D and W_M are the acoustic power of dipole and monopole.
Since all the equations are derived under the assumption of $kd \ll 1$ it is clear[1] that the sound power radiated by a dipole is always much lower than the one radiated by a monopole. The ratio becomes smaller as the wavelength λ increases, that means that the monopole is much more efficient than a dipole especially at low frequencies.

2.2.3 Quadrupole

As the dipole is defined through the combination of two monopoles oscillating out of phase, a quadrupole is defined as that acoustic source made of two dipoles close to each other and oscillating with a 180° phase-shift. As a dipole has one axis, the quadrupole has two. The physical mechanism through which a quadrupole excites the surrounding fluid is based on the fluctuating stresses that are applied to the medium (monopoles work with oscillation or mass variation, dipoles with fluctuating forces along the axis). An example of these stresses can be found in gas flows where the viscous stresses within the gas act as quadrupoles.
Two kind of quadrupole (lateral and longitudinal) can be obtained according to the disposition of the dipoles but in both cases their acoustic

[1] $kd = 2\pi d/\lambda \ll 1$

power can be compared to the one emitted by a monopole and the following relationship stands

$$\frac{W_Q}{W_M} \sim \left(\frac{d}{\lambda}\right)^4 \tag{2.8}$$

where now W_Q is the acoustic power of the quadrupole. This means that the power radiated by a monopole is greater than the one emitted by a quadrupole and, comparing (2.8) and (2.7) it can be found that the quadrupole is the least intense among the sources since it is even less intense than the dipole.

2.3 Aero-Acoustics Background

The elementary sources presented in the previous section are a modelling description of most of the possible acoustic emitters that can be found. This work deals with aero-acoustic, i.e. a branch of the acoustic that focuses on the noise generated by the motion of a gas. This science was born in the 1952 with the first aero-acoustical theory that had been developed by Lighthill [35] for unbounded fluctuating flows in a uniform medium. After that, several other studies have been conducted with some improvements and generalizations proposed by Curle [15] in 1955 including the effect of fixed solid boundaries, by Powell [46] and Howe [25] respectively in 1960 and 1975 splitting the effects of the vorticity and of the mean flow on the acoustic wave and by Ffowcs Williams-Hawkings [22] in 1969 extending Curle's investigation to moving bodies.

All these theoretical formulations, anyway, have been derived under strong assumptions that are not satisfied in most of the engineering applications. In these situations, the numerical approach helps to describe those phenomena that are too complex to be analytically described by an aeroacoustic theory. Modelling assumptions are anyway required in the numerics too and an exhaustive description may be obtained only with very expensive simulations from the computational point of view. Anyway, in most of the engineering applications, the maximum accuracy is not required since people are interested in few aspects of the whole phenomenon. A smart choice of the numerical model according to the information of interest helps to save computational time and resources.

All the numerical approaches that deals with aero-acoustics are studied by the *Computational Aero-Acoustics* (CAA) that is defined as that sci-

ence that deals with the numerical description of the aerodynamic noise, with its generation mechanisms, propagation and even prediction. The complexity of the execution of a detailed numerical simulation that returns a complete description of both the fluid-dynamic and the acoustics is too high for any engineering application. Such a computation, in fact should take care of all the numerical issues of both the CFD and the CAA. Their differences are so wide (as can be seen in table 2.1) that their proper treatment requires resources usually not available in the industrial world. Let's assume for instance to be interested in the fluid-dynamic characterization of a valve through which a gas flows at low Mach number. Such a characterization can be done with a steady simulation, on a domain that exploit any possible symmetry of the geometry, neglecting compressibility effects and with turbulence models that describe the small-scales effects. But when a noise prediction on the same valve is desired, its accurate numerical description must be completely different as the noise propagation is an unsteady phenomenon whose computation must take care of the solid walls that reflect the wave, the compressibility effects and all the frequencies the acoustic wave is made of. But, if

	Computational Fluid-dynamics	**Computational Acoustics**
Time dependency	steady/unsteady	unsteady
Frequency range	driven by turbulence	audible
Domain	source region	far-field
Compressibility	according to Mach number	necessary
Numerical schemes	-	low dispersion and diffusion

Table 2.1: *Differences about the technical and physical aspects to be cared of during numerical simulation of fluid-dynamics and acoustics.*

not interested in a description of all the acoustic features, some of the technical constraints mentioned in table 2.1 can be relaxed simplifying the numerical resolution of the acoustic simulations.

In fact, different CAA approaches have been proposed in literature [13, 53]. They are classified in

- **Direct methods** compute both the unsteady flow and the acoustic field thereby generated during the same simulation [53]. Navier-Stokes equations are a suitable tool for managing both the processes since they describe both the fluid-dynamic variation and the acoustic vibrations. Their numerical resolution is performed thanks to DNS (Direct Numerical Simulation) or to LES (Large Eddy Simulation). The former aims to a detailed description of the phe-

nomenon from the largest scales to the Kolmogorov scale, while the latter introduces models for the description of the turbulence dynamic of the small scales reducing the computational burden of the simulation.
The issues to be faced by a direct simulation regard the techniques for simulating both the noise generation connected to the fluid-dynamic and its propagation in the far-field. The disparity between the two phenomena requires the application of models and numerical techniques that are able to describe, on turn, the most critical one in any region. For instance, a detailed description of fluid-mechanics is usually achieved with a steady, incompressible simulation on a fine grid around the source. On the other side, the acoustic requires a wider domain for the evaluation of the noise far from the source and an unsteady compressible simulation: these differences forces to 'waste' resources to describe the fluid-mechanics even where not needed. Furthermore, the acoustic propagation in the audible frequency range may be conduced on a coarser mesh in the source region than the one needed for the flow simulation. All these differences are summarized in the table 2.1 that highlights how the two phenomena require different numerical techniques and models for their evaluation [40, 51].

- **Hybrid methods** solve the acoustic problem after the fluid-dynamic one, in two separated steps. The problem is in fact decomposed in noise generation and noise propagation following two different numerical methods. A CFD simulation is first run in order to evaluate the flow-field responsible for the generation of noise around the source region in the near-field. Once the noise production is described, its propagation is managed by an acoustic model that can be based on the resolution of PDEs or acoustic analogies.
  Hybrid approaches are usually appreciated for those simulations where the evaluation of the noise is made too far from the noise to be computed with a direct approach.
  The CFD simulation can be carried out at different accuracies with DNS, LES, RANS (Reynolds Averaged Navier-Stokes) or combined approaches as DES (Detached Eddy Simulation). It is anyway important that they describe the noise generation mechanisms in order to return all the data needed for the noise propagation. In industrial applications the most demanding methods as DNS or LES are usually infeasible and alternative methods for the noise

generation have been developed based on the synthetic generation of noise from the RANS output.
On the other hand, the complexity of the acoustic model depends on the physics of the noise propagation and on its interaction with the flow and with solid bodies. The acoustic analogies describe the noise very far from the source where it can be modelled as compact (2.4). Wave equations as the APE *Acoustic Perturbation Equations* describe the local effects of noise and are a tool for the description of the noise propagation in a more general flow condition. Their application will be discussed in details in section 2.5

2.4 Acoustic Analogies

The term *acoustic analogy* refers to a method for the description of the acoustic propagation through an equation whose left-hand side is a wave operator while its right-hand side contains other terms that are treated as an acoustically equivalent source term. The concept of analogy can be actually referred to any field of study when its fundamental equation is written with an equivalent source term. In acoustics, the physics of the propagation of a wave in a uniform stagnant fluid is described by the wave equation

$$\frac{\partial^2 \rho'}{\partial t^2} - c_0^2 \nabla^2 \rho' = 0, \tag{2.9}$$

where ρ' indicates the density fluctuations and c_0 is the speed of sound in standard conditions. For an isentropic flow $c_0^2 = \partial p / \partial \rho$ that, for a stagnant fluid, means

$$c_0^2 = \frac{p'}{\rho'}. \tag{2.10}$$

The solution $\rho'(\mathbf{x}, t)$ of equation (2.9) returns the value of the density fluctuations in space and time. In a uniform stagnant fluid, the receiver (point in which the noise is calculated) is characterized by a pressure p_0, a density ρ_0 and a speed of sound c_0 that are equal in any place of the space at any time [9]. Any departure from these conditions (non-uniform medium) introduces new terms in equation (2.9). It is possible to talk about *acoustic analogy* when all these new terms are collected in the right-hand side and, for the receiver, are considered as an equivalent acoustic source that emits noise in a uniform fluid.

2.4.1 Lighthill Analogy

The first, most famous acoustic analogy was derived by Lighthill [35] for the description of the density fluctuations in a uniform stagnant medium. The derivation of the analogy starts from the non-homogeneous mass and momentum conservation laws

$$\begin{cases} \dfrac{\partial \rho}{\partial t} + \dfrac{\partial \rho u_i}{\partial x_i} = m & \text{(2.11a)} \\ \dfrac{\partial (\rho u_i)}{\partial t} + \dfrac{\partial (P_{ji} + \rho u_j u_i)}{\partial x_j} = f_i + m u_i & \text{(2.11b)} \end{cases}$$

where m is the mass injection per unit of time, $\mathbf{f}$ the force density and $\mathbf{P} = p\mathbf{I} - \boldsymbol{\tau}$ the opposite of the fluid stress tensor[2].

When no mass injection nor external forces are applied (no monopole m nor dipole $\mathbf{f}$), the system (2.11) can be simplified and, taking the time derivative of (2.11a) and the divergence of (2.11b), rewritten as a second order partial differential equation

$$\frac{\partial^2 \rho'}{\partial t^2} - c_0^2 \frac{\partial^2 \rho'}{\partial x_i^2} = \frac{\partial^2 T_{ij}}{\partial x_i x_j}, \tag{2.13}$$

where $T_{i,j}$ is the Lighthill's stress tensor defined as

$$T_{ij} = \rho u_i u_j - \tau_{ij} + \left(p' - c_0^2 \rho'\right) \delta_{ij}. \tag{2.14}$$

Unlike equation (2.9) which is derived neglecting second order fluctuations, equation (2.13) is an exact equation as no approximations are introduced and all the non-linear terms are collected in the source term. Lighthill's stress tensor works as equivalent source term and its formulation (2.14) helps to distinguish three fundamental mechanisms at the base of the aero-dynamic noise generation:

- the Reynolds stress tensor $\rho u_i u_j$ that collects the non-linear terms (the velocities in a stagnant fluid are just the acoustic fluctuations) and describes the noise generation due to turbulence;

[2]The same system, written with the vectorial notation is

$$\begin{cases} \dfrac{\partial \rho}{\partial t} + \nabla \cdot (\rho\, \mathbf{u}) = m & \text{(2.12a)} \\ \dfrac{\partial (\rho\, \mathbf{u})}{\partial t} + \nabla \cdot (\mathbf{P} + \rho\, \mathbf{u}\, \mathbf{u}) = \mathbf{f} + m\, \mathbf{u} & \text{(2.12b)} \end{cases}$$

- the viscous forces τ_{ij} that are usually very small compared to Reynolds stresses;
- the deviation from an isentropic behaviour where equation (2.10) is valid and $p' - c_0^2\rho'$ is equal to zero. An alternative interpretation of this Lighthill's stress tensor's term is the deviation of the speed of sound c from the reference one c_0 valid only at the listener's position. For low Mach numbers all these effects are very low and their contribute is order of magnitude lower than the Reynolds stresses.

For low Mach numbers the Lighthill's stress tensor can be thus approximated with the only contribute coming from the Reynolds stresses $T_{ij} \sim \rho u_i u_j$.

Lighthill's equation can also be rewritten in terms of pressure fluctuations $p' = c_0^2\rho'$ as

$$\frac{1}{c_0^2}\frac{\partial^2 p'}{\partial t^2} - \nabla^2 p' = \frac{\partial^2 T_{ij}}{\partial x_i x_j}, \tag{2.15}$$

and its analytical solution [23] is made of a volume integral over the source region

$$p(\mathbf{x}, t) = \int_V \frac{\dfrac{\partial^2 T_{ij}}{\partial x_i x_j}\left(\mathbf{y}, t - \dfrac{|\mathbf{x}-\mathbf{y}|}{c}\right)}{4\pi|\mathbf{x}-\mathbf{y}|}\,\mathrm{d}^3\mathbf{y}, \tag{2.16}$$

where V represents the source region volume. Few considerations must be done:

- the vector $\mathbf{y}$ represents the position inside the source region (volume V);
- the vector $\mathbf{x}$ represents the position of the receiver, external to the sound region;
- inside the source region different elementary monopole sources are present[3], each of them characterized by an intensity equal to $\frac{\partial^2 T_{ij}}{\partial x_i x_j}$;
- each elementary monopole is characterized by a different intensity and phase;

[3]From a mathematical point of the pressure field generate by a monopole is described by an integral, a dipole produces a pressure described by the divergence of an integral and a quadrupole by the double divergence of an integral.

- the difference of the phases is taken into account with the retardation time $t - \frac{|\mathbf{x}-\mathbf{y}|}{c}$;
- if the source is assumed compact, small phase differences can be neglected (and so the retardation times);
- if the source is assumed compact, $\mathbf{x}$ must be far enough from the source region and its distance from a point in the source region can be approximated with its own position $r = |\mathbf{x} - \mathbf{y}| \approx \mathbf{x}$.

The assumption of compactness of the source region is crucial for a formal simplification of the equation (2.16) that can be rewritten as

$$p(\mathbf{x}, t) = \frac{\partial^2}{\partial x_i x_j} \int_V \frac{T_{ij}\left(\mathbf{y}, t - \dfrac{r}{c}\right)}{4\pi r} \, \mathrm{d}^3\mathbf{y}. \tag{2.17}$$

The differential operator $\frac{\partial^2}{\partial x_i x_j}$ can be moved outside of the integral thanks to mathematical procedures [23]. This operation highlights the nature of the acoustic source related to the Lighthill's stress tensor that is made of a **quadrupole**, while in equation (2.16) the source is described as a series of different monopoles.
It must be noted that, if the retardation times are neglected because of the source compactness assumption, the differential operator must be moved outside of the integral because, otherwise, the summation of the different in-phase monopoles contributions would reduce to zero and there would be no sound produced.

2.4.2 Ffowcs Williams - Hawkings Analogy

Solutions (2.16) and (2.17) describe the value of the acoustic pressure in space and time due only to the flow fluctuations described by Lighthill's stress tensor. Anyway, other sources of noise can be present and the most relevant improvements to Lighthill analogy have been derived for the extension of the analogy to the prediction of the acoustic pressure in a uniform flow with oscillating solid bodies [15, 22]. The presence of a fluctuating body introduces two additional sources of noise, i.e. a dipole due to the presence of a body immersed in the flow that is therefore excited by fluctuating forces and a monopole due to the oscillating motion of the body itself. In this situation the acoustic pressure fluctuations are

described as [22]

$$p(\mathbf{x},t) = \frac{\partial^2}{\partial x_i x_j}\int_V \frac{T_{ij}\left(\mathbf{y}, t - \dfrac{|\mathbf{x}-\mathbf{y}|}{c}\right)}{4\pi|\mathbf{x}-\mathbf{y}|}\,\mathrm{d}^3\mathbf{y} + \\ -\frac{\partial}{\partial x_i}\int_S \frac{f_i\left(\mathbf{y}, t - \dfrac{|\mathbf{x}-\mathbf{y}|}{c}\right)}{4\pi|\mathbf{x}-\mathbf{y}|}\,\mathrm{d}S(\mathbf{y}) + \frac{\partial}{\partial t}\int_S \frac{\rho\mathbf{v}\left(\mathbf{y}, t - \dfrac{|\mathbf{x}-\mathbf{y}|}{c}\right)\cdot\mathbf{n}}{4\pi|\mathbf{x}-\mathbf{y}|}\,\mathrm{d}S(\mathbf{y}) \tag{2.18}$$

where S is the surface that encloses the volume V, $\mathbf{v}$ is the velocity at which the body's surface is moving and $\mathbf{n}$ the normal to that surface. The dipole contribute is described by the second integral on the right-hand side, while the monopole due to the oscillating body is connected to the last surface integral.

2.4.3 Lilley Analogy

Further efforts in the development of the Lighthill's analogy have been done by Philips [45] and Lilley [37] in order to take into account the effect of a mean sheared flow on the acoustic propagation. Noise spectrum and waves directivity are influenced by the characteristics of the flow in which they are propagating and its effect can be relevant in the evaluation of the noise intensity far from the source.
Phillips and Lilley modified the classical wave operator (equation (2.15)left-hand side) including convective terms in the total time derivative $\frac{D(\cdot)}{Dt}$ where

$$\frac{D(\cdot)}{Dt} = \frac{\partial(\cdot)}{\partial t} + \mathbf{u}\cdot\nabla(\cdot). \tag{2.19}$$

The final equation developed by Lilley is written for the variable $\Pi = \ln(p)$ in the form of a third-order equation

$$\frac{D}{Dt}\left\{\frac{D^2\Pi}{Dt^2} - \frac{\partial}{\partial x_i}\left(c^2\frac{\partial\Pi}{\partial x_i}\right)\right\} + 2\frac{\partial u_i}{\partial x_j}\frac{\partial}{\partial x_i}\left(c^2\frac{\partial\Pi}{\partial x_i}\right) = \\ -2\gamma\frac{\partial u_i}{\partial x_j}\frac{\partial u_j}{\partial x_k}\frac{\partial u_k}{\partial x_j} + \Psi, \tag{2.20}$$

where Ψ contains other terms connected to entropy fluctuation and viscous effects (usually negligible).

Respect to the previous analogies described in sections 2.4.1 and 2.4.2, no analytical solution is available since the free-space Green function is not known for Lilley's equation [3]. Moreover, the numerical resolution of this equation results to be complicated. For this reason, when the acoustic propagation occurs in a non-uniform sheared flow it is convenient to solve the problem with different numerical approaches. One of the possible choice is the resolution of the Acoustic Perturbation Equations (APE) described in the following section.

2.5 Acoustic Perturbation Equations

When the acoustic wave propagates in a non-uniform sheared flow the evaluation of the noise through an acoustic analogy becomes more complicated since no analytical solution can be derived. In addition to this, the complexity of the phenomenon increases so much that the fundamental equations from which the analogies' wave operator are derived needs to be modified. The conservation equations of mass, momentum and energy for an inviscid fluid are described by the Euler equations

$$\begin{cases} \dfrac{\partial \rho}{\partial t} + \dfrac{\partial \rho u_j}{\partial x_j} = 0 & \text{(2.21a)} \\ \dfrac{\partial \rho u_i}{\partial t} + \dfrac{\partial \rho u_j u_i}{\partial x_j} + \dfrac{\partial p}{\partial x_i} = 0 & \text{(2.21b)} \\ \dfrac{\partial \left(e + \frac{1}{2}u_i^2\right)}{\partial t} + u_j \dfrac{\partial \left(e + \frac{1}{2}u_i^2\right)}{\partial x_j} + \dfrac{\partial p u_j}{\partial x_j} = 0 & \text{(2.21c)} \end{cases}$$

where e is the specific internal energy and $\frac{1}{2}u_i^2$ is the kinetic energy per unit of mass. The system (2.21) describes the dynamics of the fluid including both the flow and the acoustic wave.
As mentioned in section 2.3, APE belong to the hybrid methods and are a system of equations that describes the generation and propagation of the noise generated by a flow field previously computed with a CFD simulation. The derivation of the APE system can be exploited in different ways [5, 16], but the most common approach is based on the description of the flow as a superposition of a mean part plus a fluctuating one which contains both the turbulent effects and the acoustic disturbances. This means that all the variables appearing in the Euler equations can be decomposed in different contributes connected to the fluid-dynamics and to the acoustics. The most common decomposition is therefore the

one based on the superimposition of a mean part, a turbulent fluctuation and an acoustic fluctuation [5, 41]. The quantities in the Euler equations are decomposed as:

$$\mathbf{u} = \overline{\mathbf{u}} + \mathbf{u}_t + \mathbf{u}_a \tag{2.22a}$$

$$\rho = \overline{\rho} + \rho_t + \rho_a \tag{2.22b}$$

$$p = \overline{p} + p_t + p_a \ . \tag{2.22c}$$

The acoustic energy produced by the flow is usually a very small fraction of the mechanical energy of the mean fluid (the ratio between the energies varies from 10^{-2} to 10^{-5}). For this reason the fluctuations (turbulent and acoustic) are orders of magnitude lower than the mean part and, furthermore, the acoustic fluctuations are even smaller than the turbulent ones. Therefore, the following relationships are valid:

$$\overline{\mathbf{u}} \gg \mathbf{u}_t \gg \mathbf{u}_a \tag{2.23a}$$

$$\overline{\rho} \gg \rho_t \gg \rho_a \tag{2.23b}$$

$$\overline{p} \gg p_t \gg p_a \ . \tag{2.23c}$$

The procedure for the derivation of the Acoustic Perturbation Equation is described in Appendix A. It is based on the decomposition of the flow (2.22) and on the assumption of consider negligible the second order acoustical fluctuations. This means that all the terms containing a product of an acoustic fluctuation (or its derivative) with another fluctuation (acoustic or even turbulent) are removed from the final equations. The resulting system is written as (see Appendix A)

$$\begin{cases} \dfrac{\partial p_a}{\partial t} + \overline{u}_j \dfrac{\partial p_a}{\partial x_j} + \gamma \left(\overline{p} \dfrac{\partial u_{aj}}{\partial x_j} + p_a \dfrac{\partial \overline{u}_j}{\partial x_j} \right) + u_{aj} \dfrac{\partial \overline{p}}{\partial x_j} = S_p & \text{(2.24a)} \\ \dfrac{\partial u_{ai}}{\partial t} + \overline{u}_j \dfrac{\partial u_{ai}}{\partial x_j} + u_{aj} \dfrac{\partial \overline{u}_i}{\partial x_j} + \dfrac{1}{\overline{\rho}} \dfrac{\partial p_a}{\partial x_i} - \dfrac{p_a}{\overline{\rho}^2 c^2} \dfrac{\partial \overline{p}}{\partial x_i} = S_{\mathbf{u}i}. & \text{(2.24b)} \end{cases}$$

The first equation (2.24a) describes the evolution of the acoustic pressure p_a during the propagation of the noise. It is influenced by the mean quantities (pressure, velocity and their derivatives) and is coupled with the acoustic particle velocity $\mathbf{u}_a$ whose evolution is described in (2.24b).

In the left-hand side of the APE system (2.24) the mean-flow influences the dynamics of p_a and $\mathbf{u}_a$ without participating in the noise production. All the terms that are connected to the noise generation are collected in the right-hand side. Following the described procedure for

the derivation of the APE system (2.24), the source terms look like

$$S_p = -\frac{\partial p_t}{\partial t} - \overline{u_i}\frac{\partial p_t}{\partial x_i} - u_{ti}\frac{\partial \overline{p}}{\partial x_i} \tag{2.25}$$

$$S_{\mathbf{u}i} = -\frac{\partial u_{ti}}{\partial t} - \frac{1}{\overline{\rho}}\frac{\partial p_t}{\partial x_i} - u_{tj}\frac{\partial \overline{u}_i}{\partial x_j} - \overline{u}_j\frac{\partial u_{ti}}{\partial x_j} - u_{tj}\frac{\partial u_{ti}}{\partial x_j} + \overline{u_{tj}\frac{\partial u_{ti}}{\partial x_j}}. \tag{2.26}$$

The most relevant terms in the noise generation are, according to order of magnitude analysis, the ones in the source term $\mathbf{S_m}$ for the acoustic particle velocity. For this reason, the source term S_p is usually neglected and considered equal to zero [5]. The analysis of the terms in equation (2.26), on the contrary, is more complex and different literature analysis proposed different formulations [3,5,16,41]. No evidence about the best choice for the description of the noise generation inside pipelines has been found and for this reason a deeper investigation of the source term $\mathbf{S_m}$ is further discussed in section 3.3.

2.5.1 APE Modelling

The left-hand side of the APE system (2.24) is a wave operator that describes the propagation of an acoustic wave in an inviscid medium with not constant nor uniform velocity and pressure fields, i.e. a non-uniform flow. This flow represents the most general (and common) framework inside of which an acoustic wave can travel.
All the terms of the system (2.24) describe a particular interaction of the acoustic wave with the flow field and no simplified formulation can be proposed that guarantees a complete modelling of the noise propagation in a non-uniform flow.. In this section, the physical meaning of the terms is analysed showing how the APE system can be modified according to the complexity of the flow in which the wave propagates. A resume of these flow conditions and how the noise propagation can be modelled is contained in table 2.2.

The simplest flow in which the acoustic wave can be propagated is the **quiet flow**, i.e. that condition characterized by a medium at rest (null velocity) with a constant pressure. This is also the classical frame used for the theoretical derivation of the wave equation

$$\frac{\partial^2 p_a}{\partial t^2} - c_0^2\frac{\partial^2 p_a}{\partial x_i^2} = 0. \tag{2.27}$$

On the other hand, several terms contained in the left-hand side of the APE (2.24) are identically equal to zero because of the particular flow

Flow	APE formulation	Equivalent wave equation
Quiet	Eq.(2.28)	Eq.(2.27)
Uniform velocity	Eq.(2.29)	Eq.(2.30)
$\nabla p \neq 0$ Uniform velocity	Eq.(2.31)	Eq.(2.32)
Non uniform	Eq.(2.24)	N-A

Table 2.2: *Modelling for the noise propagation in different flow conditions with APE and wave equation.*

conditions. The system is thus reduced to

$$\begin{cases} \dfrac{\partial p_a}{\partial t} + \gamma \overline{p} \dfrac{\partial u_{aj}}{\partial x_j} = 0 & \text{(2.28a)} \\ \dfrac{\partial u_{ai}}{\partial t} + \dfrac{1}{\overline{\rho}} \dfrac{\partial p_a}{\partial x_i} = 0. & \text{(2.28b)} \end{cases}$$

With the introduced simplifications, the variables p_a and $\mathbf{u}_a$ are decoupled and the system is equivalent to the a second order partial differential equation that is exactly the classical wave equation for the acoustic pressure (2.27).
The four terms in the system (2.28) are thus the ones that describe the wave propagation at its speed, neglecting the interaction with the flow.

If the medium is in motion with a **mean uniform velocity** $\overline{\mathbf{u}}$ (and constant pressure) the velocity of the propagation of the acoustic wave is influenced by this flow. Respect to the previous system, two more terms containing the mean flow are introduced in the APE system that now looks like

$$\begin{cases} \dfrac{\partial p_a}{\partial t} + \gamma \overline{p} \dfrac{\partial u_{aj}}{\partial x_j} + \overline{u}_j \dfrac{\partial p_a}{\partial x_j} = 0 & \text{(2.29a)} \\ \dfrac{\partial u_{ai}}{\partial t} + \dfrac{1}{\overline{\rho}} \dfrac{\partial p_a}{\partial x_i} + \overline{u}_j \dfrac{\partial u_{ai}}{\partial x_j} = 0. & \text{(2.29b)} \end{cases}$$

Despite the introduction of the new terms which include the mean velocity field $\overline{\mathbf{u}}$, the variables are still decoupled and it is possible to obtain again a second order equation that describes the evolution of the acoustic pressure as

$$\frac{\partial^2 p_a}{\partial t^2} - c^2 \frac{\partial^2 p_a}{\partial x_i^2} = 0, \tag{2.30}$$

where c is the velocity of propagation that takes into account for the convection of the mean flow field and $c^2 = c_0^2 + u^2$ where u is the absolute value of the velocity vector $\overline{\mathbf{u}}$. In two dimensions the wave propagates with a velocity that, as is better discussed in the case analysed in section 3.1.1, is different according to the direction in which it is travelling ($c = c_0 + u$ or $c = c_0 - u$).

It is even possible that an acoustic wave propagates within a flow with **non uniform pressure** but uniform velocity. Also in this case, two terms are responsible of the description of the interaction of the acoustic wave with the pressure gradient. The terms that contains derivatives of the mean pressure are added to the APE system (2.28) obtaining

$$\begin{cases} \dfrac{\partial p_a}{\partial t} + \gamma \overline{p} \dfrac{\partial u_{aj}}{\partial x_j} + u_{aj} \dfrac{\partial \overline{p}}{\partial x_j} = 0 & \text{(2.31a)} \\ \dfrac{\partial u_{ai}}{\partial t} + \dfrac{1}{\overline{\rho}} \dfrac{\partial p_a}{\partial x_i} - \dfrac{p_a}{\overline{\rho}^2 c^2} \dfrac{\partial \overline{p}}{\partial x_i} = 0. & \text{(2.31b)} \end{cases}$$

It is still possible to decouple the system and write a second order equation for the acoustic pressure, but now the wave operator is more complex because p_a appears also as zero-order term multiplied for the gradient of the mean pressure

$$\frac{\partial^2 p_a}{\partial t^2} - c_0^2 \frac{\partial^2 p_a}{\partial x_i^2} + p_a \left(\frac{1}{\overline{\rho}} \frac{\partial^2 \overline{p}}{\partial x_i^2} + \frac{1}{\overline{\rho}^2 c_0^2} \left(\frac{\partial \overline{p}}{\partial x_i} \right)^2 \right) = 0. \tag{2.32}$$

Unlike the previous case in which the non-null velocity field changed only the speed of the wavefronts, the effect of these new terms is a change in the amplitude of the acoustic perturbations.

The last generalization that can be added is the effect of a **non-uniform mean flow** that is mathematically described by the introduction of the remaining two terms in which the gradient of $\overline{\mathbf{u}}$ appears ($\gamma p_a \frac{\partial \overline{u}_j}{\partial x_j}$ for the p_a equation and $\overline{u}_j \frac{\partial u_{ai}}{\partial x_j}$ in the $\mathbf{u}_a$ one). In this conditions, the APE wave operator become exactly the one described by the system (2.24) except for the source terms. Since the source terms and the interaction of the acoustic wave with a non-uniform mean flow field are very important in the applications investigated in this work, they are discussed in detail in sections 3.2.4.

CHAPTER 3

Numerical Resolution of APE

The Acoustic Perturbation Equations are a system of two coupled equations that describe the evolution in time of the acoustic pressure p_a and the acoustic particle velocity $\mathbf{u}_a$. Their left-hand side is a wave operator that deals with the propagation of the noise. Its generation is modelled by the source term in the right-hand side: this acoustic source can be of any typology, i.e. not only related to aero-dynamic noise. The APE are indeed a suitable system for the resolution of problems that goes beyond the aero-acoustic framework since the source terms can be related to any other noise generation mechanism.

In this work the APE formulation used for the acoustic analysis is described by the system (2.24) presented in section 2.5. The equations are derived from the Euler one under the assumption of isentropic flow and with the linearisation of the acoustic quantities. In this work, their numerical resolution has been performed thanks to a new in-house code implemented in OpenFoam [24].

The first part of this chapter describes the technical issues associated to the APE's numerical resolution paying particular attention to the development of a new solver that faces numerical instabilities. This new

solving algorithm is validated thanks to the comparison with analytical solutions and literature results. These test are not about aero-acoustics since the noise generation is not related to turbulence effect. On the contrary the solver is tested on the propagation of the noise emitted by all the fundamental acoustic sources (monopole, dipole and quadrupole) and on the influence of a sheared flow (typical of the internal flows) on the acoustic wave.
In the second part of the chapter the application of the APE to the aero-acoustic problem is introduced and the Stochastic Noise Generation and Radiation (SNGR) model for the synthetic generation of the turbulent fluctuations is described.

3.1 Implementation and Resolution of the APE

The implementation and resolution of the APE system (2.24) are performed in OpenFoam, an open-source software for the resolution of Partial Differential Equations (PDE) based on the finite-volume approach. OpenFoam is a C++ library in which CFD tools are implemented: solvers for different flows, boundary conditions, turbulence models, thermo-physical models and several other applications for the pre-processing (mesh design and flow initialization) and post-processing analysis are included. Not belonging to the CFD world, the Acoustic Perturbation Equations are not implemented in the library provided by the official software.
For this reason, their implementation and resolution has been thus performed in this work. Particular attention has been dedicated to the following numerical issues:

1. algorithm for the resolution of the time-marching APE equations (solver);
2. methods for the resolution of linear systems associated to the PDEs;
3. discretization of the derivatives (in space and time);
4. choice of the mesh size;
5. choice of the time step.

All these aspects are crucial in order to guarantee the stability and the accuracy of the resolution and an inadequate choice of one among them can compromise the whole result.

This section is particularly focused on the importance of the APE solver on the stability and accuracy of the results (point 1). On the contrary, the other numerical settings mentioned in the points 2 to 5 are not here deeply discussed but they will be specified only when needed.

3.1.1 New Solver for the APE System

The solver for the APE must be designed as an algorithm that manage the resolution of a second order hyperbolic system. Such a system has the same structure as the one for compressible Navier-Stokes equations which, in OpenFoam, are solved by the solver `rhoPimpleFoam`. This algorithm is designed for the resolution of unsteady, compressible flows and, at each time step, it manages the coupling between the different equations through nested iterative cycles and through the predictor-corrector method. The correction of the velocity field due to the newest pressure calculated inside the corrector step is performed with an explicit update of the velocity field based on the diagonal and off-diagonal matrices associated to the velocity equations. That means that, if $\mathbf{U}$ is defined as the discretized velocity vector and P the discretized pressure, the linear system that describes the velocity equation (2.24b) can be written as

$$\mathrm{C}\mathbf{U} - \mathbf{R} = -\nabla \mathrm{P}, \tag{3.1}$$

where $\mathbf{R}$ is the vector that contains all the terms in which the velocity doesn't appear (except the pressure gradient). The C matrix, in the finite volume framework, is split in a diagonal matrix A and a off-diagonal one H'. Matrix H, defined as

$$\mathrm{H} = \mathbf{R} - \mathrm{H}'\mathbf{U} \tag{3.2}$$

is introduced for writing the linear system as

$$\mathrm{A}\mathbf{U} = \mathrm{H} - \nabla \mathrm{P}. \tag{3.3}$$

The calculation of the velocity field after the correction of the pressure is performed with an algebraic operation that in the `rhoPimpleFoam` solver is described by the command

$$\mathtt{U} = \mathtt{HbyA} - \mathtt{rAU} * \mathtt{fvc} :: \mathtt{grad}(\mathtt{p}); \tag{3.4}$$

where `HbyA` stands for the ratio between H and A, `rAU` is the inverse of the A matrix and the method `fvc::grad(p)` returns the discretized

pressure gradient vector.

Because of the nature of the equations, the same solving algorithm has been applied to the APE but instabilities issues arose. Here are presented the test conducted for the identification and solving of these problems.
The benchmark case on which the solver has been tested is the propagation of the acoustic wave generated by a pulsating monopole in a uniform field with a constant not-null velocity. The monopole excitation is mathematically modelled by a source term in the acoustic pressure equation (2.24a) while the source term of the acoustic velocity equation (2.24b) is null. The test is run with non-dimensional quantities, that means that the variables in APE system are scaled with the grid spacing dx, the speed of sound c_0 and the density ρ_0 at standard conditions. The non-dimensional variables (indicated with an asterisk) are:

$$x^* = \frac{x}{\mathrm{dx}} \qquad c^* = \frac{c}{c_0} \qquad t^* = \frac{t\, c_0}{dx} \qquad u^* = \frac{u}{c_0} \qquad p^* = \frac{p}{\rho_0 c_0^2}. \tag{3.5}$$

The source term for the acoustic pressure equation is

$$S_{mono} = \sin\left(\omega t^*\right)\, \exp\left\{-\alpha\left(x^{*2} + y^{*2}\right)\right\}, \tag{3.6}$$

where the pulsation ω is set equal to $\omega = 2\pi/30$ and the parameter $\alpha = \ln(2)/9$. Thanks to the scaling (3.5), the speed of sound is equal to 1, the wavelength of the resulting acoustical wave is $\lambda^* = 15$ and the period T^* is equal to 15 too. The uniform velocity field inside of which the noise is propagated is described by a mean velocity from left to right that guarantees a Mach number equal to 0.5. Limitations on the size of the time step used for the time marching are derived from the CFL condition. The Courant number C for CFD is

$$C = \frac{U\Delta t}{\Delta x}. \tag{3.7}$$

Acoustic simulations are governed by the acoustic Courant number C_a, an extension of C which takes into account the speed of sound in addition to the fluid velocity

$$C_a = \frac{(U + c)\Delta t}{\Delta x}. \tag{3.8}$$

In this benchmark the time step is set to 0.1 for a $C_a = 0.15$.
Another fundamental quantity in the acoustic analysis is the number of

points that are used to describe a harmonic oscillation. The number of Points Per Wavelength PPW is defined as

$$\mathrm{PPW} = \frac{\lambda}{\mathrm{dx}} \tag{3.9}$$

and it is a fundamental quantity in order to avoid aliasing effects.

The propagation of the noise emitted by the monopole (3.6) is computed on a square domain with the source located in the origin of the Cartesian axes. A qualitative visualization of the acoustic field is displayed in figure 3.1. The acoustic wave is perturbed by the presence

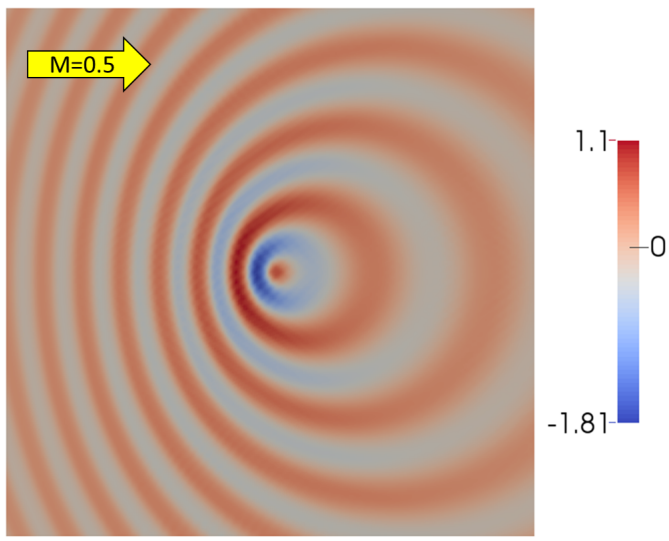

Figure 3.1: *Acoustic pressure emitted by the pulsating monopole* (3.6) *at time* $t^* = 270$. *Flow from left to right with M=0.5.*

of the mean flow (from left to right) that changes the velocity at which the wavefronts travel through the medium. Since the frequency is fixed by the pulsation of the source, the wavelength changes according to the propagation velocity $U + c\,\cos\theta$ where θ is the angle with the positive horizontal axis. The change of the travelling velocity is clear looking at the position of the wavefronts: on the left side of the domain the wave travels at the velocity $U - c$ and its fronts are much closer than the ones on the right (velocity $U + c$). In particular, the wavelength of the fronts

that propagate along the horizontal axis (aligned with the mean flow) are

$$\lambda_l = \frac{1-M}{f} = 15 \qquad \lambda_r = \frac{1+M}{f} = 45. \tag{3.10}$$

A quantitative investigation of the reliability of the implemented solver is performed comparing the APE results with the analytical solution. As shown in section 2.5.1, when the APE are applied to the propagation of the noise in a field with uniform velocity and pressure, the acoustic variables can be decoupled and the APE become equivalent to the inhomogeneous wave equation (2.30). Its analytical solution is obtained with the convolution of source term (the monopole (3.6) in this example) with the Green function [2].
In figure 3.2 the acoustic pressure computed with the APE is compared to the analytical solution (red line). The two series of numerical values (blue and black dots) are obtained with different time steps that correspond to an acoustic Courant number C_a equal to 0.15 and 0.3 (temporal spacing $\mathrm{dt} = 0.1$ and 0.2). The blue dots ($C_a = 0.3$) are affected by dif-

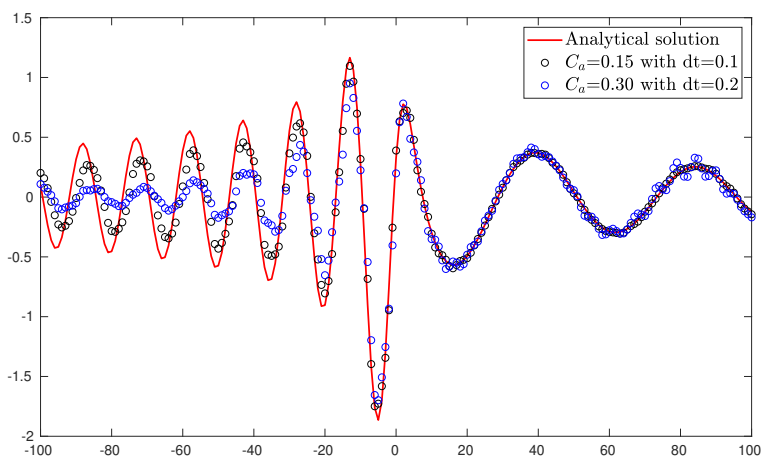

Figure 3.2: *Acoustic pressure on the x-axis emitted by a pulsating monopole: analytical (red line) and numerical solution with acoustic Courant number 0.3 (blue dots) and 0.15 (black dots);* $\mathrm{dx} = 1$.

fusion (underestimated amplitude) and dispersion (different travelling velocity) on the short-wavelength side, while instabilities and oscillations arise on the first front of the right-propagating wave. On the other

side, the reduction of the acoustic Courant number to $C_a = 0.15$ leads to a decrease in diffusion and to the absence of the oscillations on the right side of the domain.
While diffusion and dispersion are errors connected to the schemes for temporal and spatial derivatives discretization, the oscillations are a stability issue that is influenced by the way in which the linear system associated to the PDE is solved. Grid spacing and temporal step are usually the two parameters that most influence the instabilities amplitude. An investigation on the instabilities is thus performed analysing the influence of the PPW (it grows with the mesh quality) and of the C_a (it enforces limits on the time step). In the previous figure 3.2 the numerical series are obtained changing the acoustic Courant number with the temporal spacing (dx is fixed). On the contrary, in figure 3.3 C_a changes with the

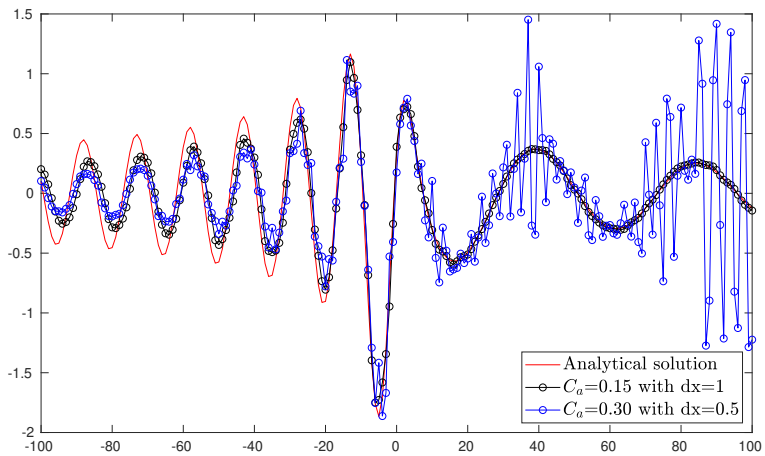

Figure 3.3: *Acoustic pressure on the x-axis emitted by a pulsating monopole: analytical (red line) and numerical solution with acoustic Courant number 0.3 (blue dots) and 0.15 (black dots);* $\mathrm{dt} = 0.1$.

spatial discretization dx ($\mathrm{dx} = 1$ and 0.5) keeping fixed the $\mathrm{dt} = 0.1$. The series at $C_a = 0.15$ in the two figure are the same, while figure 3.2 $C_a = 0.3$ is obtained with $\mathrm{dx} = 1$ and $\mathrm{dt} = 0.2$ and figure 3.3 $C_a = 0.3$ with $\mathrm{dx} = 0.5$ and $\mathrm{dt} = 0.1$ instead. At the same $C_a = 0.3$ the oscillations on the right-propagating wavefront in figure 3.3 are more enhanced that figure 3.2 and their amplitude is higher than the actual amplitude of the acoustic wave. This is an instability issue that make the noise estima-

tion completely unreliable because it is dominated by numerical errors higher than the physical values.
On the other side, the diffusion is lower because it is known that is an issue mostly due to the temporal discretization.

The increased amplitude of the oscillations suggests that the main cause of those instabilities it is exactly the spatial discretization. If on simple benchmark cases it is possible to find out the right choice of dx and dt, in real applications there are no clues that help to define their optimum values.
An alternative approach for managing these issues has been investigated at the light of the evidences suggested by the oscillations behaviour. Their dependency on C_a shows a greater influence of dx than dt: this means that the numerical issues that creates the instabilities may be connected to some explicit equation in the solving algorithm. Such an investigation allow to identify the critical equation in the solver based on `rhoPimpleFoam` as the explicit update of the velocity during the corrector step (3.4).

This step has been replaced by the implementation of a new algorithm based on the update of the acoustic particle velocity through the resolution of its PDE and not thanks to the algebraic operation [18]. This modi-

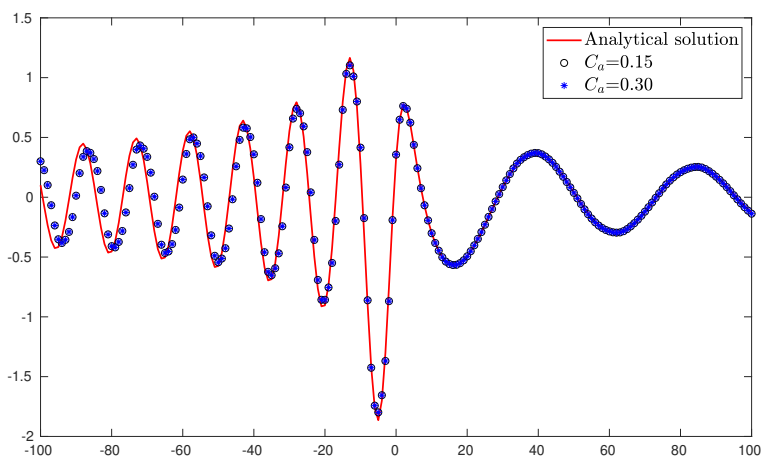

Figure 3.4: *Acoustic pressure on the x-axis emitted by a pulsating monopole computed with the new solver: analytical (red line) and numerical solution with acoustic Courant number 0.3 (blue stars) and 0.15 (black dots);* $\mathrm{dx} = 1$.

fication basically moves the iterations needed for managing the acoustic velocity-pressure coupling from the predictor-corrector loop's internal cycle to the external one that solves on turn the APE system's two equations.
The new solver has been tested on the same benchmark and the results obtained with C_a equal to 0.3 and 0.15 are displayed in figure 3.4. No oscillations on the right-propagating wavefront are now generated thanks to the numerical stability achieved with the new algorithm. Dispersion and (especially) diffusion are improved too and the difference between the computed results and the analytical solution is limited to the different velocity of propagation of the left-travelling wave.
The influence of the acoustic Courant number is also removed as can be seen by the overlap of the two numerical series.

3.2 APE Validation

This section is about the validation of the implemented APE system (2.24) with analytical solution and literature results. The first tests are performed on the acoustic propagation in a quiet field with the noise emitted by the three fundamental acoustic sources described in section 2.2. This cases are used for testing the APE with the most general acoustic sources (not only with the ones connected to aero-acoustics). Monopoles, dipoles, and quadrupoles are indeed acoustic sources that represents the most generic noise generation mechanisms. Analytical solutions are used as comparison for the APE results.
Other tests are then performed with a flow field similar to the one expected in the industrial applications, i.e. a sheared flow. Due to the complexity of these cases, no analytical solutions are available and the acoustic pressure returned by the APE is compared to literature results.

3.2.1 Monopole

The physical description of the behaviour of a monopole has been discussed in section 2.2.1. In the present paragraph the APE are applied for the emitted noise propagation in a quiet medium. The noise radiation is managed by the wave operator in the left-hand side is the one described by equations (2.28), while the noise generation is governed by source terms in the right-hand side.
With a quiet medium the wave equation (2.27) can be used as wave operator as well. Its equivalence with the APE system (2.28) has been

shown in section 2.5.1 for the homogeneous equation. Similar consideration can be also done for the non-homogeneous case: if S_p and $\mathbf{S_u}$ are the source terms respectively in (2.28a) and (2.28b), the inhomogeneous wave equation becomes

$$\frac{\partial^2 p_a}{\partial t^2} - c_0^2 \frac{\partial^2 p_a}{\partial x_i^2} = \frac{\partial S_p}{\partial t} - c_0^2 \frac{\partial S_{\mathbf{u}i}}{\partial x_i}. \tag{3.11}$$

In right-hand side of the wave equation (3.11), the zero-order derivatives represent a monopole, the first-order ones a dipole while quadrupole is described by second-order ones. The source term S_p is thus a monopole source, while $\mathbf{S_u}$ is a dipole or, if it contains other spatial derivatives, a quadrupole.

The monopole here simulated is described by a source term $S_p = \sin(2\pi/30t^*)\exp\left(-\ln(2)\frac{x^{*2}+y^{*2}}{9}\right)$. The instantaneous pattern of acoustic pressure is displayed in figure 3.5 that, as expected, is made of concentric wavefronts whose intensity depends only on their distance from the origin and decreases moving far from the source.

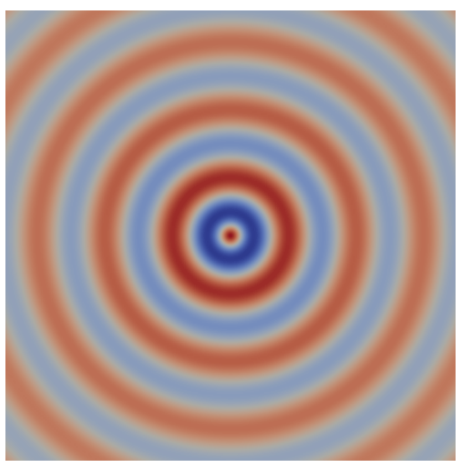

Figure 3.5: *Acoustic pressure emitted by a pulsating monopole at* $t^* = 150$.

For the noise propagation in quiet medium an analytical solution is computable and the numerical result along the horizontal axis is compared to it (figure 3.6). The acoustic pressure p_a computed with the APE is overlapped to the analytical solution. From the physical point of view it can be noticed the expected decrease of the intensity of the peaks of

the acoustic pressure moving far from the monopole described in section 2.2.1.

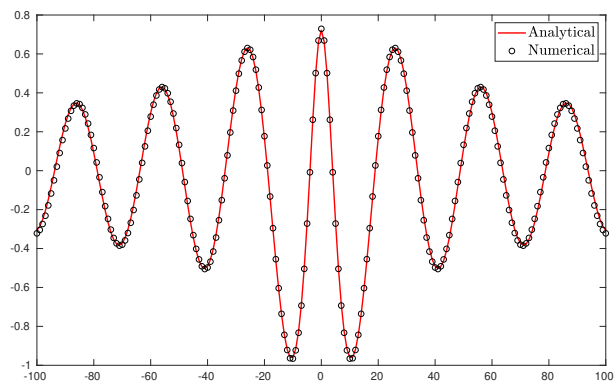

Figure 3.6: *Comparison of the analytical solution and numerical results of the acoustic pressure along the x-axis emitted by a pulsating monopole at* $t^* = 150$.

3.2.2 Dipole

A dipole that radiates sound in a quiet field is modelled by a spatial derivative terms in the right-hand side of (3.11), i.e. by a force. In the APE system it is thus modelled by $\mathbf{S_u}$ since in the wave equation it appears under the divergence operator.
The main features of a dipole were discusses in section 2.2.2. Here, the APE are solved for the computation of the noise radiated by a dipole which is described by the source term

$$\mathbf{S_u} = \begin{bmatrix} \sin\left(2\pi t^*/15\right)\cos\left(10\pi/x^*\right)\exp\left(-\ln(2)\dfrac{y^{*2}}{9}\right) \\ 0 \end{bmatrix}.$$

Its directivity pattern is shown in figure 3.7.

Unlike the monopole, now it is evident that the pressure intensity changes with the polar angle and that is equal to zero along the axis of the dipole placed at 90° respect to the horizontal axis. At the sides of the axis the wavefronts have opposite signs that attest the phase-shift of the waves emitted by the two monopoles. This is even more evident when the solution is sampled along the horizontal axis (figure 3.8): the

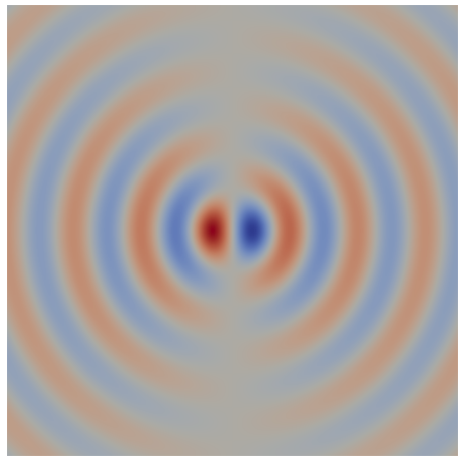

Figure 3.7: *Acoustic pressure emitted by a pulsating dipole at* $t^* = 150$.

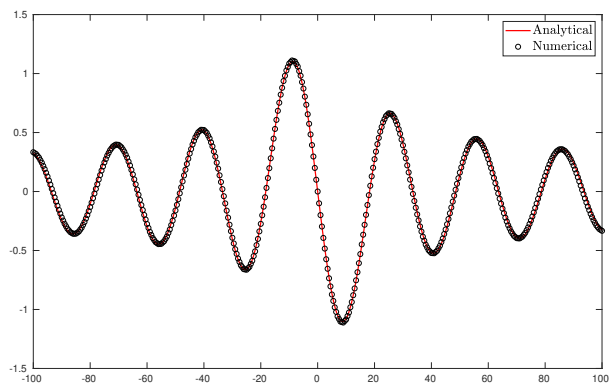

Figure 3.8: *Comparison of the analytical solution and numerical results of the acoustic pressure along the x-axis emitted by a dipole at* $t^* = 150$.

acoustic pressure is no more symmetric as in the monopole radiation but now it is antisymmetric because of the 180° phase shift.
Figure 3.8 shows the agreement between the APE numerical result and the analytical solution in this case too.

3.2.3 Quadrupole

A quadrupole, whose physical description is treated in section 2.2.3, is modelled by a source terms under a second order spatial derivative in the wave equation (3.11). This means that, when $\mathbf{S_u}$ in the APE is written as a spatial derivative it represent a quadrupole excitation of the surrounding medium. Here, the directivity pattern of a lateral quadrupole (figure 3.9) is computed through the resolution of the APE system with the source term

$$\mathbf{S_u} = \sin\left(2\pi t^*/30\right) \begin{bmatrix} \sin\left(\pi/20x^*\right)\exp\left(-\ln(2)\dfrac{y^{*2}}{9}\right) \\ \sin\left(\pi/20y^*\right)\exp\left(-\ln(2)\dfrac{x^{*2}}{9}\right) \end{bmatrix}$$

with $(x^*, y^*) \in [-10, 10] \times [-10, 10]$.

Since a quadrupole is modelled as two close dipoles, the directivity of

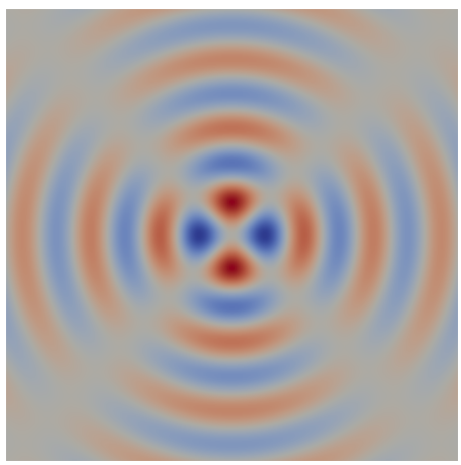

Figure 3.9: *Acoustic pressure emitted by a pulsating lateral quadrupole at* $t^* = 150$.

the noise is now characterized by the presence of two axes of low noise.

Even in this case, the APE solver has been tested and figure 3.10 shows the accordance between the analytical solution and the numerical data.

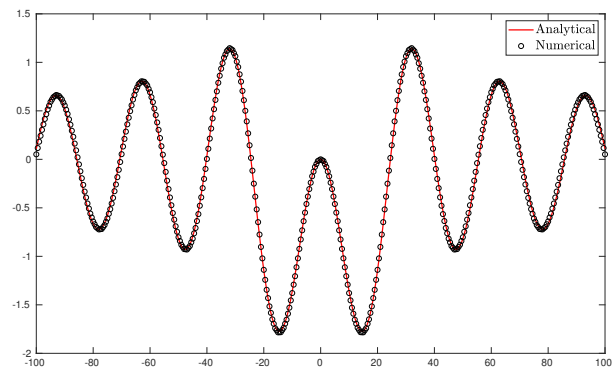

Figure 3.10: *Comparison of the analytical solution and numerical results of the acoustic pressure along the x-axis emitted by a quadrupole at* $t^* = 150$.

3.2.4 Propagation in Sheared Flow

So far, the APE have been tested on the propagation of the noise emitted by the fundamental acoustic sources and radiated into a quiet medium. Anyway, in industrial applications a flow inside ducts is always present and it is often described by a non-uniform profile because of the perturbation induced by singularities as, for instance, the control devices. For this reason, the APE have also been solved on two cases that are about the noise propagation in a flow with non-uniform velocity and pressure. The results are compared with literature references because no analytical solutions are available in such complex phenomena.

The first test-case deals with the propagation of the noise radiated by a pulsating monopole in a sheared flow whose mean velocity profile is described by the hyperbolic tangent $U = 0.5\tanh(y^*/25)$. The source is placed at the origin at the axis and the only difference with the set-up described in the paragraph 3.2.1 is represented by the mean flow. Since no analytical solution is available for such a complex flow, the comparison of the numerical results is made with a reference solution that can be found in literature [16].
The visualization of the acoustic wave emitted by the monopole is displayed in figure 3.11: the mean flow affects the directivity of the acoustic wave that now is no more characterized by spherical wavefronts.

A quantitative comparison with literature results is done looking at the intensity of the acoustic pressure along the $y^* = 70$ horizontal line

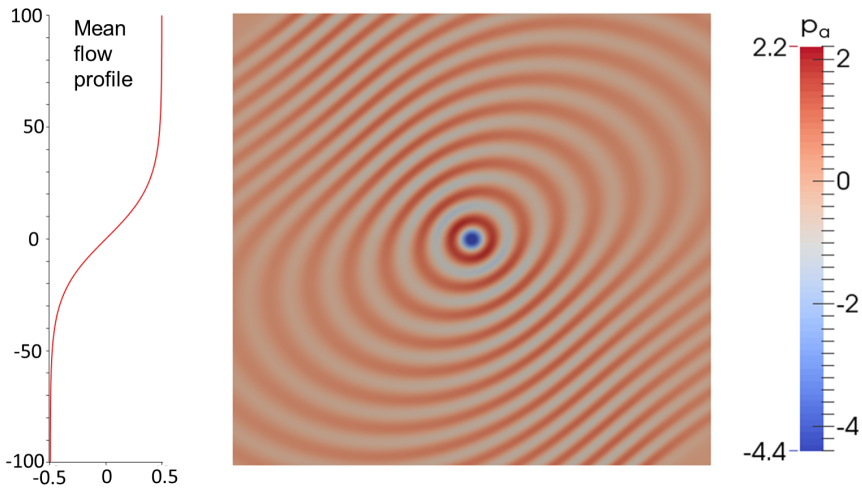

Figure 3.11: *Mean velocity profile and acoustic pressure emitted by a pulsating monopole in a sheared flow at* $t^* = 180$.

as reported in [16] (figure 3.12). The amplitude of the pressure is per-

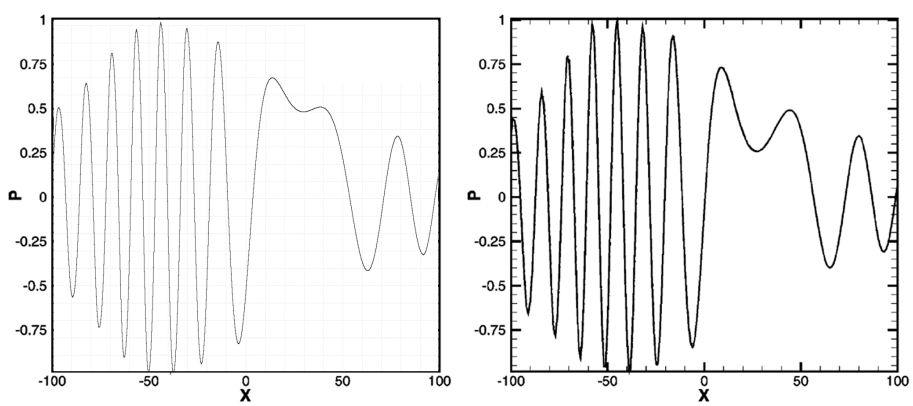

(a) *APE* **(b)** *Reference solution [16]*

Figure 3.12: *Acoustic pressure at the time* $t^* = 180$ *emitted by a pulsating monopole in a sheared mean flow computed with the APE solver (a) and obtained from literature [16] (b).*

fectly described by the APE and it is in accordance with the literature evidences. The small difference on the first sink on the right of the origin

is due to numerical diffusion, while dispersion affects the wave as can be seen by the phase at the boundaries of the domain. These issues are associated to the numerical schemes (temporal and spatial) that are implemented in OpenFoam that cannot reach higher orders than the third, while it is well-known that the numerical dispersion is removed only with higher-order schemes [51, 52]. Such an error is anyway acceptable for the purpose of this work because the spectral analysis goes beyond the interest in the evaluation of the SPL of the noise inside pipelines.

Another comparison with literature has been performed simulating the noise propagation in a flow whose profile is similar to a jet, exactly as the flow expected inside pipes in industrial applications. In this case the velocity profile is described by $U = 0.5/\cosh\left[(1+\sqrt{2})y^*/10\right]$ and the sound is emitted once again by a pulsating monopole. The comparison with literature results is shown in figure 3.13 where the acoustic pressure isolines are plotted. The diffusion effects noticed in the previous test are still present and the results computed with the APE smooth out the lowest-intensity isolines in the back of the monopole and in the front of the propagating waves. Despite these numerical inaccuracies, all the other isolines are in accordance with the reference solution, i.e. the APE properly describe the peaks of the intensity of the acoustic pressure. This is confirmed by the formation of the 'lobes' of noise around the jet that describe the directivity of the wave; according to literature, the angle at which the maximum noise is obtained is defined by $\theta = \cos^{-1}(1/(1+M))$ where M is the Mach number that here is imposed equal to 0.5. The directivity of the lobes computed with the APE is about $49°$ that is very close to the literature value of $\theta \approx 48°$. The error introduced in the change of directivity of noise is so low that can be quietly assumed negligible.

The results returned by the APE in the tests just described show the goodness of the implemented solver that does not introduce numerical instabilities. The evaluation of the intensity of the acoustic pressure is always in accordance with literature results. Small errors due to diffusion and dispersion are introduced by the numerical schemes used for the discretization, respectively, of the temporal and spatial derivatives. Because of the limitation of the schemes implemented in the OpenFoam standard library no better results can be obtained under these aspects.
Because of the aforementioned reasons, the APE, as implemented, have

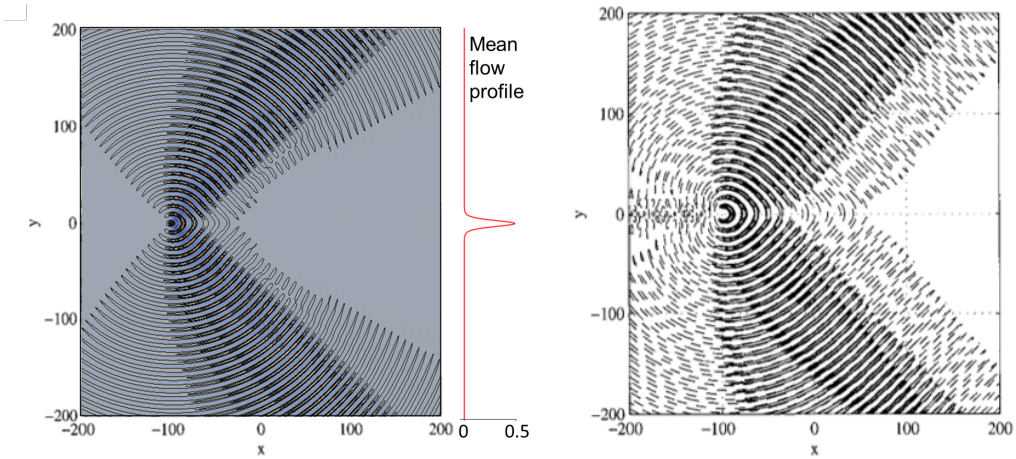

(a) *APE* **(b)** *Reference solution [2]*

Figure 3.13: *Acoustic pressure at the time* $t^* = 900$ *emitted by a pulsating monopole in a jet computed with the APE solver (a) and obtained from literature [2] (b). Isolines from* 10^{-2} *to* 10^{-3} *(step* 10^{-3}*) and* 10^{-4}.

been then applied to the aero-acoustics for the prediction of control devices' noise emissions.

3.3 APE for Aero-Acoustics

In the previous section 3.2 it has been discussed how the source terms of APE can be modelled for the description of the fundamental acoustic sources such as monopoles, dipoles and quadrupoles. In aero-acoustics, a small branch of acoustics, the sources are more complicated than the fundamental ones because they are connected to all the non-linear contributes associated to the turbulence. The Lighthill analogy has been already discussed in section 2.4.1 showing that the effects of the turbulence are collected in the Lighthill tensor T_{ij} defined by equation (2.14). The derivation of the source terms for the APE is discussed in details in Appendix A and section 2.5: according to literature [5] it is possible to neglect the contribute of the source term S_p for the acoustic pressure, while different formulations of $\mathbf{S_u}$ have been derived in different papers. The common point to all the possible expressions for the source term $\mathbf{S_u}$ is that it depends on the turbulent effects as described in equation (2.26). In literature, different considerations (order of magnitude analysis and filtering operations) led to the different formulations of $\mathbf{S_u}$ [7]. In this

work two possible expressions are considered. The first one [5, 48] is

$$\mathbf{S_u} = -\mathbf{u}_t \cdot \nabla \overline{\mathbf{u}} - \overline{\mathbf{u}} \cdot \nabla \mathbf{u}_t - \mathbf{u}_t \cdot \nabla \mathbf{u}_t. \tag{3.12}$$

Its derivation is based only on the orders of magnitude analysis that reveals that the main terms are the ones associated to the interaction between the turbulent and mean flow field (shear noise), and to the self-noise generated by the turbulence-turbulence interaction.
The second expression of the $\mathbf{S_u}$ source term that is used in this work is [3, 41]

$$\mathbf{S_u} = \overline{\mathbf{u}_t \cdot \nabla \mathbf{u}_t} - \mathbf{u}_t \cdot \nabla \mathbf{u}_t \tag{3.13}$$

and is characterized by a mean equal to zero.

The computation of the turbulent velocity fluctuations is a necessary step required for the evaluation of the APE's acoustic source terms. Two possible approaches are feasible for the computation of the turbulence through CFD: the first one evaluates the turbulent field at each time step in every point of the domain thanks to the resolution of an unsteady DNS or LES. This is the most complete way to describe the turbulence but not the most efficient because of the numerical burden associated to that kind of simulations.
The second approach is based on the reconstruction of the turbulent velocity field from information about the mean flow as the mean velocity, pressure and density that can be computed with a RANS simulation. The reconstruction of the turbulent velocity is then made with the use of a Stochastic Noise Generation and Radiation model (SNGR) that allows to write the turbulent fluctuations exploiting the statistical quantities of the turbulence. This approach is much faster than the previous one and it is the proper choice for industrial purposes. In fact, because of its high computational cost, the first approach is usually not feasible in an industrial framework where the companies seek for results in a short time.
In this work the turbulent velocities are thus computed with a SNGR model that has been implemented in OpenFoam. Next sections are about the main features and characteristics of the model implemented and used in chapter 4.

3.3.1 Stochastic Noise Generation and Radiation (SNGR) Model

The Stochastic Noise Generation and Radiation method is an algorithm for the synthetic generation of turbulent quantities from the information

from an averaged flow field. Turbulence is a very complex phenomenon whose detailed description goes beyond the purpose of this work, but its main features and characteristic quantities can be found for instance in [34]. However, turbulence is not a deterministic phenomenon nor a completely stochastic one: turbulent structures in space and time arise and their evolution is described thanks to their statistics. The most important turbulence theory has been formulated by Kolmogorov in 1941 [33] for isotropic turbulence. The analysis of the turbulence statistics is developed in the Fourier space and the synthetic generator of the turbulent velocity thus follows the same approach making use of Fourier modal decomposition. A description of some of the possible synthetic generators can be found in [40].

This work makes usage of a synthetic generator that writes the turbulent velocity as a finite sum of Fourier modes. Two formulations of the turbulent velocity are considered: the first one (Karweit method) creates a field that takes into account only the spatial correlation [5, 8, 31] and reconstruct $\mathbf{u}_t$ as

$$\mathbf{u}_t\left(\mathbf{x},t\right) = 2\sum_{n=1}^{N} \tilde{u}_n \cos\left[\mathbf{k}_n \cdot \mathbf{x} + \psi_n\right] \boldsymbol{\sigma}_n. \tag{3.14}$$

The second formulation (Bailly method), presented in [1, 3], write $\mathbf{u}_t$ as

$$\mathbf{u}_t\left(\mathbf{x},t\right) = 2\sum_{n=1}^{N} \tilde{u}_n \cos\left[\mathbf{k}_n \cdot \left(\mathbf{x} - \overline{\mathbf{u}}t\right) + \psi_n + \omega_n t\right] \boldsymbol{\sigma}_n. \tag{3.15}$$

Such a formulation creates, in each point $\mathbf{x}$ of the domain, a temporal series of turbulent velocities that are not independent from their previous values, but are correlated in time according to the turbulence theory. In addition to the temporal correlation, the $\mathbf{u}_t$ field still maintains the same spatial correlation as the Karweit method (3.14).
The contributes of the terms that appear in the Fourier series are:

- N is the number of Fourier modes used to describe the turbulent velocity. The number of these modes is chosen in order to guarantee an accurate discretization of the energy spectrum preserving the total energy.
- $\tilde{u}_n$ is the amplitude of the n-th Fourier mode ($\boldsymbol{\sigma}$ is a unit vector) and describes the intensity of the turbulence associated to one mode.

The energy of the turbulent mode is extracted from the discretization of the energy spectrum $E(k)$.

- $\mathbf{k}_n$ is the wave vector correspondent to the n-th Fourier mode.
- $\mathbf{x} - \overline{\mathbf{u}}\ t$ takes into account for the spatial correlation of the turbulence considering also the convection of the turbulent structures due to the mean flow.
- ψ_n is the phase of the n-th Fourier mode.
- ω_n is the pulsation of the n-th Fourier mode and it describes the temporal correlation of the turbulent structures. It is introduced for the accounting of the turbulent velocities' temporal correlation.
- $\boldsymbol{\sigma}_n$ is the directivity unit vector of the n-th Fourier modes.

Some of these variables are deterministic, while others need a random process to be generated. Their detailed description is treated in the next sections.

3.3.1.1 Energy spectrum

The deterministic quantities that are generated by SNGR model according to turbulence statistics [33] are the intensity of the Fourier modes $\tilde{u}_n$ and the intensity of each wave vector, i.e. the wave number k_n. The most important quantity in the description of the turbulence is its energy spectrum $E(k)$ that describes the quantity of mechanical energy associated to each spatial length-scale $1/k$. The theoretical definition of the energy spectrum is based on the auto-correlation function of the velocity field. Because this is exactly the unknown in the SNGR, other models have been developed in order to describe it with just the mean flow variables. In this work the Modified Von-Karman spectrum [4, 40] has been used for the $E(k)$ modelling:

$$E(k) = \frac{2}{3} A \frac{K}{k_e} \frac{(k/k_e)^4}{\left[(k/k_e)^2 + 1\right]^{17/6}} \exp\left[-2(k/k_K)^2\right], \tag{3.16}$$

where K is the turbulent kinetic energy, k_e is the most energetic wave number and k_K is the Kolmogorov wave number, i.e. the smallest scale at which viscous forces are less intense than the inertial ones and do not dissipate energy. The value of k_e is imposed equal to $k_e = 1.453 \frac{9\pi}{55} \frac{1}{L}$

where L is the integral length scale, while the definition of the Kolmogorov wave number is obtained again from the mean flow quantities as

$$k_K = \frac{\epsilon^{1/4}}{\nu^{3/4}}, \tag{3.17}$$

where ϵ is the energy dissipation rate and ν is the viscosity of the fluid. The shape the energy spectrum $E(k)$ in a point of the domain can be visualized in figure 3.14 in the natural scale and in the bi-logarithmic on. In particular figure 3.14(b) proves that the shape of the spectrum in the inertial band is in accordance with the theoretical description of the "5/3" turbulence law.

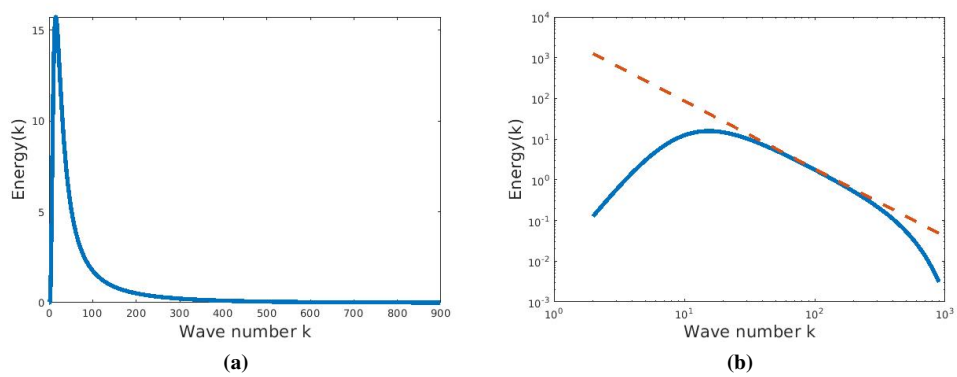

Figure 3.14: *Modified Von-Karman spectrum (a) and comparison with $k^{-5/3}$ law (dashed line) in log-log scale (b).*

The energy spectrum $E(k)$ is a continuous variable that needs to be approximated through its discretization in N intervals. The upper extreme of the n-th interval is evaluated as

$$k_n = \exp\left[\ln(k_1) + (n-1)\Delta k\right] \qquad \forall n = 1, ..., N \tag{3.18}$$

where $k_1 = k_e/5$ and $\Delta k = \frac{\ln(k_N)-\ln(k_1)}{N-1}$. In turn, $k_N = \frac{2\pi}{7\Delta x}$ with Δx defined as a characteristic dimension of the grid spacing.
From the discretized energy spectrum it is possible to evaluate the amplitude k_n of the wave vectors $\mathbf{k}_n$ that appears inside the Bailly model, but also the intensity of each Fourier mode because

$$\tilde{u}_n = \sqrt{E(k_n)\Delta k_n} \tag{3.19}$$

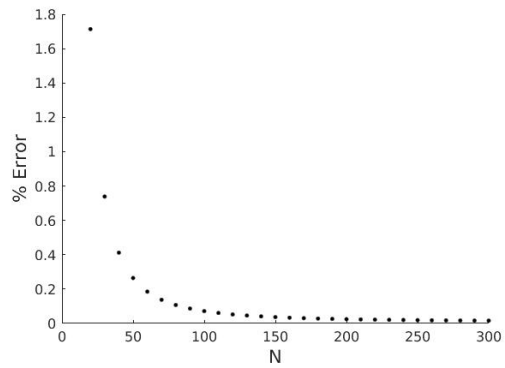

Figure 3.15: *Relative error on the integral of $E(k)$ changing the number of intervals N.*

where $\Delta k_n = k_n - k_{n-1}$.

In order to guarantee a good reconstruction of the turbulent field it is important that the number N of the Fourier modes is high enough to obtain a good description of the spectrum. In this work N is set equal to 200 that is enough to ensure that the relative error between the integral of the continuous spectrum and the discretized one is lower than 0.05% as shown in figure 3.15.

3.3.1.2 Random Variables in SNGR models

The stochastic processes in the SNGR model are about the random generation of some terms that appears in equation for the turbulent velocity $\mathbf{u}_t$. In the Bailly method described by equation (3.15), for each of the N Fourier modes, a random generation process is required for the evaluation of:

- the direction of the wave vector $\mathbf{k}_n$;
- the phase ψ_n;
- the pulsation ω_n;
- the direction of the Fourier modes $\boldsymbol{\sigma}_n$.

Since the direction of a vector is defined by two quantities (longitudinal and azimuthal angles), six variables must to be synthesized for each wave vector (directions of $\mathbf{k}_n$ and $\boldsymbol{\sigma}_n$, phase ψ_n and the pulsation ω_n). The SNGR method described in [1, 3] removes one of the degrees of

freedom with the introduction of the incompressibility assumption that, in the Fourier space, corresponds to an orthogonality relationship between the wave vector and the direction of the turbulent velocity. This means that

$$\mathbf{k}_n \cdot \boldsymbol{\sigma}_n = 0 \qquad \forall n = 1, .., N. \tag{3.20}$$

One of the angles required for the characterization of the direction of $\boldsymbol{\sigma}_n$ is thus defined by this equation. A graphical visualization of the relative positions of the wave vectors $\mathbf{k}_n$ and $\boldsymbol{\sigma}$ is displayed in figure 3.16. According to that figure, the angles that need to be synthesized

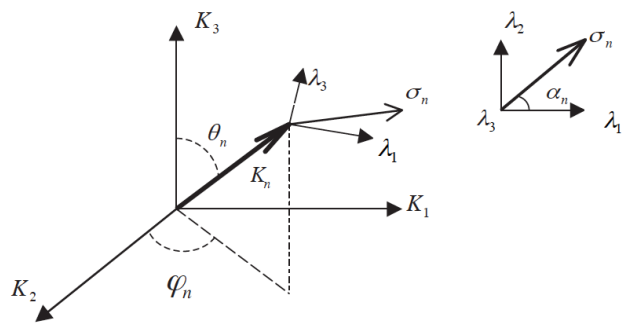

Figure 3.16: *Position of the wave vector* $\mathbf{k}_n$ *and the direction of the n-th Fourier mode* $\boldsymbol{\sigma}_n$.

are ϕ_n, ϑ_n and α_n. The direction of the vector $\mathbf{k}_n$ is chosen randomly on a unit sphere, while α_n is synthesized with uniform probability in $[0, 2\pi]$. The same distribution is assumed for the description of the phase ψ_n, while the pulsation is taken from a Gaussian $\mathcal{N}(\omega_{tn}, \omega_{tn}^2)$ where $\omega_{tn} = \sqrt{2K/3}\, k_n$ [1,40].

In the Bailly method all the five random variables must be synthesized for all the N Fourier modes, but their values do not change during the time advancement since the temporal correlation is managed by the variable t inside the cosine in equation (3.15). The computational burden of this approach is negligible if compared to the APE's resolution burden because, after the first iteration, no other random generations are required. In addition to this, the data stored during the simulation are only the values of the five random quantities.

The synthesis of the random variables in the Karweit method described by equation (3.14) involves the same quantity except the pulsa-

tion ω_n. Even though less variables need to be synthesized, this approach results to be more expensive than the Bailly one because, since the time advancement is not managed by the variable t, at each time step it is required to synthesize all the four variables for all the N modes.

CHAPTER 4

Numerical Investigation of the Noise Generated by an Orifice

In Chapter 3 the numerical tools for the computation of fluid-dynamic noise generation and propagation in a medium have been discussed. The hybrid approach based on the resolution of the APE system has been implemented and tested on benchmark cases that have shown its reliability in the prediction of the noise intensity, whatever its source. In industrial applications the source of noise is definitely more complex than the fundamental sources and, in the case of the noise produced by flow-control devices, the aero-acoustics theory suggests that it corresponds to the high-turbulent region. This area is usually localized at the outlet of a flow-control device. A very small amount of noise is produced inside the body of the valve and transmitted outside of it [28], while the interest in the noise prediction is focused on that part of acoustic energy that is generated at the outlet, convected downstream and propagated outside of the pipe. Of course, several types of control valves are available on the market but most of them are characterized by a flow that, at their outlet, is made of one jet or more interacting jet coming from different paths.

For this reason, the jet may be considered as the reference configuration for the investigation of the noise emitted by control devices.
In this chapter the APE system (2.24) is applied and solved for the characterization of the acoustic emission of a transversal perforated plate with a single perforation whose axis is aligned with the pipe's one. The nominal diameter of the pipe inside of which the plate is installed is equal to 3" ($D = 77.5$mm). In the rest of the work, the perforated plate will be also referred to as resistor or orifice.

4.1 Fluid-Dynamic Characterization of the Orifice

The orifice used in the simulations presented in this chapter is the one described in the technical draw in figure 4.1. Its relevant features are

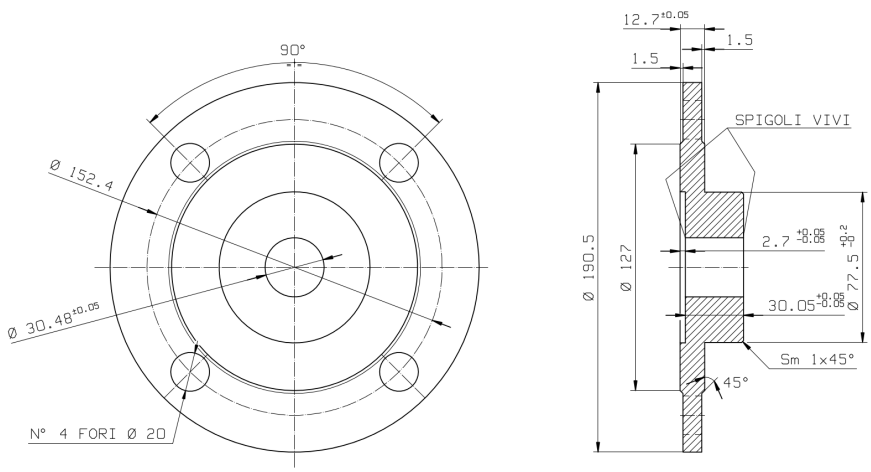

Figure 4.1: *Technical draw of the orifice. Property of Pibiviesse S.r.l.*

the dimension of the perforation and its thickness. The diameter of the orifice is $d = 30.48$ mm that corresponds to a porosity $\beta = 0.4$ that is defined as

$$\beta = \frac{d}{D}. \tag{4.1}$$

The fluid-dynamic characterization of a hydraulic device is made through some quantities defined in the international standard [26, 29, 44]:

- $X = \Delta p / p_1$ is the pressure drop ratio, i.e. the pressure drop divided for the pressure upstream of the device (inlet pressure);

- $F_L = \sqrt{(p_1 - p_2) / (p_1 - p_{\text{vc}})}$ is the liquid pressure recovery factor where p_2 is the outlet pressure and p_{vc} the one within the vena contracta;
- X_{cr} is the pressure drop ratio at the velocity in the vena contracta of a compressible fluid is equal to the speed of sound;
- X_T is maximum pressure drop ratio over which, increasing Δp, no increase in flow-rate is obtained for a compressible fluid;
- Y is the expansion factor that is a coefficient introduced for compressible fluids in order to compute them with similar equations to the ones introduced for incompressible fluids;
- C_V is the flow coefficient and describes the flow-rate that passes through a device with a unity pressure drop.

For the tested device represented in figure 4.1, previous works stated that its F_L is equal to 0.745 [39]. The liquid pressure recovery factor is used for the estimation of $X_T \cong 0.85 F_L^2$ and $X_{\text{cr}} \cong 0.47 F_L^2$ for an ideal gas [44]. The flow coefficient is computed as

$$Y\, C_V = \frac{1}{27.3} \frac{Q_m}{\sqrt{\rho_1 \Delta p}}, \tag{4.2}$$

where $Y = 1 - \frac{X}{3X_T}$ for an ideal gas, Q_m is the mass flow rate (in kg/h) and ρ_1 is the inlet density. The flow coefficient of the studied orifice computed with RANS simulation is about 34.5 [17].
The RANS simulations are performed in OpenFoam running the computation on a simplified geometry that exploits the symmetry of the domain and of the perforated plate. Since the software works in Cartesian coordinates (not cylindrical), a slice of pipe corresponding to one fourth of the pipe is used for the CFD simulation (inner angle equal to 90°). The mesh is a structured hexahedral one, designed in order to guarantee a $y^+ \approx 85$ far from the orifice for the undisturbed flow.

The flow displayed in figure 4.2 refers to the one developed imposing a pressure drop $\Delta p = 1$ bar with an upstream pressure $p_1 = 5$ barA. It's dynamic is characterized by the formation of a jet along the axis of the pipe with the confinement of the vena contracta inside the orifice. In fact, its enlargement is partially obstructed by the walls of the orifice whose thickness had been designed in order to guarantee the reattachment of the vena contracta inside of the resistor, before it can reach the trailing

edge. The influence of the orifice's thickness on the pressure is such that, after the drop on the leading edge due to the transformation of potential energy in kinetic one, the energy-recovery does not take place continuously but it is interrupted in correspondence of the trailing-edge. The pressure curve (black) in figure 4.2 describes this effect with its change in convexity.

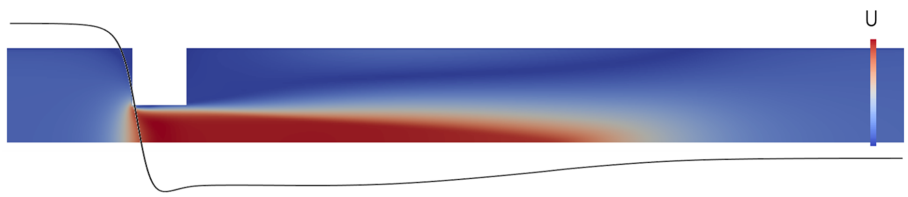

Figure 4.2: *Velocity (coloured contours) and pressure along the axis of the pipe (black line) on a slice of the pipe. Results from RANS simulation with* $p_1 = 5$ *barA and* $p_2 = 4$ *barA.*

4.2 Noise Prediction with APE

In section 3.3 it has been discussed the possibility to use different models for the evaluation of the source term $\mathbf{S_u}$ and algorithms for the synthetic generation of the turbulent velocity. Both of them influence the APE prediction because they respectively change the intensity of the acoustic source and the properties of the turbulence necessary for the evaluation of the APE source term. Several models have been developed in literature: in this work the attention is focused on testing the effects of the Karweit method (3.14) and the Bailly one (3.15) for the generation of the turbulent velocity $\mathbf{u}_t$ in the SNGR, and on the source term modelling according to the equations (3.12) and (3.13). No evidences of the best choice for industrial applications has been found in literature and for this reason, this section is focused on their analysis in order to find the most suitable method. The evaluation of the goodness of one method is done thanks to the comparison of the noise prediction with the results returned by a Large Eddy Simulation.
The coupling of the two algorithms for noise synthesis and the two source term's modelling equations returns four possible combinations:

- Karweit method for SNGR and source term (3.12) from Bechara's work: this source term will be called $\mathbf{S}_{\mathbf{u}KB}$ and the corresponding

formulation APE$_{KB}$;

- Karweit method for SNGR and source term (3.13) with zero-mean: this source term will be called $\mathbf{S}_{\mathbf{u}\overline{K}}$ and the corresponding formulation APE$_{\overline{K}}$;
- Bailly method for SNGR and source term (3.12) from Bechara's work: this source term will be called $\mathbf{S}_{\mathbf{u}BB}$ and the corresponding formulation APE$_{BB}$;
- Bailly method for SNGR and source term (3.13) with zero-mean: this source term will be called $\mathbf{S}_{\mathbf{u}\overline{B}}$ and the corresponding formulation APE$_{\overline{B}}$.

From the numerical point of view, the computational burden of all the four APE formulations is comparable among them. Their complexity depends only on the number of operations performed by the SNGR: the Karweit method synthesizes just one variable less than the Bailly approach (the pulsation ω_n) but has the disadvantage to synthesize all the other quantities at each time step in order to create a temporal series. The Karweit method it is thus more expensive than the Bailly one, but its burden is anyway much lower than the one associated to the resolution of the APE linear system. Their influence on the total burden associated to the APE resolution is thus comparable among them.

As pointed out, the first step of this work is about the identification of which among the four models is the most suitable for the noise prediction emitted by the jet downstream of the orifice. Their reliability is thus tested thanks to the comparison of their results with the noise computed by a LES solution. In order remove all possible errors coming from a different description of the fluid-dynamic, the mean flow field used for the resolution of the APE system is the time-averaged one returned by the LES instead of the mean one coming from RANS [19]. The settings used for the LES are described in the next section 4.2.1.
For the resolution of the APE a uniform structured mesh is built and the equations are solved with totally reflective boundary conditions on the walls of the pipe and non-reflecting ones on the numerical boundaries (inlet and outlet). The time advancement is made with a time-step equal to 10^{-7}s and the simulation is run till a time $T = 2$ ms, after which the distribution of the acoustic pressure inside the pipe reaches a stable configuration, terminating its transient from the initial silent condition. The

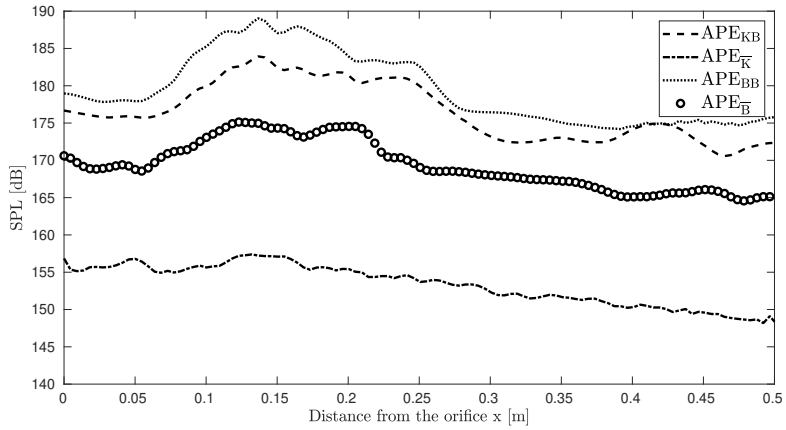

Figure 4.3: *Sound pressure level downstream of the orifice computed with different models applied on APE.*

noise intensity predicted by the four APE models is evaluated thanks to the Sound Pressure Level (SPL) on the walls of the pipe. The expected trend of the noise emitted by a flow-device is similar to the one described by Kirkwood in [32] that focused on the experimental investigation of perforated plates noise emissions. Kirkwood measured the noise along the pipe and described its trend as a curve made of a fast increase of SPL close to the device followed by a fast decrease and a slower one far enough from the resistor.
The SPL trends returned by the APE with all the tested models are visualized in figure 4.3.

Except for the $\mathrm{APE}_{\overline{K}}$, all the other curves has a shape in accordance with the one described in literature. Anyway, the four formulation return noise predictions shifted among them. The $\mathrm{APE}_{\mathrm{BB}}$ computes the highest noise, followed by $\mathrm{APE}_{\mathrm{KB}}$ and by $\mathrm{APE}_{\overline{B}}$. The lowest formulation is the $\mathrm{APE}_{\overline{K}}$ whose SPL prediction is about 25/30 dB lower than the one computed with the $\mathrm{APE}_{\mathrm{BB}}$. A further comparison with the four different methods is necessary for the identification of the best model. This is done looking at the acoustic pressure inside the pipe. Figure 4.4 shows the instantaneous p_a pattern on a slice of the pipe, downstream of the orifice, returned by the different models described before. The patterns of the four cases are qualitatively similar among them: the acoustic pressure is distributed with alternate structures with negative and positive intensity. They are located in the shear layer around the potential

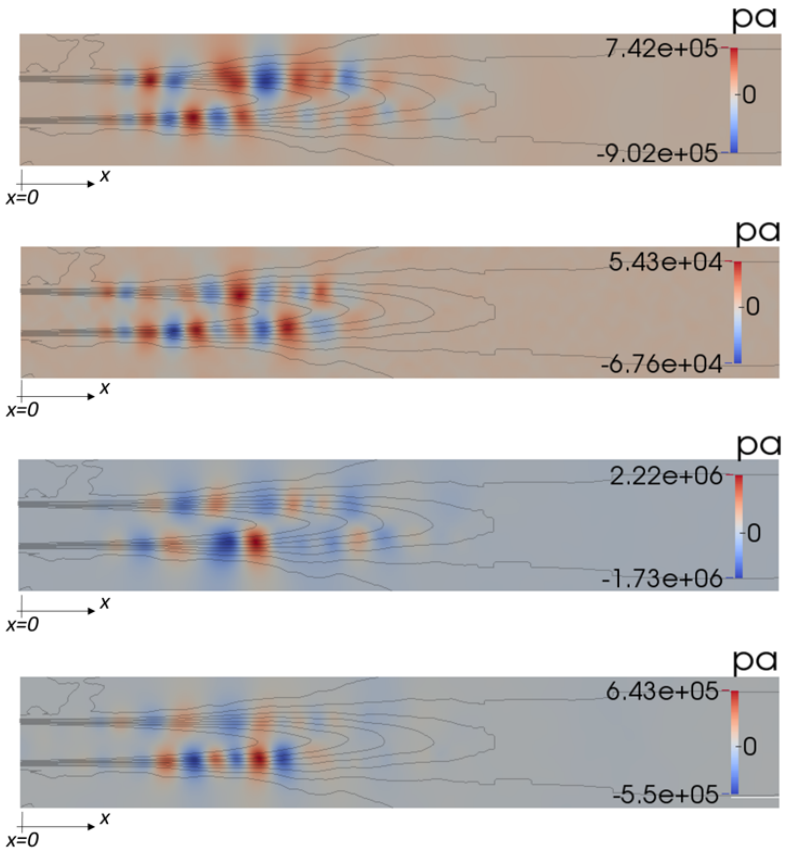

(a) $\mathrm{APE}_{\mathrm{KB}}$

(b) $\mathrm{APE}_{\overline{K}}$

(c) $\mathrm{APE}_{\mathrm{BB}}$

(d) $\mathrm{APE}_{\overline{B}}$

Figure 4.4: *Instantaneous acoustic pressure p_a at time $T = 2ms$ calculated with different APE models applied on the system* (2.24)*. Contours of the mean axial velocity. Orifice's trailing edge at $x = 0$.*

core (not within it) and at the end of the jet decreasing their intensity moving far from the orifice.
Differences among the four models are about the intensity (as expected from the SPL considerations) and the dimension of the structures:

- if the source term $\mathbf{S_u}$ is modelled as (3.12) (figure 4.4.(a)-(c)) the amplitude of the acoustic pressure is higher than the respective one computed with the zero-mean source term (3.13) with the same SNGR model (figure 4.4.(b)-(d));

- if the Karweit method is used for the synthesis of the turbulent velocity (figure 4.4.(a)-(b)) the amplitude of the acoustic pressure is lower than the respective one computed with the Bailly method describing the source term in the same way (figure 4.4.(c)-(d));

- the structures returned by the Bailly method with the description of the source term (3.12) ($\mathrm{APE_{BB}}$ in figure 4.4.(c)) are bigger than the other simulations. This mean that they are propagated with a different wavelength and are generated with a different frequency.

All these considerations are in accordance with the trend described in figure 4.3 but do not help to understand which is the most suitable formulation. For this reason, a further comparison with the results coming from a LES is required.

4.2.1 Comparison with LES

A Large Eddy Simulation is performed for computing the SPL emitted by the orifice and for using it as further comparison for the APE models introduced in the previous section. LES belongs to the so-called CAA direct approaches: its advantage is that no acoustic model is required for the noise propagation since it is computed together with the fluid-dynamic simulation [53].
The geometry on which the LES is run is the complete 3D pipe without any symmetry plane because of the three-dimensional behaviour of the turbulence (figure 4.5). The inlet of the pipe is placed $15d$ upstream of the resistor and the outlet $25d$ downstream of it, far enough to avoid the influence of the outlet on the computed fields. The modelling of the subgrid turbulence is made through a one-equation model developed by Yoshizawa [54] based on the resolution of a transport equation for the kinetic energy K_{SGS}. The simulation is run on a uniform, Cartesian grid

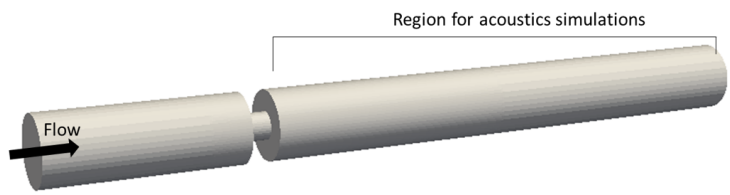

Figure 4.5: *3D domain for LES simulation.*

with a spacing that allows to compute the sound propagation up to almost 70 kHz according to the formula $f_{max} = c_0/(5\Delta x)$ [11] where c_0 is the speed of sound in the free field and Δx is the spacing of the grid. The dimension of the filter for the application of the subgrid model is computed as the cube root of the cells' volume. The time spacing is adapted at each time step in order to keep the Courant number lower than 0.75, and the whole simulation is run for about 200 characteristic periods D/U_j where U_j is the velocity of the jet developed at the outlet of the orifice.
The physics of the gas inside the pipe is described by the ideal gas model (dry air) whit viscosity and specific heat that change with temperature according respectively to Sutherland's law and JANAF polynomial.
The movement of the fluid is imposed through the assignment of boundary conditions with the pressure values on the inlet patch (total pressure equal to 5 barA) and at the outlet (static pressure equal to 4 barA). With this pressure drop, a Mach number equal to 0.7 is reached inside the jet and the Reynolds number referred to the mean velocity in the pipe is $5.3 \cdot 10^5$. Wave transmissive boundary conditions are also added on these patches in order to avoid numerical reflection of the incident waves. On the other boundaries of the domain (walls of the pipe and orifice) no-slip condition is imposed while their thermodynamic behaviour is modelled as adiabatic. The external temperature is imposed equal to the ambient one at 300 K.

The velocity field computed with the LES is averaged over the different time steps and the time-averaged velocity is used for the definition of the length of the jet at the orifice outlet. Its profile along the axis of the pipe is shown in figure 4.6 and helps to define the jet length equal to about $4d$. Unlike the RANS simulation, LES provides details also on the turbulence distribution of the flow inside the pipe. In aero-acoustics the noise generation takes place only in the regions characterized by high

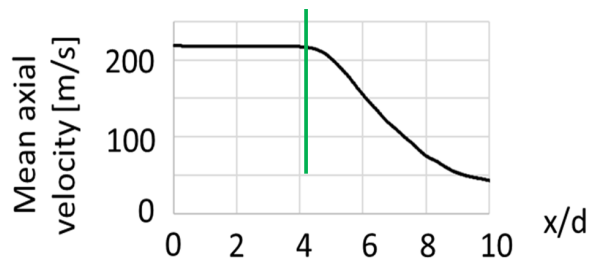

Figure 4.6: *Time-averaged velocity along the axis of the pipe.*

turbulence. The vorticity $\boldsymbol{\omega} = \nabla \times \mathbf{u}$ is an indicator of high-turbulence region and according to Powell-Howe theory of vortex sound [25] it is a necessary condition for the generation of the flow-induced noise. Its distribution is visualized in figure 4.7 and it shows that $\boldsymbol{\omega}$ reaches its highest intensity in the annular shear layer around the potential core and at the end of the jet filling each transversal section of the pipe.

Powell-Howe theory states that the presence of $\boldsymbol{\omega}$ is just a neces-

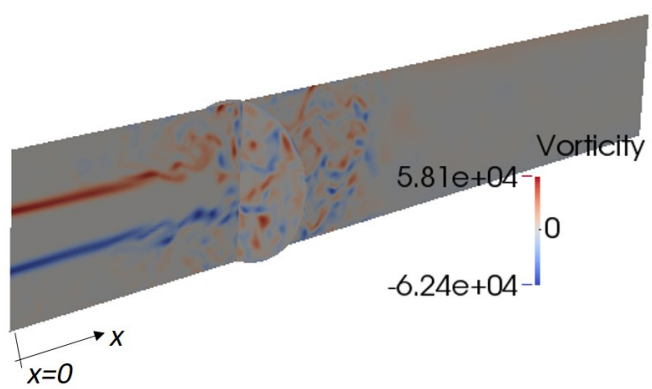

Figure 4.7: *Instantaneous vorticity field: visualization of the components of $\boldsymbol{\omega}$ orthogonal to the surfaces (ω_y in the longitudinal section and ω_x in the transversal section). Flow from left to right.*

sary condition (not sufficient) for noise generation: the definition of the acoustic source region is thus performed through the turbulent kinetic energy K (that can be derived from the RANS simulation as well). In the Acoustic Perturbation Equations, the region of domain where the source

terms are not equal to zero is defined as the part of the domain where K is higher than a a percentage of its maximum value assumed in the domain. Here the percentage is chosen equal to the 20% in accordance with [41]. The evaluation of the source region is made with the time-average of K computed as half of the trace of the averaged subgrid scale stress tensor

$$\mathrm{K} = 0.5\left(\overline{u'u'} + \overline{v'v'} + \overline{w'w'}\right). \tag{4.3}$$

Figure 4.8 shows the distribution of the turbulent kinetic energy so calculated and its intensity suggests that the biggest generation of noise is located downstream of the potential core of the jet and not in the mixing layer where the vorticity reaches its peak.

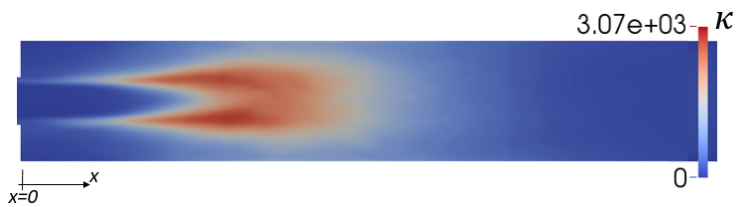

Figure 4.8: *Time-averaged turbulent kinetic energy from LES downstream of the orifice. Flow from left to right.*

According to the procedure described in [11] it is possible to compute the acoustic pressure from the LES output and compare it with the results obtained by the APE described in the previous section that were run with the mean quantities from the LES here presented. The SPL evaluated on the walls of the pipe is compared with the one plotted in figure 4.3 in order to define which combination of models (sources and SNGR) is the one which that shows the better accordance with LES results. The noise computed with the Bailly method for the SNGR and the source term with zero-mean ($\mathrm{APE}_{\overline{B}}$) is the one that return the closest SPL curve to the LES noise as shown in figure 4.9. The accordance of the two curves is almost perfect in all the regions (close to the orifice and far from it) since both describe the increase of noise in the region close to the end of the jet ($x = 4d$) with the following decrease of intensity with a slope that changes about at $x = 9d$. Such a comparison suggests that, among the four models combination, this is the best choice that returns the most reliable prediction for the considered orifice.

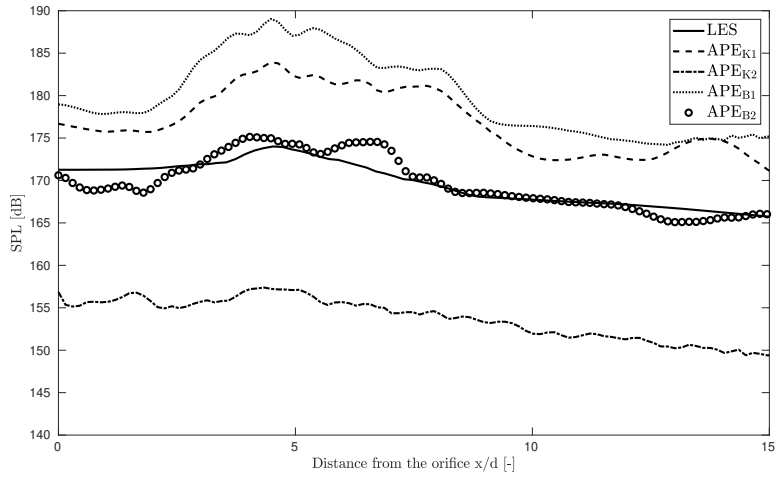

Figure 4.9: *Sound pressure level downstream of the orifice computed with LES and different models applied on APE.*

4.2.2 Influence of the Flow-Rate on the Noise Emission

The APE$_{\overline{B}}$ has been identified as the model that can be used for the prediction of the noise emitted by the orifice. The analysis of the influence of the boundary conditions on the noise emission is always a relevant topic in industrial applications because of the different flow-conditions in which control devices usually works (temperature, density and pressure). Here the influence of the pressure drop at the sides of the orifice (with fixed upstream pressure) has been investigated. This is a typical procedure for the fluid-dynamic characterization of a device that allows, for instance, to evaluate its flow coefficient C_V [29].

Some of the tests performed on the orifice are described in table 4.1.

p_1 [barA]	p_2 [barA]	X	Q_m [kg/s]	Re	SPL$_{\max}$[dB]
5	4.63	0.07	0.38	$3.47\cdot 10^5$	160.77
5	4.42	0.11	0.47	$4.23\cdot 10^5$	165.24
5	4.28	0.15	0.51	$4.62\cdot 10^5$	166.74
5	4.07	0.18	0.56	$5.12\cdot 10^5$	168.96
5	4	0.2	0.58	$5.26\cdot 10^5$	169.53

Table 4.1: *Simulations on the orifice changing the pressure drop at its sides*

The simulations are run with the APE from the RANS mean field (fastest approach in industrial applications). The pressure drop is imposed such

that the pressure drop ratio X is kept lower than the critical one $X_{\mathrm{cr}} = 0.35$ for the studied orifice (subsonic regime).
The reduction of the downstream pressure induces an increase of all the

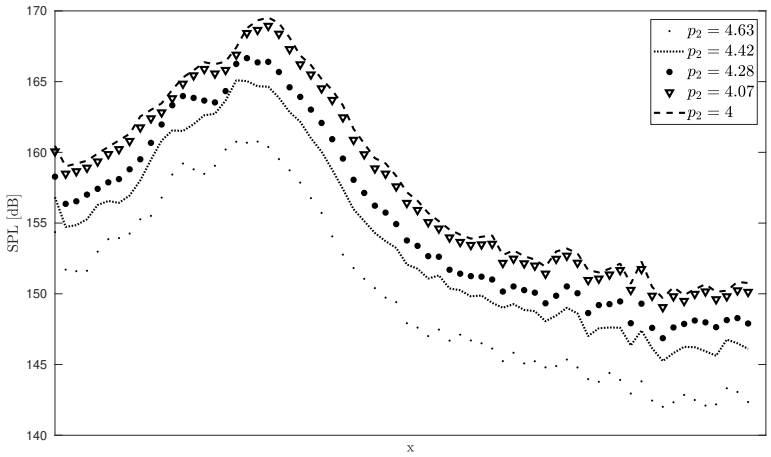

Figure 4.10: *SPL on the walls of the pipe changing the pressure drop at the sides of the orifice.*

other fluid-dynamic quantities (flow-rate and Re) but also of the noise intensity. This is justified by the increase of the mechanical energy associated to the flow-rate: the noise is a fraction of the mechanical energy that is generated by its dissipation and therefore it increases with the flow-rate.
The trend of the SPL along the walls of the pipe is not influenced by the pressure drop, but the SPL curves are just shifted. The mismatch between the most intense noise and the lowest one is about 9 dB. Finally, another influence of the pressure drop on the SPL curves is on the position of the noise peaks that move downstream increasing the flow-rate following the jet length.

4.2.3 Acoustic Pressure Inside the Pipe

The SPL curves computed with LES and with APE$_{\overline{B}}$ displayed in figure 4.9 are not perfectly coincident in the region around the peak of noise. Such a difference is investigated with a comparison of the acoustic pressure inside the pipe: from the APE$_{\overline{B}}$ results (figure 4.4.(d)) it is evident the formation of alternated p_a structures localized in the shear layer with

a growing intensity moving downstream up to reach their maximum just after the end of the jet (figure 4.4.(d)). This is exactly the position where the peak of the SPL is located and along the walls of the pipe there is a correspondence between the SPL trend and the intensity of the acoustic pressure.
The decrease of noise after its peak is justified by the decay of the intensity of these structures. Furthermore, the change in the slope of the SPL curve's decreasing branch placed about at $x = 9d$ suggests that the acoustic influence of these structures does not goes further than that section. Their influence is just localized to their very-near field. In fact, if the noise far from the orifice was due to emission of the structures it should not change its behaviour moving away from the end of the jet where the most intense structures are located.
On the other side, it is clear that the fast decrease of SPL just downstream of the peak is an indicator of the local effect of the acoustic pressure structures and of the fast decay suffered by the noise generated by them. The noise far from the orifice must be thus produced by another source that is the one placed at the end of the jet where, according to the turbulent kinetic energy in figure 4.8, is located the region of strongest noise generation.

The considerations just explained are even enforced by the comparison of the acoustic pressure field from $\text{APE}_{\overline{B}}$ with the one computed with LES. The pressure fluctuations returned by LES are visualized in figure 4.11. At a first glimpse the qualitative pattern looks a bit different than the one from the $\text{APE}_{\overline{B}}$ (figure 4.4.(d)). The structures in the shear

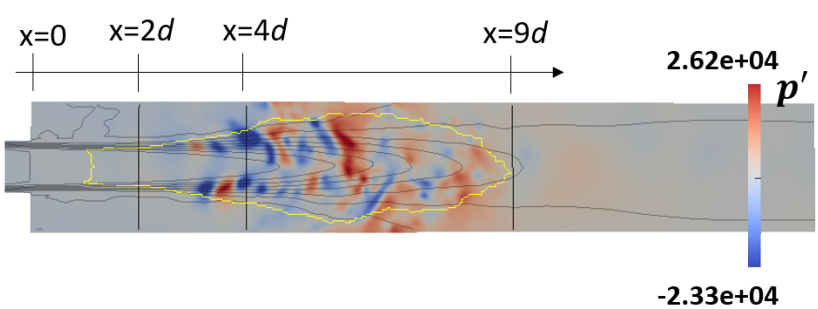

Figure 4.11: *Instantaneous acoustic pressure field downstream of the orifice on a longitudinal section of the pipe and contours of the time-averaged longitudinal velocity calculated with LES. In yellow the boundary of the acoustic source region; in grey contours of the mean axial velocity.*

layer are still present but their dimension and intensity are lower than the one computed with the APE. Despite such differences, their generation mechanism and dynamics inside the pipe are exactly the same described by the APE system. The birth of these structures, in fact, happens about at half length of the jet in the annular shear layer and it is due to the interaction of pre-existing pressure perturbations with the flow. In particular in the shear layer the gradient of the velocity and the vorticity (figure 4.7) are very high and give a contribute to the noise generation and to the refraction of the acoustic wave. The structures are then convected by the mean flow towards the end of the potential core where they are no more confined in the shear layer but fill the transversal section of the pipe.
The difference between LES and APE$_{\overline{B}}$ acoustic pressure is that APE overestimates the intensity and the dimension of the structures; when they are convected downstream they locally hide the contribute of the other chaotic structures not confined in the shear layer. For a better characterization of the phenomenon it is possible to define four regions downstream of the orifice according to the information from LES about both fluid-dynamics and the acoustics:

1. just downstream of the orifice (between 0 and $2d$) the shear layer has a very low thickness and it is filled by high vorticity that, nevertheless, here does not generate noise [25];

2. between $2d$ and $4d$ the thickness of the shear layer increases and the interaction of the pre-existing noise with the sheared flow induces the generation of further noise in the form of order structures of alternate negative and positive acoustic pressure;

3. the structures are convected downstream towards the end of the jet and enter the region between $4d$ and $9d$ where the potential core is no more present and the turbulent flow fills each transversal section of the pipe. In this region, according to the turbulent kinetic energy, the most intense part of the source region is located. The acoustic pressure pattern is no more so ordered as in the previous region but it is more chaotic (figure 4.11)

4. downstream of $9d$ the turbulence vanishes and the intensity of the acoustic pressure decreases fast.

As already pointed out, the structures generate a noise that decays very fast. Such a statement is enforced by the comparison of both p_a

and SPL computed with LES and $\text{APE}_{\overline{B}}$. In the shear layer the acoustic pressure returned by $\text{APE}_{\overline{B}}$ is almost one order of magnitude higher than the one from LES, but APE's SPL peak is just 1 dB higher than the one from LES. The noise produced by the structures in the shear layer decays so fast that on the walls its contribute is already smoothed. The structures hereby described play a key-role in the definition of the shape of the curve of the SPL on the walls with its local increase of noise, but their influence on the noise outside of the shear layer is negligible because of their fast decay.

4.3 New Modified APE

The results obtained from the tested APE and from the LES highlighted the irrelevance of the acoustic structures in the shear layer on the noise far from the orifice. The applicability of the APE to industrial problems encourages to find the fastest formulation for obtaining the desired information. In the field of valves manufacturers, the reference international standards characterize the noise emission of a device with the SPL evaluated 1 meter downstream of it [28]. When this distance is far enough from the device it is useless to spend time and resources for the description of the near field structures detected in the shear layer. A smart numerical approach should be based on the reduction of computational time for the description of those structures that do not influence the noise prediction in the position indicated by the standards. For this reason a new formulation of APE is here proposed without the terms that describe the noise generation mechanism in the shear layer.

In order to identify them, a deeper comprehension of the physical meaning of the terms in the APE system (2.24) is needed. In [16] a different interpretation of the APE is given: the system is not derived with the flow decomposition (2.22) but with the application of a filter on the Euler equations' source terms that modifies them exciting only the acoustic modes. Since the source term of the acoustic pressure equation (2.24a) has been considered negligible, here the discussion is focused on the equation for the acoustic particle velocity. When the filter is applied to the momentum balance equation of the linearized Euler equations, its filtered source term that excites only the acoustic modes can be written as the gradient of a potential field $\nabla\Phi$. The potential Φ is decomposed in three terms that represent different contributes to the noise generation

[16]

$$\nabla\Phi_1 = \overline{\mathbf{u}}\cdot\nabla\mathbf{u}_a + \mathbf{u}_a\cdot\nabla\overline{\mathbf{u}} \tag{4.4a}$$

$$\nabla\Phi_2 = \frac{\nabla\overline{p}}{\overline{\rho}} \tag{4.4b}$$

$$\nabla\Phi_3 = \mathbf{u}_t\cdot\nabla\mathbf{u}_t + \mathbf{u}_t\cdot\nabla\overline{\mathbf{u}} + \left(\mathbf{u}_t\cdot\nabla\mathbf{u}_t\right)'. \tag{4.4c}$$

When the flow is isentropic, simplifications can be introduced on these three terms: $\nabla\Phi_1$ and $\nabla\Phi_3$ are the only two terms that generate noise while $\nabla\Phi_2$ can be moved to the left-hand side since it does not work as source term. The comparison of these three term with the acoustic particle velocity equation (2.24b) suggests that, in the APE system (2.24), $\nabla\Phi_3$ is included inside the source term $\mathbf{S_u}$, while $\nabla\Phi_1$ is moved to the left-hand side because it contains the acoustic particle velocity. Even though $\nabla\Phi_1$ is on the left-hand side of (2.24), it is a noise generator. Furthermore, it can be manipulated and thanks to irrotationality of $\mathbf{u}_a$, it can be rewritten as

$$\nabla\Phi_1 = \nabla\left(\overline{\mathbf{u}}\cdot\mathbf{u}_a\right) + \overline{\boldsymbol{\omega}}\times\mathbf{u}_a, \tag{4.5}$$

where $\overline{\boldsymbol{\omega}}$ is the vorticity of the mean velocity. This formulation helps to clarify the interaction of the acoustic wave with the mean flow and with its mean vorticity, and their influence on the noise generation mechanisms. These effects are in fact the responsible of the generation of the structures in the shear layer. For this reason and with the purpose described before to reduce to complexity of the APE system, the new formulation of APE is obtained removing the terms contained in $\nabla\Phi_1$. The new modified APE system is thus

$$\begin{cases} \dfrac{\partial p_a}{\partial t} + \overline{u}_j\dfrac{\partial p_a}{\partial x_j} + \gamma\left(\overline{p}\dfrac{\partial u_{aj}}{\partial x_j} + p_a\dfrac{\partial \overline{u}_j}{\partial x_j}\right) + u_{aj}\dfrac{\partial\overline{p}}{\partial x_j} = 0 & \text{(4.6a)} \\ \dfrac{\partial u_{ai}}{\partial t} + \dfrac{1}{\overline{\rho}}\dfrac{\partial p_a}{\partial x_i} - \dfrac{p_a}{\overline{\rho}^2 c^2}\dfrac{\partial\overline{p}}{\partial x_i} = S_{\mathbf{u}i}. & \text{(4.6b)} \end{cases}$$

The equation for the acoustic pressure is exactly the same as the previous APE system. The removal of the two terms described by $\nabla\Phi_1$ has effect only on the left-hand side of the equation for $\mathbf{u}_a$. The source term $\mathbf{S_u}$ is modelled as suggested by the analysis presented in section 4.2 with the Bailly SNGR and the zero-mean source.

From the numerical point of view, the simplification introduced in the new formulation changes the structures of the linear system associated to the equation for the acoustic particle velocity. In the APE system (2.24) $\mathbf{u}_a$ is an implicit quantity and the matrix of the linear system has non-null off-diagonal terms connected to its derivatives. In the new formulation the matrix for equation (4.6b) is diagonal and this simplification allows to change the method for the resolution of the system from an iterative approach to a faster direct one. In addition to this, the coupling between the two equations (acoustic pressure and acoustic particle velocity) is extremely reduced and less iterations are required in order to reach the convergence at each time step. The overall reduction of computational time is about the 20%.

4.3.1 Acoustic Prediction with the Modified APE

The new APE formulation is now applied to the same case described before and, as for the comparison made in section 4.2.1, it is run with the mean field obtained from the time-averaged quantities from LES. As expected, the acoustic pressure is distributed in the domain with a

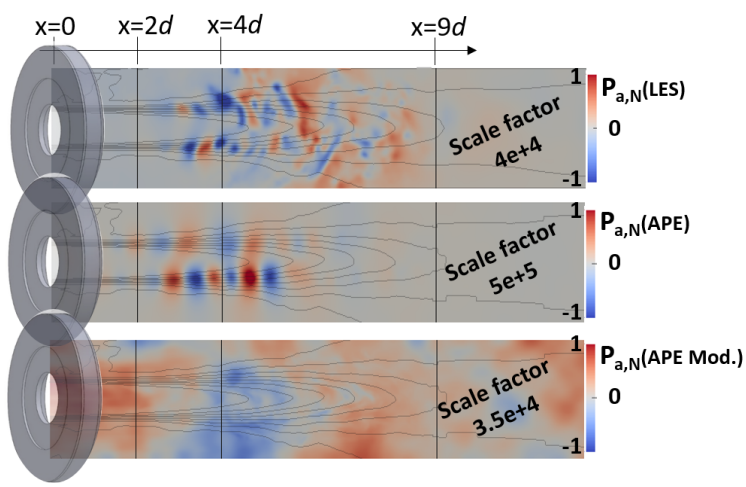

Figure 4.12: *Instantaneous acoustic pressure p_a computed with different numerical methods: LES, APE system* (2.24) *and new modified APE* (4.6). *Different scales according to the own values.*

completely different pattern from the ones computed with the previous methods. Figure 4.12 compares the output of the different simulations

scaled with a proper factor in order to have a similar qualitative representation of the acoustic pressure pattern. The results show that the typical structures described in the previous sections are not generated in the shear layer by the new modified APE. The terms in $\nabla\Phi_1$ are thus the only responsible for the generation of those structures, whose nature is due only to the mutual interaction between the acoustic wave and the sheared flow field.
Despite the absence of those structures, the results coming from the new APE are interesting because of the intensity of the acoustic pressure that is of the same order of magnitude of the oscillations described by the LES. Further comparison can be done looking at the SPL curve on the walls (figure 4.13): as expected close to the orifice the SPL does not have the typical hill-shaped profile due to the increasing intensity of the structure in the shear layer, but far from the resistor it overlaps the noise computed with the complete APE system (2.24). This is a further confirm that the p_a structures affect the noise only locally with the peak of SPL close to the end of the jet, but their influence on the radiated sound is completely negligible.

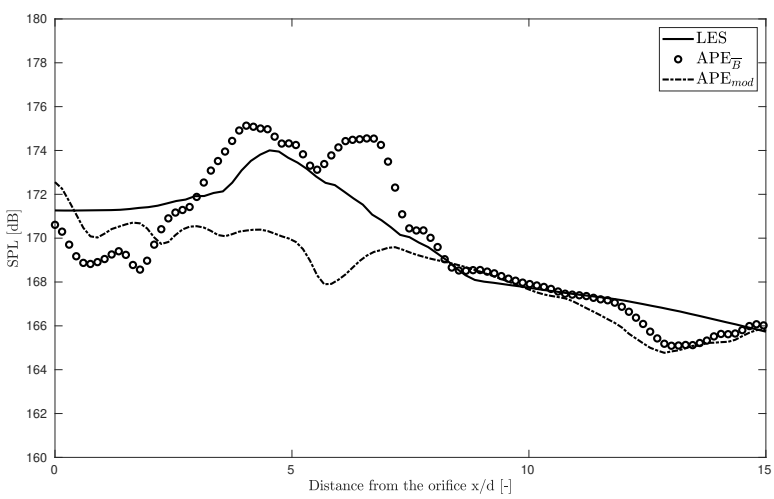

Figure 4.13: *Sound pressure level downstream of the orifice computed with different APE systems.*

In industrial applications the interest in the noise prediction is concentrated on the noise 1 meter downstream of the valve. When such a distance is far enough from the control device it is thus possible to apply

the new APE (4.6) for a successful noise prediction. The disclaimer between near and far is given by the dimension of the jet: for instance, in the case of the orifice, the dimension of the jet is given by the diameter of the perforation. It is thus possible to state that when the diameter of the orifice is small enough to have $9d < 1$ m the new APE formulation is able to return, with a lower computational burden, the same prediction as the previous APE formulation (2.24).

4.4 Main Results with APE

The application of the Acoustic Perturbation Equations for the prediction of the internal Sound Pressure Level emitted by an orifice has been investigated. The APE are solved after a compressible RANS simulation (fastest CFD approach) coupled with a SNGR model for the synthesis of the turbulent velocity. The choice of the fluid-dynamic models (RANS+SNGR) is driven by the necessity to apply this numerical analysis to industrial applications that claim for results in very short time.
The APE formulation has been chosen among several literature formulations: it is directly derived from the Euler equations with the decomposition of the flow in a mean part and in turbulent and acoustic fluctuations. Linearization of the second order acoustic quantities has been performed.
Two SNGR models (Karweit method and Bailly one) has been compared: they are selected because of their low computational burden and low quantity of stored data.
The combination of the two possible SNGR models with two possible source term formulations gives four possible combinations that have been compared among them and with a LES solution. All the four APE formulations describe the generation of acoustic pressure structures in the shear layer due to the interaction of pre-existing noise with the sheared flow. The APE formulation written with the Bailly method for the SNGR and the zero-mean source term returns SPL on the pipes' wall similar to the LES one. Despite such a similarity, the intensity of the acoustic pressure of the structures in the shear layer is overestimated by the APE. The nature of these structures has been investigated and it has been found that their contribute to the noise is just local and the sound they generate decays very fast. For this reason, the difference between the APE and the LES is more evident on the intensity of the acoustic pressure inside the domain (in the shear layer) than on the SPL evalu-

ated on the walls.
Furthermore, the noise far from the orifice has been computed neglecting the influence of these structures with a new APE formulation. This new system is preferable to the first APE formulation because of its reduced computational time obtained thanks to the simplification of the mathematical terms that describe the generation of the acoustic pressure structures in the shear layer. As supposed, the SPL prediction returned by the new APE formulation far from the orifice is in accordance with the noise computed with the other methods even though the structures in the shear layer are not described.
The international standards measure the noise 1 meter downstream of the tested device: for all those devices which develop a small jet at their outlet, the new APE formulation is thus a reliable and faster system for SPL computation.

CHAPTER 5

Numerical Evaluation of Valves' Parameters in International Standards for Industrial Aerodynamic Noise

In this chapter another approach for the estimation of valves' noise emission is presented. In chapter 4, APE have been introduced and a physical description of the noise generation mechanisms has been provided. A new fast APE formulation has been formulated in order to reduce the computational time as much as possible. Anyway, industries are also asked to be able to characterize their products in an even faster way based on the identification of valves' parameters that allow the noise prediction according to international standards. Several standards have been developing manuals with world-wide accepted procedures for testing and characterization of the flow-control devices. Example of the international standards are the *Organisation Internationale de Normalisation* **ISO**, the *International Electrotechnical Commission* **IEC** and the *Instrumentation, System, and Automation Society* **ISA**. In this work, the IEC international standard is used as reference for the noise prediction procedure in control valves.

The purpose of the study presented in this chapter is the numerical estimation of those parameters that characterize a control devices and whose values must be known to valves' manufacturers.
In the first part of the chapter the IEC international standard for aerodynamic sound in control valves is described. The focus is then moved on the estimation of a particular parameter A_η which plays a fundamental role in the definition of the amount of mechanical energy converted into noise.

5.1 Reference IEC International Standard for Control Valve Aerodynamic Noise

The reference international standard for aerodynamic noise prediction used in this work is the IEC 60534-8-3 [28] which describes a procedure for the acoustical characterization of a control valve. The purpose of this standard is the estimation of the external noise perceived 1 meter away from the pipe's outer wall and 1 meter downstream of the valve body. The equations that define valve's working regimes and all the quantities involved in the acoustic characterization are described by the procedure in different steps:

1. the mechanical power of the flow is evaluated from hydraulic and fluid-dynamic quantities;
2. the internal acoustic power is computed as a portion of the mechanical power;
3. the internal sound is decomposed in frequency bands;
4. the contribute of each frequency is transmitted outside of the pipe through its walls;
5. the noise is propagated 1 meter far from the external pipe and the SPL is evaluated.

A graphical representation of the steps of the IEC procedure is visualized in figure 5.1.

The first hydraulic and fluid-dynamic quantities that are introduced are the pressure at the sides of the valve (p_1 measured $2D$ upstream of the valve and p_2 evaluated $6D$ downstream [29]), the upstream density ρ_1 and temperature T_1 and the mass flow rate Q_m. The *liquid pressure recovery factor* F_L and the differential pressure ratio $X = \Delta p/p_1$ are

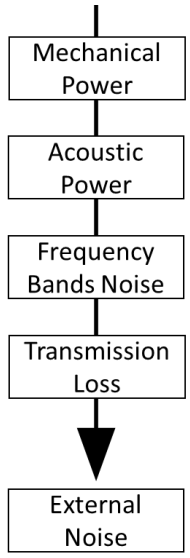

Figure 5.1: *Scheme of the IEC procedure for valve aerodynamic noise prediction [28]*

then introduced for the computation of the characteristics of the flow in the vena contracta, i.e. its pressure p_{vc}, its temperature T_{vc}, Mach number M_{vc} and speed of sound c_{vc}.
The differential pressure ratio is used for the definition of the flow regime in which the valve operates (in this work the flow always belongs to the subsonic regime). The quantities evaluated in the vena contracta are, on the contrary, computed as function of the parameter F_L. This is one of the four parameters that be provided by the valves' producers for their devices' acoustical characterization. From the information about the flow in the vena contracta, the mechanical power of the flow is calculated as

$$W_m = \frac{Q_m \left(M_{\mathrm{vc}}\, c_{\mathrm{vc}}\right)^2}{2}. \tag{5.1}$$

The acoustic power W_a is a fraction of the mechanical one. Their ratio is defined by the acoustical efficiency factor $\eta = W_a/W_m$ whose computation is performed as

$$\eta = 10^{A_\eta} F_L^2\, M_{\mathrm{vc}}^3, \tag{5.2}$$

where A_η is the *valve correction factor for acoustical efficiency* and it is the second parameter required for the characterization a control-device.

The internal sound pressure level on the walls of the pipe is then computed from the acoustic power W_a and from the outlet density ρ_2, the outlet speed of sound c_2 and the related Mach number M_2. A spectral decomposition of this noise in one-third octave bands associating a proper intensity to each central frequency. The shape of the spectrum is modelled according to the peak frequency f_p that defines the band with the highest acoustic energy. For the definition of f_p two other fundamental parameters for the acoustic characterization must be introduced: they are the *valve style modifier* F_d and the *Strouhal number for peak frequency calculation* St_p. The former is used for the evaluation of the diameter of the jet at the outlet of the valve

$$D_j = 4.6 \cdot 10^{-3} F_d \sqrt{C_V \; F_L}. \tag{5.3}$$

The Strouhal number St_p is then involved in the computation of the peak frequency

$$f_p = \frac{St_p \; M_{\mathrm{vc}} \; c_{\mathrm{vc}}}{D_j}. \tag{5.4}$$

Once the spectrum of the noise is computed, each frequency band is transmitted outside of the pipe through the walls according to the transmission loss function. The amount of noise dissipated during the passage through the walls depends on the frequencies and on the characteristics of the pipe as thickness, natural frequency and material.

The external noise is finally propagated 1 meter far from the pipe with a cylindrical law.

In all the steps here described, four parameters about the fluid-dynamic and acoustic behaviour of the valve have been introduced (F_L, A_η, F_d, St_p). Their usage in the procedure for noise prediction is described in figure 5.2. The four parameters are the quantities that characterize each flow-control device and that must be provided by valves' manufacturers. Their estimation is described in the next sections: the discussion starts from the fluid-dynamic parameters F_L and F_d and then deals with the acoustic ones A_η and St_p.

5.1.1 Estimation of the Fluid-Dynamic Parameters $\mathbf{F_L}$ and $\mathbf{F_d}$

The liquid pressure recovery factor F_L and the valve style modifier F_d are the two parameters connected to the fluid-dynamics. The former is connected to the fraction of energy that is recovered downstream of

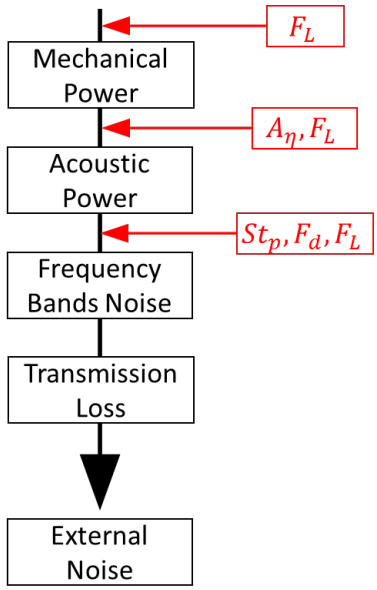

Figure 5.2: *Scheme of the IEC procedure for valve aerodynamic noise prediction [28]*

the valve with the conversion from kinetic energy to potential and it is defined as

$$F_L = \sqrt{\frac{p_1 - p_2}{p_1 - p_{\mathrm{vc}}}}. \tag{5.5}$$

The latter is defined as a geometric ratio between the hydraulic diameter of a single flow passage d_H and the equivalent circular diameter d_0 of the total passage area

$$F_d = \frac{d_H}{d_0} = \frac{4A_H/I_W}{\sqrt{4n_0\ A/\pi}}, \tag{5.6}$$

where A_H is the area of a single flow passage, I_W its wetted perimeter and n_0 the number of independent and identical flow passages.

Both the parameters have a definition that, for complex devices, is not applicable because the vena contracta cannot be easily identified and because often there are flow passages with different shapes and areas. For this reasons, the international standards [29] defines other ways to estimate them with different formulations. The F_L, for instance is evaluated with increasing pressure drop tests (upstream pressure p_1 fixed) until the choked flow is reached and the maximum flow-rate is evaluated.

The F_d on the contrary can be evaluated according to a procedure described in [29] with test where the Reynolds number is so low that a laminar flow is obtained.

These procedures are suggested for experimental campaigns but, in principle, they can be followed by numerical simulations too. Indeed, for the numerical evaluation of the F_L it is possible either to use its definition (in simple geometries as the orifice) or to simulate the choked flow with multiphase models that take into account the generation of vapour bubbles when the liquid pressure goes under the liquid vapour pressure [21, 38, 49].
The valve recovery factor, on the contrary, needs a very simple CFD simulation because it is computed with a low-Reynolds laminar flow and no turbulence model is thus required.

Their computation is feasible with numerical methods that require a reasonable computational time independently from the size of the simulated device. This is the biggest advantage of the numerical approach respect to the experimental one that, especially with big-sized devices, is very expensive because of the costs of realization of the valve and of the plant on which it can be tested.

5.1.2 Estimation of the Acoustic Parameters $\mathbf{A}_\eta$ and $\mathbf{St_p}$

The parameters that describe the acoustic behaviour of a device are the valve correction factor for acoustical efficiency A_η and the Strouhal number for peak frequency St_p. In the IEC 60534-8-3 international standard there are no equations or definitions for those quantities that can be used for their estimation on new devices. On the contrary, only general information on their values for particular devices are indicated in a table that is here reported in figure 5.3.

In addition to those information, A_η is suggested to be equal to "-4 for a pure dipole noise sources as for free jets in a big expansion volume" [28]. It is also stated that it can be dependent on the differential pressure ratio X but, nevertheless, the tabulated A_η values for different valves do not change with the flow conditions.
The range for the St_p parameter changes between 0.1 and 0.3 for free jets, but the reported values are in the range between 0.19 and 0.3. Unlike A_η the Strouhal number for peak frequency is not assumed to change with the flow conditions.

Valve or fitting	*Flow direction*	A_η	St_p
Globe, parabolic plug	Either	-4,2	0,19
Globe, V-port plug	Either	-4,2	0,19
Globe, ported cage design	Either	-3,8	0,2
Globe, multihole drilled plug or cage	To open	-4,8	0,2
Globe, multihole drilled plug or cage	To close	-4,4	0,2
Butterfly, eccentric	Either	-4,2	0,3
Butterfly, swing-through (centered shaft), to 70°	Either	-4,2	0,3
Butterfly, fluted vane, to 70°	Either	-4,2	0,3
Butterfly, 60° flat disk	Either	-4,2	0,3
Eccentric rotary plug	Either	-3,6	0,3
Segmented ball 90°	Either	-3,6	0,3
Drilled hole plate fixed resistance	Either	-4,8	0,2
Expander	Either	-3,0	0,2
NOTE 1 These values are typical only. Actual values are stated by the manufacturer. NOTE 2 Section 8 should be used, for those multihole trims, where the hole size and spacing is controlled to minimize noise.			

Figure 5.3: *Table 4 from IEC 60534-8-3 [28] with the suggested values for the A_η and St_p parameters for particulars devices.*

The IEC table in figure 5.3 is the only reference provided by the international standard for the definition of the values of A_η and St_p. The reliability of the values indicated in the table is questioned in section 5.2.1. A good estimation of A_η in particular is crucial for the noise prediction because a variation of 0.1 in its value leads to a variation of 1 dB in the prediction of the external noise.

No direct methods are proposed by the IEC for the evaluation of St_p and A_η; the only way to deduce their values is through the computation of related quantities and to the inversion of the equations presented in the international standards. With an experimental approach the St_p is can be evaluated measuring the peak frequency with a microphone and inverting equation (5.4), assuming F_d known.
Similar approach can be followed by numerics even though an expensive (from the computational point of view) CAA simulation should be solved.

The estimation of A_η can be only performed from the acoustical efficiency η (5.2) that, on turn, must be computed as the ratio between the mechanical and the acoustic power. In the experimental approach the

real challenge is the measurement of the acoustic power of the source inside the pipe. On the contrary, with a numerical approach and acoustic models it is possible to estimate the same quantity as illustrated in the next sections.

5.2 Estimation of A_η Curve from CFD

The most critical parameter among the four that the valves' manufacturers have to provide for the acoustical characterization of their devices is the valve correction factor for acoustical efficiency A_η. In fact, in the previous sections it has been shown that the fluid-dynamic parameters F_L and F_d can be computed with numerical simulation and with equations from the IEC standard (section 5.1.1).
Among the acoustic parameters (A_η and St_p) the valve correction factor for acoustical efficiency is the one that most influence the external noise as can be seen with a sensitivity analysis on those two parameters. Figure 5.4 describes the noise emitted by a perforated plate according to the IEC procedure changing the acoustical parameters in the ranges indicated in the standard. A perforated plate correspond to a "drilled hole plate fixed

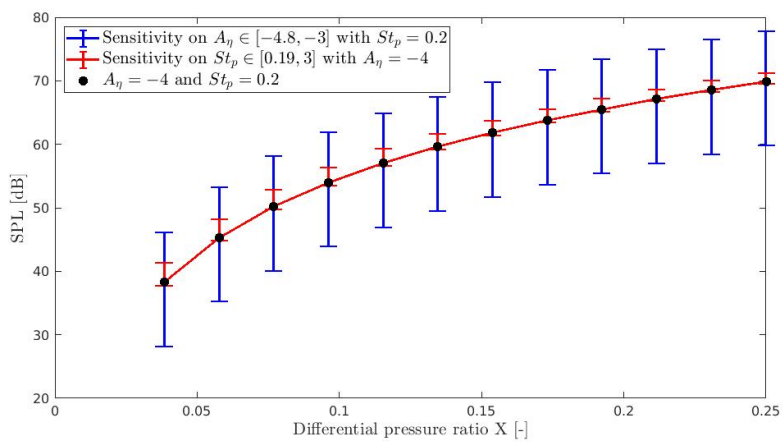

Figure 5.4: *Variability of the external noise evaluated according to the IEC procedure with the acoustic parameters A_η and St_p.*

resistance" in figure 5.3 and its characteristic values are $A_\eta = -4.8$ and $St_p = 0.2$. In figure 5.4 the two parameters changes in the range described by the IEC, i.e. $A_\eta \in [-4.8, -3]$ and $St_p \in [0.19, 0.3]$. The incidence of the variability of A_η is much higher than the one due to the

uncertainty on St_p: the noise changes up to 18 dB changing the values of A_η while the variation due to St_p is limited to no more than 3.6 dB. The black-dotted curve is obtained with $A_\eta = -4$ that is the general value for a dipole source (it is not set equal to -4.8 as suggested by the table because this is one of the extreme of the A_η range) and with $St_p = 0.2$ that is the one suggest for the drilled holed resistance.

Because of the major influence of the valve correction factor for acoustical efficiency on the external noise, the focus of the developed research has been moved on A_η. In particular the work here presented is about the identification of acoustical models that, from CFD simulations, are able to estimate A_η taking into account its dependency on the flow conditions.

5.2.1 Experimental Evidences

The necessity of a more detailed investigation on A_η is justified by its variability with the flow and by its high incidence on the noise prediction. In addition to this, some previous experimental data [39] are also available for a qualitative analysis on A_η. In [39] the noise emitted by a perforated plate (different from the one here considered and described in figure 5.6) was measured with external microphones for a statistical analysis on the best combination of the valves' parameters that return a noise estimation close to the measurements. Figure 5.5 suggests few considerations on the trend of A_η:

- the experimental data describe a noise higher than the one returned with the prediction according to IEC. The value of A_η used for the two black series are not coherent with experimental evidences;
- as expected, the black series are shifted among them of 8 dB because of a constant difference of 0.8 in the A_η values;
- the distance of the experimental red series from the black ones is not constant.

The first consideration suggests that the A_η values indicated by the IEC standard are not good enough to be in accordance with experimental data. The most important consideration is anyway the third one: A_η is not constant changing the pressure drop at the sides of the valve. In fact, the second observation shows that two different values of A_η return curves that are shifted of a constant amount. This does not happen for

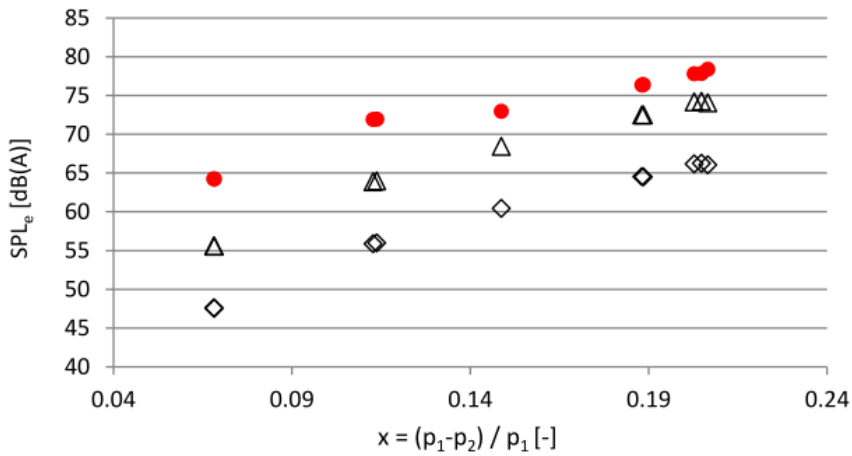

Figure 5.5: *Noise prediction according to IEC with A_η=-4 (△) and A_η=-4.8 (◊) and experimental data (●). Figure from [39]*

the experimental data. The assumption of working with a constant A_η as indicated in the table in figure 5.3 is not consistent with the experimental evidences. A good characterization of A_η can be thus obtained only if its prediction returns a value that changes with the pressure drop.

5.2.2 Acoustic Model for the Numerical Estimation of W_a

The estimation of A_η, as already pointed out, cannot be fulfilled with its direct evaluation but it is made through the values assumed by the acoustical efficiency η. The point is thus moved to the modelling of the acoustic power W_a and the mechanical one W_m, whose ratio defines η. The equation for the mechanical power is indicated by the IEC (5.1). On the contrary, the international standard's equation cannot be used for the evaluation of W_a because it assume the parameter A_η to be known. This equation states that

$$W_a = \left(10^{A_\eta} F_L^2 \, M_{\mathrm{vc}}^3\right) W_m. \tag{5.7}$$

An alternative method for the modelling of the acoustic power is based on literature acoustic models developed according to Lighthill's theory. It has been discussed about the fundamental sources' acoustic power in section 2.2 and it has been shown that it is possible to estimate their intensity's order of magnitude, regardless the type of the source. In aero-acoustics the power of the sources is connected to the characteristic

quantities of the flow as velocity, density and distances. For the fundamental sources (monopole, dipole and quadrupole), the following points are valid:

- A monopole is characterized by the acoustic power $W_M = \frac{4\pi r^2 p_{\mathrm{rms}}^2}{\rho_0 c}$ (2.6). The characteristic length for the radius r is a typical dimension of the domain L, while the pressure p_{rms} can be related with dimensional analysis to the product of $\rho_0 U^2$ where U is for instance the mean flow velocity. The order of magnitude of the acoustic power of a monopole is thus

$$W_M \approx \frac{\rho_0 L^2 U^4}{4\pi c} \approx \frac{\rho_0 L^2 U^3}{4\pi} M. \tag{5.8}$$

  The sound power radiated by an aerodynamic monopole scales with the fourth power of the flow velocity.

- The power of a dipole is $(d/\lambda)^2$ times greater than the one from a monopole. The wavelength λ scales as Lc/U and the radiated power thus scales as

$$W_D \approx \frac{\rho_0 d^2 U^6}{3\pi c} \approx \frac{\rho_0 d^2 U^3}{3\pi} M^3, \tag{5.9}$$

  that means the power radiated by a dipole scales with the sixth power of the velocity. For a subsonic flow a monopole radiates a sound power higher than the dipole because their ratio goes with the second power of the Mach number.

- An aeroacoustic quadrupole radiates a power whose ratio with the monopole's one is described by equation (2.8). For a lateral quadrupole the power is

$$W_Q \approx \frac{\rho_0 d^2 U^8}{15\pi c^5} \approx \frac{\rho_0 d^2 U^3}{15\pi} M^5 \tag{5.10}$$

  and it scales with the eighth power of the mean flow velocity. The denominator in equation (5.10) changes with the type of quadrupole: a more general law was derived by Lighthill [35, 36] in the *eighth power law* that states

$$W_Q = K_L \frac{\rho_0 d^2 U^8}{c^5} \tag{5.11}$$

  where K_L is a constant.

In the aero-acoustics theory the turbulence that generates noise is modelled as a quadrupole. The eighth power law is thus a valid approach for the estimation of the acoustic power of the quadrupole inside the fluid.
Further developments of the Lighthill's theory focused on the derivation of acoustic models for the definition of the acoustic power density $\mathcal{P}$, i.e. the power per volume unity radiated by the turbulent flow. One of the models write it as [47]

$$\mathcal{P} = \alpha_P \, \epsilon M_t^5, \tag{5.12}$$

where α_P is a constant, ϵ is the turbulent dissipation rate and M_t is the turbulent Mach number defined as the ratio between the turbulent velocity and the local speed of sound.
The quantities involved in equation (5.12) refer to the flow turbulent properties and their evaluation can be exploited with CFD numerical simulations. Furthermore, under the assumption of isotropic turbulence, the turbulent velocity can be written as function of the turbulent kinetic energy K and the equation (5.12), known as Proudman equation, can be rewritten as

$$\mathcal{P} = \alpha_P \, \epsilon \left(\frac{\sqrt{2K/3}}{c} \right)^5 . \tag{5.13}$$

With this new formulation, the numerical computation of the quantities that appear inside equation (5.13) is simpler than the previous one because it is no needed to compute the turbulent velocity, but information on the turbulent kinetic energy are enough. Steady RANS simulations are the fastest approach that returns all the information about K and ϵ needed for the estimation of the acoustic power density. This method is exactly the one that is used in this work for the analysis presented in section 5.3.
According to literature, the value of the constant α_P varies in that range from 0.629 to 13. In this work, a re-scaled model it is used and the constant is set equal to 3.804 [50].
Once the acoustic power density is computed from the CFD simulation and the Proudman acoustic model, the acoustic power W_a of the source region is numerically evaluated integrating $\mathcal{P}$ over the source region

$$\widehat{W_a} = \int_{S.R.} \mathcal{P}(\mathbf{x}) \, d\mathbf{x}^3. \tag{5.14}$$

The source region, as in the APE, is localized where the turbulent kinetic energy is higher than the 20% of the maximum K computed in the domain.

The hat will be use to distinguish the acoustic power $\widehat{W_a}$ computed with CFD simulation and the acoustic model, from W_a obtained following the equations described by the IEC procedure.

5.2.3 Computation of A_η from the Numerical Acoustic Power

The valve correction factor for acoustic efficiency A_η can be estimated thanks to the numerical computation of the acoustic power presented in the previous section. In fact, according to the equations presented in the IEC, the acoustic power is a function of A_η and they are connected as indicated by equation (5.7). The dependency of A_η from the acoustic power can be thus written as

$$A_\eta = \log_{10}\left(\frac{W_a}{F_L^2\, M_{\mathrm{vc}}^3\, W_m}\right). \tag{5.15}$$

The value of A_η is computable from this equation only if all the quantities on the right-hand side in equation are known. If the recovery factor F_L is known, the IEC standard give other equation for a trivial evaluation of the Mach number in the vena contracta M_{vc} and of the mechanical power W_m.
The intensity of the acoustic power W_a, on the contrary, cannot be computed from the IEC without using A_η. That is the reason why a procedure for the numerical estimation of the acoustic power $\widehat{W_a}$ has been proposed in the previous section with the equation (5.14). When $\widehat{W_a}$ is substituted into equation (5.16), it is possible to obtain an estimation of A_η as

$$A_\eta = \log_{10}\left(\frac{\widehat{W_a}}{F_L^2\, M_{\mathrm{vc}}^3\, W_m}\right). \tag{5.16}$$

This is the equation that is used in the following sections for the computation of A_η from the numerical simulations.

5.3 Numerical Prediction of the External Noise Produced by ISA Orifice

The numerical model for the estimation of A_η is applied again to an orifice, but with another geometry respect to the one presented in section 4.1. The new one is described by the ISA international standard [30] and it is chosen because its $F_L = 0.86$ is defined in the manual allowing

to take this data as a non-questionable parameter among the four that characterize a control device. For an orifice the F_d is computable with its definition and it is equal to 1.
The technical draw of the orifice is displayed in figure 5.6.

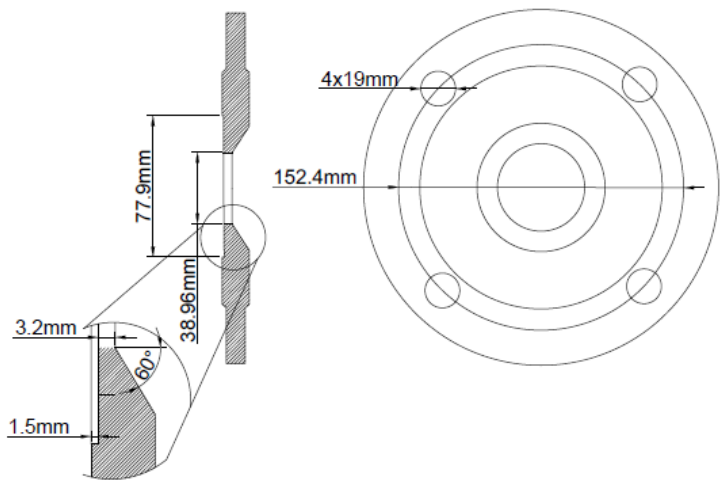

Figure 5.6: *Technical draw of the orifice described in the ISA international standard [30].*

The acoustic power has been here computed with different pressure drops at constant upstream pressure $p_1 = 5.2$ barA. The pressure drop goes from 0.1 bar to 1.3 bar that correspond to a flow whose jet Mach number is close to 0.8.

For the application of the Proudman model described in the previous section it is necessary to compute the turbulent quantities as the turbulent kinetic energy K and the turbulent dissipation rate ϵ with a compressible RANS simulation [20]. The simulation is run on a three dimensional domain for sake of simplicity in the integration over the source region, but it could be even run on the same slice of pipe as the one used for the RANS described in section 4.1.

The acoustic power density $\mathcal{P}$ is then computed in all the domain and then it is integrated over the source region in order to obtain an estimation of the acoustic power of the source. The trend of the acoustic power with the pressure drop is shown in figure 5.7. The acoustic power predicted with the acoustic model $\widehat{W_a}$ is between the curves obtained

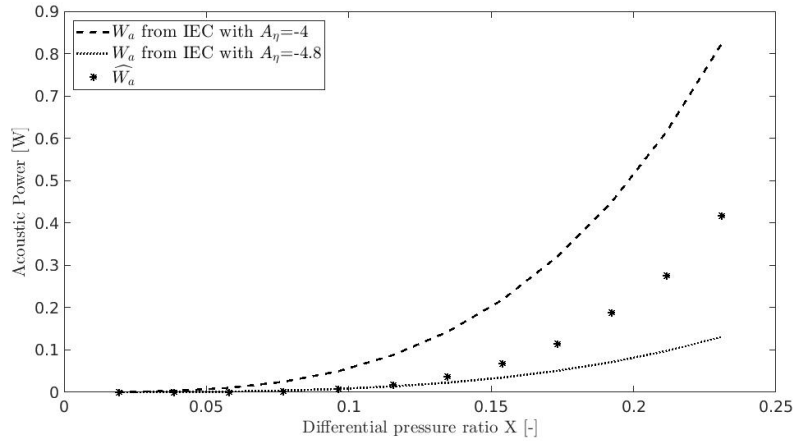

Figure 5.7: *Acoustic power depending on the differential pressure drop ratio X: comparison of the values return from the IEC procedure with A_η=-4 and -4.8, and of the numerical prediction $\widehat{W_a}$.*

applying the IEC procedure with a fixed value of A_η equal to -4 and -4.8. As in the experimental data described in figure 5.5, these values are chosen because they are the values indicated by the international standard for a generic drilled holed plate as the orifice, and the generic value for an acoustic source not included among the valves in table 5.3. The curve with $A_\eta = -4.8$ returns a lower value than the one with $A_\eta = -4$ because, as can be seen in equation (5.7), it means that a lower fraction of mechanical energy is converted into acoustic one.
The results returned by the numerical simulations with the application of the Proudman equation stand between those two curve suggesting that the numerical prediction is coherent with what is expected by the IEC.

All the three series in figure 5.7 grows according to power laws. The dependency of the acoustic power is not actually connected to the pressure drop but to the flow velocity as indicated in the laws described for the fundamental sources (5.8), (5.9) and (5.10). A logarithmic representation of the acoustic power allows to see the slope of the curves and to compare them also at small pressure drops. Figure 5.8 shows the acoustic power depending on the velocity of the jet (characteristic velocity for the phenomenon). The slope of the series evaluated with the IEC procedure is different from the one computed with the numerical model: the IEC series grows about with the sixth power of the velocity while the $\widehat{W_a}$ one with the eighth power in accordance with (5.10). The difference

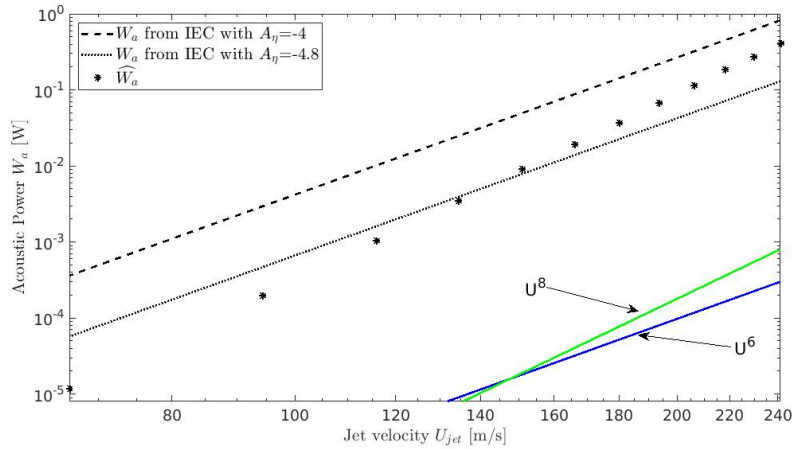

Figure 5.8: *Acoustic power depending on the velocity of the jet U_j in logarithmic scale: comparison of the values return from the IEC procedure with A_η=-4 and -4.8, and of the numerical prediction $\widehat{W_a}$. In the corner blue and green lines show the slope of the U^6 and U^8 curves.*

in the slope of the series must be searched in the modelling of the valve correction factor A_η. In fact, in the equation that describes the acoustic power evaluated according to the IEC procedure (5.7), the only way to modify its dependency on the velocity is to assume that A_η changes with the flow conditions (the other involved parameter F_L is not dependent on the pressure drop). The Mach number M_{vc} scales with the velocity and the mechanical power with its cube. In order to have $\widehat{W_a} \sim U^8$ is thus necessary to ask for

$$10^{A_\eta} \sim U^2 \tag{5.17}$$

that means

$$A_\eta \sim 2 \log_{10} U. \tag{5.18}$$

This theoretical analysis is confirmed by the graphical representation of the curve of A_η computed from the equation (5.16) and displayed in figure 5.9. The series of the values assumed by A_η is, for low pressure drops, under the -4.8 line that is crossed only over a certain pressure drop. When the downstream pressure is much lower than the upstream one, on the contrary, A_η assumes values that are close to the one suggested by the IEC since it stands between the values -4 and -4.8. Its numerical prediction is thus consistent with what expected by the international standards, but has the big advantage to describe its variation

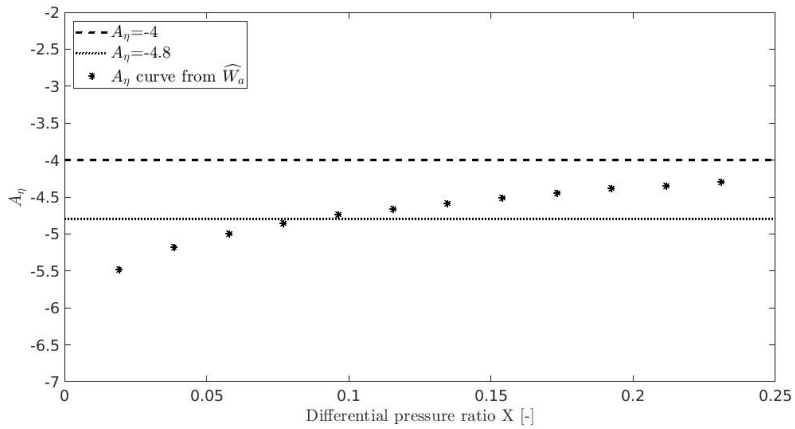

Figure 5.9: *Curve of the valve correction factor for acoustic efficiency A_η numerically computed with the acoustic power $\widehat{W_a}$. The horizontal lines represent the values -4 and -4.8 suggested by the IEC for a generic source and for a perforated plate.*

with the flow conditions, which the IEC is blind to.

The values of A_η lower than -4.8 for low pressure drops can be further investigated considering the Mach number over which the A_η series crosses the -4.8 line. Figure 5.10 represents the same series as figure 5.9 but with the Mach number on the x-axis. The numerical A_η becomes higher than -4.8 for a Mach number close to 0.4 that corresponds to a flow whose compressibility effects are low. With low compressibility, low noise is expected too and this is confirmed by the estimation of the external noise computed starting from the numerical acoustic power $\widehat{W_a}$ represented in figure 5.11. Once again, the curve of the numerical noise is lower than the curves from IEC for low pressure drop and in particular for a Mach number lower than 0.4. Even though this results means that numerics is underestimating the noise emission (not conservative prediction) it must be highlighted that this error is committed for an external SPL that is lower than 40 dB (noise intensity lower than a normal conversation). For significant noises, on the contrary, the prediction with the numerical acoustic power is higher than the curve with $A_\eta = -4.8$ and goes towards the value -4 suggesting that the acoustical efficiency η of the orifice grows with the pressure drop. Finally, for the orifice, it is possible to state that the value of $A_\eta = -4.8$ suggested by the IEC table 5.3 is not reliable for high Mach numbers where the acoustic efficiency is actually higher. This inaccuracy of the IEC procedure in the

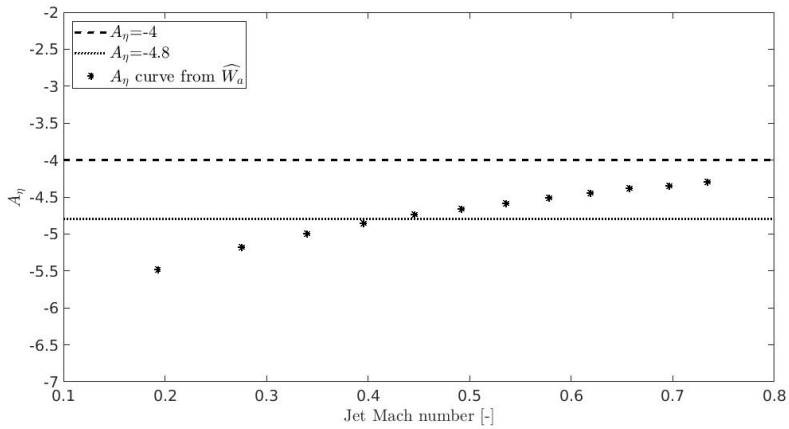

Figure 5.10: *Curve of the valve correction factor for acoustic efficiency A_η numerically computed with the acoustic power $\widehat{W_a}$ with the jet Mach number on the x-axis. The horizontal lines represent the values -4 and -4.8 suggested by the IEC for a generic source and for a perforated plate.*

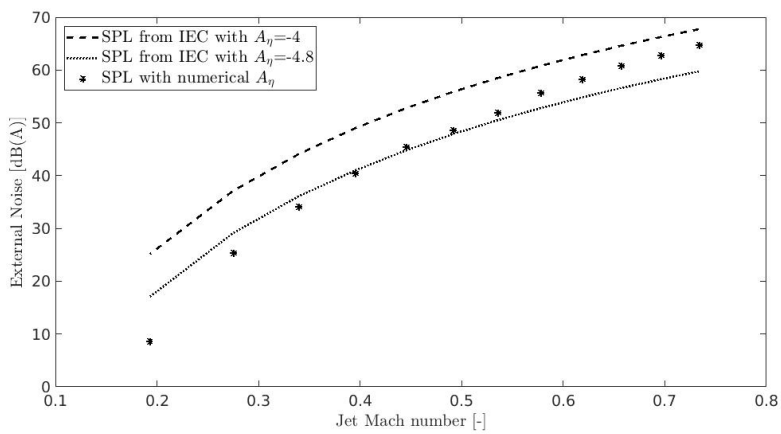

Figure 5.11: *External noise in the position indicated by IEC 60534-8-3, depending on the differential pressure drop ratio X: comparison of the values return from the IEC procedure with A_η=-4 and -4.8, and of the numerical prediction $\widehat{W_a}$.*

description of the A_η values may be connected to the fact that, as state in the introduction of the document IEC 60534-8-3, the values are validated with test made using air at moderate pressure and temperatures. The results here described are thus an interesting advancement respect to the indications provided by the IEC.

5.4 Main Results from the Application of Numerics on the IEC Procedure

The IEC 60534-8-3 international standard for the prediction of the noise emission of flow-control devices has been described in order to find out how the numerics can support the valves' manufacturers in the definition of the main acoustic features of their devices. The procedure for the noise prediction takes into account the device's characteristics with the introduction of four parameters, two connected to the fluid-dynamic behaviour and two to the acoustic one. The formers are the liquid pressure recovery factor F_L and the valve style modifier F_d whose values can be evaluated with procedures described by other IEC manuals and that can be followed both by experimental campaigns and by numerical simulations. The experimental approach is usually longer and more expensive because it needs the realization of the device and of the test plant, while the numerical approach results to be faster and cheaper.
The acoustic parameters that describe a control device are the Strouhal number for peak frequency St_p and the valve correction factor for acoustical efficiency A_η. Unlike the fluid-dynamic parameters no procedures or equations for their characterization is provided by the IEC standard, but their values are just tabulated for some devices under the assumption to be constant changing the flow conditions. The reliability of this assumption is questioned in this work in the light of previous experimental works that suggested a not constant behaviour of the A_η parameter. The numerics is here used for the study on A_η because it has been shown that its influence on the noise prediction is much more effective than the uncertainty on the Strouhal number.
It has been then explained how numerics can be used in collaboration with the IEC procedure for the prediction of A_η through the computation of the acoustic power. A literature model for the description of the acoustic power density has been used to predict the acoustic power of an orifice described in the ISA international standard. From the mean turbulent quantities computed with numerical CFD simulations it has been evaluated the orifice's acoustic power under different increasing pressure drop from 0.1bar up to 1.2bar. It has been shown that the numerical acoustic power lays between the values computed with the IEC procedure assuming $A_\eta = -4$ and -4.8 which are provided as typical values for a generic acoustic source and a generic perforated plate. The dependency of the acoustic power on the velocity of the flow is different

between the one returned by the literature model and by the IEC, and this difference must be ascribed to the assumption of constant A_η. Removing this constraint, a curve of A_η has been derived and it goes with twice the logarithm of the flow velocity.

Finally, a comparison on the external noise shows that the numerical prediction is lower than the IEC one only for SPL lower than 40 dB(A) (harmless noise) while it is in accordance with the IEC prediction for jet Mach numbers higher than 0.4. In these conditions the noise prediction stands between the curves with $A_\eta = -4$ and -4.8 with a progressive approach to the -4 curve suggesting that the value -4.8 indicated by the IEC for the perforated plates is not reliable.

The results here described are thus an advancement in the characterization of the A_η parameter whose values indicated in the IEC are simply validated with test at low pressure and assuming it not dependent on the flow conditions.

CHAPTER 6

Experimental Plant Design

In addition to the numerical approach, further information on the aerodynamic noise can be obtained thanks to experimental proofs. For this reason, the last part of this work is focused on the design of a new experimental plant on which can be performed tests whose results may be also compared to the numerical ones. In particular, the campaigns will be about the study of the influence of the pressure drop, the pressure drop ratio and the absolute pressure on the noise emission. In fact, none of these quantities controls the noise generation by itself but they all gave a contribute to the final results. For instance the pressure drop defines the flow coefficient C_V which is an important parameter to be used in the procedure for the noise prediction described by the international standards [28, 29]. Even more important is the differential pressure drop ratio X that appears in most of the equation in the IEC procedure. On the other side, it is not possible to state that the noise depends only on X because the absolute pressure influences the density of the air and the flow-rate. The dependency of the noise on all these factors needs to be investigated in detail and only a study based both on the numerical and on the experimental approach can return a complete description of the

phenomenon.

In addition to this, the experimental data can actually be used for a calibration of the coefficients that appear in the numerical models and for a comparison on more complex geometries than an orifice that are closer to the industrial world. In fact, even though the orifice is the most important fundamental configuration in aero-acoustics, it is actually true that the valves' manufacturers are interested in more complex devices. Testing real valves is difficult to be managed as already mentioned in the motivation of the numerical study at the beginning of this work. Indeed, the costs of realization of a valve are very high (materials, machines usage and time) and it is even more complicated to design and manage a proper plant on which these devices could be tested according to the reference international standards. A previous plant had already been realized [12, 14, 39, 42] but several issues were found about the quality of the air (humidity and dirt), about the measurement of hydraulic quantities as the velocity of the fluid, about the air-supply that fed the plant and by external noises. For all these reasons, the new plant wants to be designed in order to have the full control of all the variables that involves the quality of the air, the fluid-dynamic quantities and the loudness of the surrounding ambient. Below, the description of the plant that has been designed for the experimental campaign is fulfilled with particular attention to the choice of the instrumentations and their positioning along the pipes.

A good control of all the variables is easier to be achieved when the tests are performed on a small plant. The reduced dimension of all the parts involves lower flow-rate, smaller tank for air storage, faster tests and also money saving. For all these reason, the plant has been designed with a 1" main line on which the testing device is installed and the acoustic measurements are taken. The section of the test line downstream of the tested device is 2000mm long [27] while the upstream one is 750mm long. The flow conditions are controlled with a pressure regulator (inlet pressure) and by a valve at the end of the line to control the flow-rate.
According to the international standard IEC 60534-2-3 [29] the housings for the measurement of pressure and temperature are taken $2D$ upstream of the device and $6D$. The flow-rate is measured upstream of the main line just at the outlet of the tank that stores the air. Its quality is guaranteed by a dryer and two filters installed after a compressor.
The acoustic pressure inside the pipe is measured with different taps

downstream of the device, while the external noise is recorded by a microphone placed inside an anechoic chamber around the orifice. The reduction of the internal noise is managed by two silencers, one mounted upstream of the main line in order to reduce all the noise coming from the flow-meter and by the tank, and one at the end of the main line for avoiding the reflection of the noise that impacts against the downstream valve. Two other silencers are mounted before the exhaust in order to reduce the external noise emissions.

A visualization of the position of the different lines and instrumentations is visualized in figure 6.1. The placement of the instruments is the one suggested by the IEC 60534-8-1 [27]. The air supply is managed

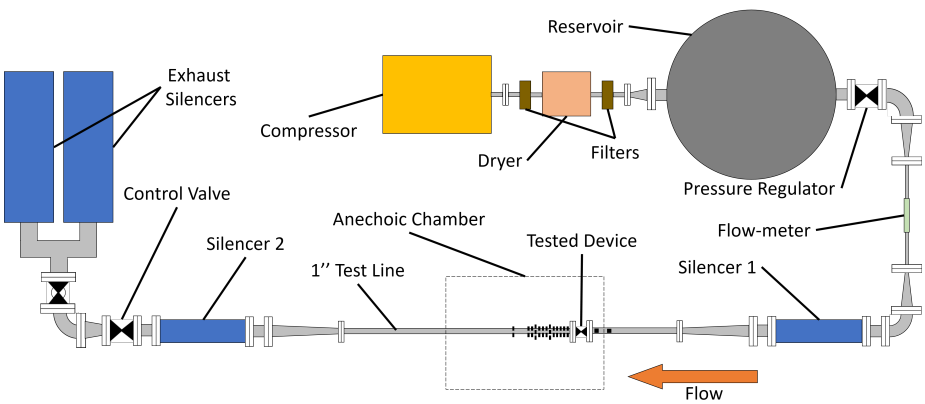

Figure 6.1: *Top-view of the plant designed for experimental campaign.*

in the first part of the plant by a Ingersoll Rand R7.5i-14 compressor that pressurizes the air up to 12 barA a with a 8.83 m^3/min flow-rate. Filters (Ingersoll Rand FA751 G and FA751 H) and a dryer (Ingersoll Rand D72IN-A) purify the air from dirt and humidity to a quality of the air that reaches the class 4/5 in the ISO 8573-1:2001. The purified air is not directly blown into the test line but it is collected in a 2 m^3 reservoir. The amount of air that flows inside the test line is managed by the control valve at the end of the section where the acoustic measurements are taken, and by a pressure reducer that fixes the pressure at the outlet of the reservoir.

The flow-rate is measured with the Coriolis Proline Promass F300 flow-meter installed on a reduced 1/2" pipe that guarantees a more precise measurement of all the flow-rate in the range 0.004-0.15 kg/s.

The silencers (1 and 2 in figure 6.1) are two Maxim 2" ILL-30 mounted

with proper fittings for a smooth change of the diameter of the pipe in order to avoid the generation of undesired noise.
The flow is finally characterized by the pressure and temperature respectively measured with two absolute pressure transducer (Cerabar M PMP51 and Tecsis P3290S075020), one differential pressure transducer Deltabar S PMD75, and with two RTD Pt100 Omega M12TXSS.

The acoustic pressure inside the pipe is measured with three microphones and three pressure sensors. The choice of the right instruments here is delicate because of the reduced dimension of the pipe, the high expected noise and because of the fragility of the microphones. The line, as already mentioned, has a diameter equal to 1" and the measurement of the acoustic pressure on the walls of the pipe becomes pretty challenging because of the curvature of the walls. The smallest microphones on the market that can be mounted with a flush installation have been identified in the 1/8" Gras 40DE. The problem associated to the installation of these microphones is that they are very fragile and the presence of eventual particles in the fluid could damage their membrane. For this reason, other sensors have been compared and the choice moved to the 1/4" PCB 113B28 pressure sensors; they functioning is completely different from the microphones and their hard membrane make them resistant to particles. On the other side, no sensors smaller than 1/4" have been found on the market and this is a critical issue since their dimension is comparable with the diameter of the pipe. A flush installation is very intrusive inside the pipe and modifies its geometry with possible affection of the internal flow. A recessed installation (sensor installed after a pin-hole on the walls) returns a measurement which is influenced by the hole and by its dimension. The possible installations of the PCB pressure sensor are displayed in figure 6.2. Because of the described issues, it has been

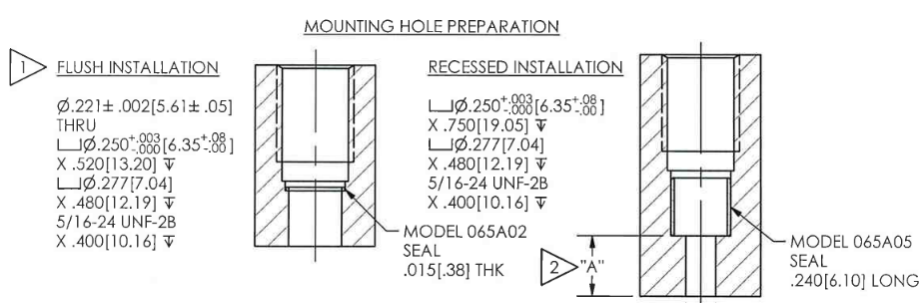

Figure 6.2: *Possible installation for the PCB113B28 pressure sensor.*

decided to install both the instruments in order to compare their data and make up for possible malfunctions of either of them. According to the description of the acoustic pressure returned by the APE presented in the chapter 4, the distribution of the acoustic pressure along the walls of the pipe varies considerably close to the tested device. For this reason, the taps for the pressure sensors and the housing for the microphones have been placed in the first 10 diameters with a constant pace of 1 diameter in order to be able to reconstruct all the SPL curve with its local peak, fast decrease and slower one.
In order to avoid external influences on the noise measurements, all the acoustic instruments are installed inside an anechoic chamber (1400 x 1000 x 1600mm LWH) placed around the testing device and along the downstream section of the test line. Another microphone (PCB 378B02) it is installed within the same chamber too and it measures the external noise 1 meter far from the pipe as indicated by the IEC international standard [28].

The last concern for a good experimental setup is the choice of the acquisition system whose scheme is visualized in figure 6.3. On the plant that has been described, the instrumentations for the hydraulic and fluid-dynamic measurements require different specifics than what is demanded by the acoustic ones. The acquisition of noise must be done with a frequency high enough to be able to describe the acoustic spectrum up to 20kHz, while lower frequencies are enough for the acquisition of the hydraulic quantities that change much slower than the acoustic ones. High-frequency modules have been identified in the National Instruments NI-9234, while for the all the other instruments the acquisition is managed by the NI-9208 module. The former module has only 4 channels that are not enough for all the 7 acoustic instruments (3 pressure sensors and 3+1 microphones) and two of them are thus installed on the plant. Nevertheless, they cannot be installed in the same way because of the different sensitivity of the pressure sensors respect to the microphones. The amplitude of the signal returned by the pressure sensors is in fact much lower than the one from the microphones and a signal conditioner PCB 482C15 is thus installed before a NI-9234 module for the amplification of the signal with a maximum possible gain of 100 times the original signal. All the three modules are installed on a chassis NI-9185 that is connected to a computer.

All the details hereby presented have already been discussed with

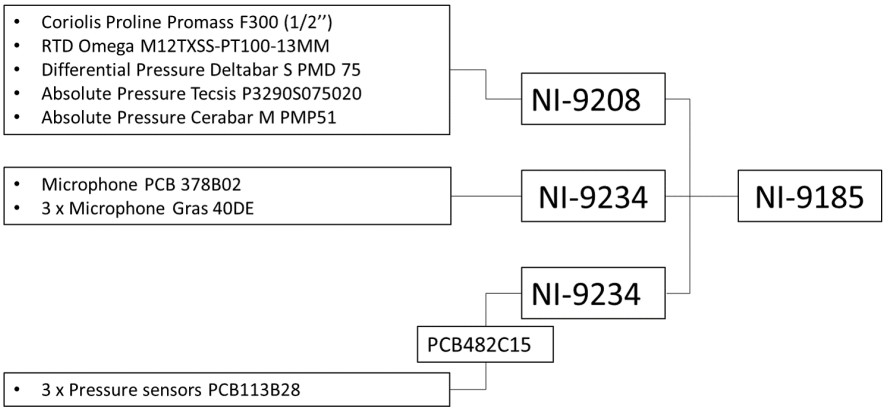

Figure 6.3: *Scheme of the sensors for the fluid-dynamic and acoustic measurements with the respective module and chassis for the acquisition system.*

the partner company that follows such a research and approved for the oncoming realization.

CHAPTER 7

Conclusions and Future Work

The research presented in this work is focused on the numerical prediction of the noise emitted by flow-control devices. The knowledge of the noise generation mechanism and the evaluation of the external noise are here computed with numerical methods overcoming the difficulties of experimental campaigns, lengthy and expensive for most of the valves.

In this work the Acoustic Perturbation Equations APE have been used as system for the propagation of the noise, that is generated by a flow computed with compressible RANS simulation and with synthetic generation of turbulence. The mean flow from RANS is used for the localization of the acoustic source region inside the pipe and for the definition of the APE source terms.

The APE has been implemented in OpenFoam and a new solver has been developed for facing all those numerical issues associated to CAA computation in the finite volume framework. The new solver has been tested and validated with analytical solutions and literature examples and its description of the intensity of the acoustic pressure is in accordance with the references. Small differences have been found on the velocity of the propagation of the acoustic wave and on its directivity but these are all

factors that, in the applications of interested, have negligible incidence.

The APE have been applied to the study of the noise emitted by an orifice installed inside a pipe. The jet generated at its outlet is characterized by a source region whose highest intensity is localized at the end of the potential core but it occupies also part of the shear layer. Different models for the description of the source term and the synthetic generation of the turbulent velocities have been compared and all return a similar qualitative distribution of the acoustic pressure (and of the SPL) inside the pipe. Differences have been found on the intensity of structures of acoustic pressure developed in the shear layer. The identification of the best couple of source models has been performed thanks to the comparison of the APE results with a LES that computes the acoustic fluctuations with a direct approach.
The noise produced downstream of the orifice is characterized by a local increase of noise due to the structures of acoustic pressure developed in the shear layer. However, the noise radiated by those structures decays in very short distances and they do not influence the noise downstream the end of the potential core. Here indeed the noise is governed by the acoustic generation mechanism located in the source region at the end of the jet.
This analysis on the role of the structures suggests that the noise far from the orifice is not influenced by them. For this reason, the terms responsible for the physical generation of these structures have been identified in the APE system and a new formulation without those two terms has been proposed. Its resolution requires 20% lower computational burden because of the simplification of the matrix of the linear system associated to its numerical resolution. The results returned by this formulation are, as expected, very different from the previous ones in the region close to the orifice where the lack of the structures induces a completely different acoustic pattern. The remarkable result is that far enough from the orifice (downstream of $9d$) the amplitude of the acoustic pressure and the SPL on the pipe's wall is in accordance with the one computed with the previous APE formulation. Such an evidence suggests that the new proposed APE system is able to predict the noise far from the orifice with the same reliability of the complete APE formulation, which on turn is able to describe the local noise generation mechanisms close to the jet's potential core too.
In industrial applications the interest in the noise prediction is focused

1 meter downstream of the tested device according to international standards. For all those devices whose jet at their outlet has a diameter such that $9d$ is shorter than 1 meter, the new APE formulation can be used for the noise prediction without the loss of any information.

The international standards used as disclaimer for the choice of the APE formulation is the reference for the valves' manufacturers who are asked to characterize their devices. In particular, they need to provide four parameters that can be used as part of a procedure for the evaluation of the noise 1 meter downstream of the device and 1 meter far from the external wall of the pipe. Among these four parameter, two are about the fluid-dynamic behaviour and their computation is well described by the proper international standards. The remaining two parameters are about the acoustical behaviour of the device and their values in the international standards are just tabulated for few devices and are constant for each of them. The assumption of invariability of these parameters with the flow conditions is very strong and it is also disproved by previous experimental results. Among the two acoustic parameters, furthermore, the valve correction factor for acoustic efficiency A_η has been identified as the one that influences the most the external SPL. The work is thus focused on the application of numerics for the estimation of this parameter and of its dependence with the flow conditions. An acoustical model for the prediction of the acoustic power density has been applied to the output of CFD numerical simulations for the computation of the acoustic power of all the source region inside the pipe. According to the equation returned by the international standard for its description, if the acoustic power is known, the A_η parameter is the only unknown quantity and its value can be thus evaluated inverting the equation. A curve of A_η values with different flow conditions has been derived for an orifice and it has been shown that it depends on the logarithm of the flow velocity.
The prediction of the noise obtained with the numerical value of A_η is close to the one returned by the international standards but it takes into account the flow influence and has a different shape. In particular, when the noise is higher than 40 dB, the numerical prediction returns an external SPL higher than the one computed with the suggested value for A_η for drilled holed plates, but lower than the one with the generic A_η for non-tabulated devices.

Finally, an experimental plant has been design with the definition of

all the required length, instrumentations, accuracy and air-quality control for the accomplishment of test in accordance with the international standards. Such a plant is projected for the realization of experimental test with small devices on a 1” line in order to collect data for a comparison with the numerical evidences presented in this work and for a deeper knowledge of all the noise generation mechanisms inside pipes. The proper instrumentations and acquisition system have been identified and their choice have been approved by the partner company for a future realization of the design plant.

APPENDIX $\mathcal{A}$

Derivation of Acoustic Perturbation Equations

The homogeneous Euler equations describe the conservation of mass, momentum and energy for an inviscid fluid without any external force:

$$\begin{cases} \dfrac{\partial \rho}{\partial t} + \dfrac{\partial \rho u_j}{\partial x_j} = 0 & \text{(A.1a)} \\ \dfrac{\partial \rho u_i}{\partial t} + \dfrac{\partial \rho u_j u_i}{\partial x_j} + \dfrac{\partial p}{\partial x_i} = 0 & \text{(A.1b)} \\ \dfrac{\partial \left(e + \frac{1}{2}u_i^2\right)}{\partial t} + u_j \dfrac{\partial \left(e + \frac{1}{2}u_i^2\right)}{\partial x_j} + \dfrac{\partial p u_j}{\partial x_j} = 0 & \text{(A.1c)} \end{cases}$$

where e is the internal energy per unity of mass.

The Acoustic Perturbation Equations APE used in this wor is presented in [5] and it is based on the decomposition of the fluid-dynamic quantities in a mean part $(\bar{\cdot})$, a turbulent fluctuation $(\cdot_t)$ and an acoustic

fluctuation ($\cdot_a$). This means:

$$\mathbf{u} = \overline{\mathbf{u}} + \mathbf{u}_t + \mathbf{u}_a; \tag{A.2a}$$

$$\rho = \overline{\rho} + \rho_t + \rho_a; \tag{A.2b}$$

$$p = \overline{p} + p_t + p_a. \tag{A.2c}$$

The concept at the base of this decomposition is that the mean flow is firstly computed with a CFD steady simulation, then the turbulent fluctuations is superimposed with a random synthetic generator (SNGR) and finally the acoustic fluctuations are left as unknowns in the APE system. In this appendix the Euler equations are manipulated for the derivation of the APE system.

A.1 Energy Equation

Equation (A.1c) is the first law of thermodynamics (thermal law equation) that describe the conservation of specific internal energy e and kinetic energy per unit of mass $\frac{1}{2}u_j^2 = E/\rho$ where E is the kinetic energy per unit of volume [34]. The conservation law for kinetic energy can be derived from the momentum equation (A.1b) multiplying it for the velocity vector with a proper scalar product

$$u_i \frac{\partial \rho u_i}{\partial t} + u_i \frac{\partial \rho u_j u_i}{\partial x_j} + u_i \frac{\partial p}{\partial x_i} = 0. \tag{A.3}$$

On the other side, from the continuity equation (A.1a) it is possible to obtain an expression for the divergence of the velocity field[1]

$$\frac{\partial u_j}{\partial x_j} = -\frac{1}{\rho}\frac{\partial \rho}{\partial t} - \frac{1}{\rho}\frac{\partial u_i}{\partial x_j} u_j = -\frac{1}{\rho}\frac{D\rho}{Dt}. \tag{A.4}$$

Manipulating equation (A.3) and taking into account equation (A.4) it is possible to obtain the conservation law for the kinetic energy

$$\rho \frac{\partial \frac{1}{2}u_j^2}{\partial t} + \rho u_i \frac{\partial \frac{1}{2}u_j^2}{\partial x_i} + u_j \frac{\partial p}{\partial x_j} = 0 \tag{A.5}$$

or, written with the total derivative

$$\rho \frac{D\frac{1}{2}u_j^2}{Dt} + u_j \frac{\partial p}{\partial x_j} = 0. \tag{A.6}$$

[1] It is used the decomposition of the divergence of a product of a scalar a with a vector $\mathbf{b}$, i.e. $\nabla\cdot(a\mathbf{b}) = a\nabla\cdot\mathbf{b} + \nabla a\cdot\mathbf{b}$.

Subtracting the equation for the kinetic energy (A.6) from the first law of thermodynamics (A.1c) it is possible to obtain an equation for the specific internal energy e as

$$\frac{De}{Dt} + \frac{p}{\rho}\frac{\partial u_j}{\partial x_j} = 0. \tag{A.7}$$

Substituting (A.4) in the energy equation (A.7) leads to

$$\frac{De}{Dt} - \frac{p}{\rho^2}\frac{D\rho}{Dt} = 0, \tag{A.8}$$

which is equivalent to the condition of an isentropic flow ($ds = 0$) according to the *fundamental law of thermodynamics for reversible processes*

$$T\, ds = de + p\, d\left(\rho^{-1}\right). \tag{A.9}$$

This means that, under the assumption of isentropic flow, equation (A.1c) is always satisfied.

The assumption of isentropic flow applied to the equation of state $p = p(\rho, s)$ for a generic gas

$$dp = c^2\, d\rho + \left(\frac{\partial p}{\partial s}\right)\bigg|_{\rho} ds \tag{A.10}$$

allows to derive the definition of the speed of sound c since stands

$$c^2 = \left(\frac{dp}{d\rho}\right)\bigg|_{s}. \tag{A.11}$$

A perfect gas (ideal gas with constant heat capacities) is characterized by the equation of state

$$p = \rho \bar{R} T, \tag{A.12}$$

and by the relationship

$$de = c_V dT \tag{A.13}$$

where $\bar{R}$ is the specific gas constant, T the temperature of the gas and c_V the specific heat at constant volume. Moreover, if the perfect gas transformation is governed by an isentropic process, it is possible to write

$$\gamma\frac{p}{\rho} = \left(\frac{dp}{d\rho}\right)\bigg|_{s} \tag{A.14}$$

where $\gamma = \frac{c_P}{c_V}$ is the specific heat ratio.
The comparison of the definition of the definition of the speed of sound for a generic gas (A.11) and equation (A.14) allows to obtain the formulation of the speed of sound for a perfect gas in an isentropic flow

$$c^2 = \gamma \frac{p}{\rho}. \tag{A.15}$$

A.2 Continuity Equation

Taking advantage of the equation (A.14) for a perfect gas in an isentropic flow it is possible to rewrite the continuity equation (A.1a) as function of the pressure

$$\frac{\partial p}{\partial t} + \gamma p \frac{\partial u_j}{\partial x_j} + u_j \frac{\partial p}{\partial x_j} = 0. \tag{A.16}$$

On this equation is possible to apply the decomposition of the flow quantities described by the equations (A.2) remembering that:

1. The mean flow is stationary and so the partial time derivative of a mean quantity is equal to zero

$$\frac{\partial \left(\bar{\cdot}\right)}{\partial t} = 0. \tag{A.17}$$

2. If the CFD simulation is run with an incompressible RANS other simplifications can be introduced:

   - the density of the fluid ρ is constant and uniform, i.e.

$$\frac{\partial \rho}{\partial t} = 0 \quad \text{and} \quad \frac{\partial \rho}{\partial x_i} = 0; \tag{A.18}$$

   - the fluid-dynamic density fluctuations are negligible since the flow doesn't change its density

$$\rho_t \approx 0; \tag{A.19}$$

   - Reynolds averaged continuity equation (written for ρ as (A.1a)) states that the divergence of the velocity field (mean and turbulent) is equal to zero

$$\frac{\partial \overline{u}_j}{\partial x_j} = 0 \quad \text{and} \quad \frac{\partial u_{tj}}{\partial x_j} = 0; \tag{A.20}$$

- Reynolds averaged continuity equation (written for p as (A.16)) for perfect gas and isentropic flow can be written as

$$\overline{u}_j \frac{\partial p}{\partial x_j} + u_{tj} \frac{\partial p_t}{\partial x_j} + \gamma \overline{p} \frac{\partial \overline{u}_j}{\partial x_j} + \gamma p_t \frac{\partial u_{tj}}{\partial x_j} = 0. \tag{A.21}$$

3. Acoustic fluctuations are usually order of magnitude lower than the turbulent ones which, on turn, are lower than the mean quantities. Second order fluctuations including acoustic fluctuations are negligible, that means that a product of an acoustic fluctuation with a turbulent (or acoustic) one is approximated to zero

$$(\cdot)_a (\cdot)_a \approx 0 \quad \text{and} \quad (\cdot)_a (\cdot)_t \approx 0 \tag{A.22}$$

The previous assumptions are applied to continuity equation (A.16) decomposed according to (A.2) obtaining

$$\frac{\partial p_a}{\partial t} + \overline{u}_j \frac{\partial p_a}{\partial x_j} + \gamma \left(\overline{p} \frac{\partial u_{aj}}{\partial x_j} + p_a \frac{\partial \overline{u}_j}{\partial x_j} \right) + u_{aj} \frac{\partial \overline{p}}{\partial x_j} = - \left[\frac{\partial p_t}{\partial t} + \overline{u}_j \frac{\partial p_t}{\partial t} + u_{tj} \frac{\partial \overline{p}}{\partial x_j} \right]. \tag{A.23}$$

According to [5] the right-hand side of (A.23) can be neglected according to order of magnitude analysis. The resulting **APE equation for acoustic pressure** is

$$\frac{\partial p_a}{\partial t} + \overline{u}_j \frac{\partial p_a}{\partial x_j} + \gamma \left(\overline{p} \frac{\partial u_{aj}}{\partial x_j} + p_a \frac{\partial \overline{u}_j}{\partial x_j} \right) + u_{aj} \frac{\partial \overline{p}}{\partial x_j} = 0. \tag{A.24}$$

A.3 Momentum Equation

The Euler momentum equation (A.1b) can be rewritten splitting the derivative of the first two terms as

$$\frac{\partial \rho}{\partial t} u_i + \rho \frac{\partial u_i}{\partial t} + \frac{\partial \rho u_j}{\partial x_j} u_i + \frac{\partial u_i}{\partial x_j} \rho u_j + \frac{\partial p}{\partial x_i} = 0. \tag{A.25}$$

Furthermore continuity equation (A.1a) suggests that the sum of the first and third term in (A.25) is equal to zero. Dividing equation (A.25) for the density ρ the momentum equation becomes

$$\frac{\partial u_i}{\partial t} + \frac{\partial u_i}{\partial x_j} u_j + \frac{1}{\rho} \frac{\partial p}{\partial x_i} = 0. \tag{A.26}$$

With the same flow decomposition and standing the assumptions introduced for the continuity equation it is possible to derive the **Acoustic Perturbation Equation for the acoustic particle velocity**

$$\frac{\partial u_{ai}}{\partial t} + \overline{u}_j \frac{\partial u_{ai}}{\partial x_j} + u_{aj} \frac{\partial \overline{u}_i}{\partial x_j} + \frac{1}{\overline{\rho}} \frac{\partial p_a}{\partial x_i} - \frac{p_a}{\overline{\rho}^2 c^2} \frac{\partial \overline{p}}{\partial x_i} = S_{\mathbf{u}i} \tag{A.27}$$

where the source term in its most complete form is

$$S_{\mathbf{u}i} = -\left[u_{tj} \frac{\partial u_{ti}}{\partial x_j} + \overline{u}_j \frac{\partial u_{ti}}{\partial x_j} + u_{tj} \frac{\partial \overline{u}_i}{\partial x_j} + \frac{\partial u_{ti}}{\partial t} - \frac{1}{\overline{\rho}} \frac{\partial p_t}{\partial x_i} + \overline{u_{tj} \frac{\partial u_{ti}}{\partial x_j}} \right]. \tag{A.28}$$

In the derivation of (A.27) the following equation derived from RANS equations has been used

$$\overline{u}_j \frac{\partial \overline{u}_i}{\partial x_j} + \frac{1}{\overline{\rho}} \frac{\partial \overline{p}}{\partial x_i} = -\overline{\frac{\partial u_{tj}}{\partial x_j}} - \overline{u_{tj} \frac{\partial u_{ti}}{\partial x_j}}. \tag{A.29}$$

Bibliography

[1] C. Bailly and D. Juve. A stochastic approach to compute subsonic noise using linearized euler's equations. In *5th AIAA/CEAS Aeroacoustics Conference and Exhibit*, page 1872, 1999.

[2] C. Bailly and D. Juve. Numerical solution of acoustic propagation problems using linearized euler equations. *AIAA journal*, 38(1):22–29, 2000.

[3] C. Bailly, P. Lafon, and S. Candel. A stochastic approach to compute noise generation and radiation of free turbulent flows. *DGLR BERICHT*, pages 669–669, 1995.

[4] M. Bauer and A. Zeibig. Towards the applicability of the modified von kármán spectrum to predict trailing edge noise. In *New Results in Numerical and Experimental Fluid Mechanics V*, pages 381–388. Springer, 2006.

[5] W. Bechara, C. Bailly, P. Lafon, and S.M. Candel. Stochastic approach to noise modeling for free turbulent flows. *AIAA journal*, 32(3):455–463, 1994.

[6] D.A. Bies, C. Hansen, and C. Howard. *Engineering noise control*. CRC press, 2017.

[7] M. Billson, L.-E. Eriksson, and L. Davidson. Acoustic source terms for the linearized euler equations in conservative form. *AIAA journal*, 43(4):752–759, 2005.

[8] M. Billson, L.E. Eriksson, and L. Davidson. Jet noise prediction using stochastic turbulence modeling. In *9th AIAA/CEAS Aeroacoustics Conference and Exhibit*, page 3282, 2003.

[9] W.K. Blake. *Mechanics of flow-induced sound and vibration, Volume 1: General Concepts and Elementary Sources*. Academic press, 2017.

[10] W.K. Blake. *Mechanics of flow-induced sound and vibration, Volume 2: Complex flow-structure interactions*. Academic press, 2017.

[11] C Bogey, C Bailly, and D Juvé. Noise investigation of a high subsonic, moderate reynolds number jet using a compressible large eddy simulation. *Theoretical and Computational Fluid Dynamics*, 16(4):273–297, 2003.

[12] F. Bossi. *Fluid-dynamic noise in control devices*. PhD thesis, 2016.

[13] T. Colonius, S. K Lele, and P. Moin. Sound generation in a mixing layer. *Journal of Fluid Mechanics*, 330:375–409, 1997.

[14] I. Colpo. *Valvole di regolazione a sfera: caratterizzazione fluidodinamica e generazione di rumore aerodinamico*. PhD thesis, 2011.

[15] N. Curle. The influence of solid boundaries upon aerodynamic sound. *Proc. R. Soc. Lond. A*, 231(1187):505–514, 1955.

[16] R. Ewert and W. Schröder. Acoustic perturbation equations based on flow decomposition via source filtering. *Journal of Computational Physics*, 188(2):365–398, 2003.

[17] L. Fenini, F.C. Bossi, and S. Malavasi. Broadband noise generated downstream of a resistor in a duct. In *Proceedings of 11th F.I.V. conference*, 2016.

[18] L. Fenini and S. Malavasi. Improvements and validation of the numerical prediction of the incipient cavitation index. In *ECCOMAS Young Investigators Conference 2017*, 2017.

[19] L. Fenini and S. Malavasi. Numerical prediction of aero-dynamic noise with a finite volume approach. In *Proceedings of FSI2 & FVI+N*, 2018.

[20] L. Fenini, S. Malavasi, and B. Papa. Integration of numerical methods with iec standard for aerodynamic noise prediction in control devices. In *ValveWorld 2018 Conference,*, 2018.

[21] G. Ferrarese et al. New method for predicting the incipient cavitation index by means of single-phase computational fluid dynamics model. *Advances in Mechanical Engineering*, 7(3), 2015.

[22] J.E. Ffowcs Williams and D.L Hawkings. Sound generation by turbulence and surfaces in arbitrary motion. *Phil. Trans. R. Soc. Lond. A*, 264(1151):321–342, 1969.

[23] M.E. Goldstein. *Aeroacoustics*. McGraw-Hill, 1976.

[24] C.J. Greenshields. Openfoam user guide. *OpenFOAM Foundation Ltd, version*, 3(1), 2015.

[25] M.S. Howe. Contributions to the theory of aerodynamic sound, with application to excess jet noise and the theory of the flute. *Journal of Fluid Mechanics*, 71(4):625–673, 1975.

[26] IEC. *IEC 60534, Industrial-process control valves - Part 1: Control valve terminology and general considerations*. IEC International Standard, 2005.

[27] IEC. *IEC 60534 Industrial-process control valves - Part 8-1: Noise considerations - Laboratory measurements of noise generated by aerodynamic flow through control valves*. IEC International Standard, 2005.

[28] IEC. *IEC 60534, Industrial-process control valves - Part 8-3: Noise considerations - Control valve aerodynamic noise prediction method*. IEC International Standard, 2010.

[29] IEC. *IEC 60534 Industrial-process control valves - Part 2-3: Flow capacity - Test procedures*. IEC International Standard, 2015.

[30] ISA. *ISA-RP75.23-1995 Considerations for Evaluating Control Valve Cavitation*. Research Triangle Park, NC, USA, 1995.

[31] M Karweit, P. Blanc-Benon, D. Juvé, and G. Comte-Bellot. Simulation of the propagation of an acoustic wave through a turbulent velocity field: A study of phase variance. *The Journal of the Acoustical Society of America*, 89(1):52–62, 1991.

[32] AD Kirkwood. *Aerdynamic noise generation in control valves*. PhD thesis, The University of Manchester, 1992.

[33] A.N. Kolmogorov. The local structure of turbulence in incompressible viscous fluid for very large reynolds numbers. In *Dokl. Akad. Nauk SSSR*, volume 30, pages 299–303, 1941.

[34] P.K. Kundu, I.M. Cohen, and H.H. Hu. *Fluid Mechanics*. Elsevier Academic Press, San Diego, 2012.

[35] M.J. Lighthill. On sound generated aerodynamically i: General theory. *Proc. R. Soc. Lond. A*, 211(1107):564–587, 1952.

[36] M.J. Lighthill. On sound generated aerodynamically ii. turbulence as a source of sound. *Proc. R. Soc. Lond. A*, 222(1148):1–32, 1954.

[37] G.M. Lilley. The generation and radiation of supersonic jet noise. *Theory of Turbulence Generated Noise*, 4(part II), 1972.

[38] S. Malavasi et al. Numerical method to provide cavitation index for control valves. In *Proceedings of the ASME 2013 Pressure Vessels & Piping. Division Conference PVP2013*, pages 1–7, 2013.

[39] G. Mazzaro. *Rumore Fluidodinamico in dispositivi di regolazione*. PhD thesis, 2014.

[40] M. Mesbah. Flow noise prediction using the stochastic noise generation and radiation approach. 2006.

[41] M. Mesbah, J. Meyers, M. Baelmans, and W. Desmet. Assessment of different parameters used in the sngr method. *Proceedings of ISMA2004*, pages 389–402, 2004.

[42] F. Nelli. *Analisi del rumore aerodinamico in dispositivi di regolazione*. PhD thesis, 2014.

[43] M.P. Norton and D.G. Karczub. *Fundamentals of noise and vibration analysis for engineers*. Cambridge university press, 2003.

[44] Parcol. *Handbook for control valve sizing*. 2016.

[45] O.M. Philips. On the generation of sound by supersonic turbulent shear layer. *Journal of Fluid Mechanics*, 9(Part 1):1–28, 1960.

[46] A. Powell. Aerodynamic noise and the plane boundary. *The Journal of the Acoustical Society of America*, 32(8):982–990, 1960.

[47] I. Proudman. The generation of noise by isotropic turbulence. *Proc. R. Soc. Lond. A*, 214(1116):119–132, 1952.

[48] H.S. Ribner. The generation of sound by turbulent jets. *Advances in applied mechanics*, 8(103-182):10, 1964.

[49] M.M.A. Rossi et al. Improvements and validation of the numerical prediction of the incipient cavitation index. In *Proceedings of the ASME 2015 Pressure Vessels & Piping. Division Conference PVP2015*, 2015.

[50] S. Sarkar and M.Y. Hussaini. Computation of the sound generated by isotropic turbulence. Technical report, Institute For Computer Applications in Science and Engineering Hampton VA, 1993.

[51] C.K.W. Tam. Computational aeroacoustics-issues and methods. *AIAA journal*, 33(10):1788–1796, 1995.

[52] C.K.W. Tam and J.C. Webb. Dispersion-relation-preserving finite difference schemes for computational acoustics. *Journal of computational physics*, 107(2):262–281, 1993.

[53] C. Wagner, T. Hüttl, and P. Sagaut. *Large-eddy simulation for acoustics*, volume 20. Cambridge University Press, 2007.

[54] A. Yoshizawa. Statistical theory for compressible turbulent shear flows, with the application to subgrid modeling. *The Physics of fluids*, 29(7):2152–2164, 1986.